UV PUMPED HOLOSTERIC OPTICAL PARAMETRIC OSCILLATOR

Yong Cui

A Thesis Submitted for the Degree of PhD
at the
University of St Andrews

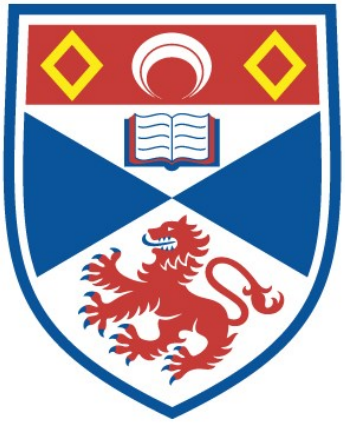

1993

UV Pumped Holosteric Optical Parametric Oscillator

Yong Cui

A thesis presented to the University of St. Andrews in application for the degree of Doctor of Philosophy.

Department of Physics and Astronomy
University of St. Andrews

January 1993

Declaration

I hereby certify that this thesis has been composed by my self, that it is a record of my own work, and that it has not been accepted in partial or complete fulfilment of any other degree or professional application.

This research work was carried out in the J. F. Allen Physics Research Laboratory in the Physics Department of the University of St. Andrews, under the supervision of Professor M. H. Dunn.

Y. Cui
January 1993

I hereby certify that the candidate has fulfilled the conditions of the Resolution appropriate to the Degree of Ph. D.

M. H. Dunn
Research Supervisor
January 1993

Acknowledgement

Firstly, I would like to thank Professor Malcolm H. Dunn for his guidance, advice and helps during the period of this work. His deep physical insight will always be an inspiration. I am grateful to Professor Wilson Sibbett for allowing me to work in his Department, and for his support and encouragement throughout. I am also pleased to have this opportunity to thank every one who has helped make my years in St. Andrews fruitful and pleasant, and in particular, I would like mention a number of people for their collaborations, assistance and patience, they are Bruce D. Sinclair, Callum J. Norrie, Cameron F. Rae, Angus Henderson, Jonathan A. C. Terry, Gordon Roberson, Dominic E. Withers, Christian Rahlff, Majid Ebrahimzadeh. The mechanical workshop, in particular Jimmy Lindsay must be thanked for fabrication of essential components for the optical parametric oscillator.

Secondly, I would like to acknowledge the Royal Society of London and the Defence Research Agency (Aerospace Division, Royal Armament Research and Development Establishment) of the United Kingdom for funding my fellowships which have supported me through out my research work.

Finally, I am grateful to my wife Tang Yan, whose challenges, encouragement, and understanding have made this work much easier.

Publications and Papers

(1) **A lithium triborate optical parametric oscillator pumped at 266 nm**
Y. Tang, Y. Cui and M. H. Dunn
in 1991 European Quantum Electronics Conference and Tenth National Quantum Electronics Conference (Heriot-Watt University, Edinburgh, August 27th-30th, 1991)
91 EQEC Technical Digest, Post-deadline paper PD 8, 14, 1991

(2) **A lithium triborate optical parametric oscillator pumped at 266 nm**
Y. Tang, Y. Cui and M. H. Dunn
Opt. Lett. **17**(3), 192, 1992

(3) **All-solid-state optical parametric oscillator for the visible**
Y. Cui, M. H. Dunn, C. J. Norrie, W. Sibbett, B. D. Sinclair, Y. Tang, and J. A. C. Terry
in Conference on Lasers and Electro-Optics (Anaheim, California, 1992)
OSA Technical Digest Series, **12**, Paper CTuR1, 198, 1992

(4) **All-Solid-State Optical Parametric Oscillator for the visible**
Y. Cui, M. H. Dunn, C. J. Norrie, W. Sibbett, B. D. Sinclair, Y. Tang, and J. A. C. Terry
Opt. Lett. **17**(9), 646, 1992

(5) **Widely tunable of all-solid-state optical parametric oscillator for the visible and near infrared**
Y. Cui, D. E. Withers, C. F. Rae, C. J. Norrie, Y. Tang, B. D. Sinclair, W. Sibbett and M. H. Dunn
Opt. Lett. **18**(2), 122, 1993

(6) **Comparison of lithium triborate and beta barium borate as nonlinear media for optical parametric oscillators**
M. H. Dunn, Y. Cui, A. J. Henderson, G. Roberson, Y. Tang, D. E. Withers, W. Sibbett, and B. D. Sinclair
Journal of Optical Society of America B, (submitted, Nov. 1992)

Abstract

The all-solid-state (or "holosteric") optical parametric oscillator has resulted from the recent development of diode-laser-pumped solid-state lasers and from recent advancements in new optically nonlinear materials. As a result, all-solid-state sources of widely tunable (ultraviolet - visible - near infrared) coherent radiation are now possible by using the radiation from diode-laser-pumped solid-state lasers, either directly or after frequency conversion, to pump optical parametric oscillators. Such devices can be made compact, efficient and reliable. The work described in this thesis explores the feasibility of obtaining widely tunable radiation from such devices, with particular reference to low threshold, high efficiency operation, so requiring only modest energies (1 mJ in ultraviolet) from the pump source. In particular, a frequency tripled or frequency quadruped Nd:YAG laser pumped by pulsed, GaAlAs diode laser bars has been used as the pump source, and lithium triborate has been used as the nonlinear medium in the optical parametric oscillator.

Two geometries of lithium triborate crystals have been investigated as the nonlinear medium. One was cut for a type II non-critical phase matching geometry, while the other was cut for a type I critical phase matching geometry. The oscillator cavities were designed for optimum focusing and mode matching aiming for operation with a low pump energy through the use of tightly focused pump radiation. The ultraviolet pump source was based on a Q-switched diode-laser-pumped Nd:YAG laser which generated pulses at 1.064 μm with energy 10 mJ and duration around 10 ns. These were then frequency up-converted to the UV at 355 nm or 266 nm, so as to be suitable for pumping the parametric oscillators. Generally, an overall conversion efficiency from 1.064 μm to 355 nm of >30% was obtained using the nonlinear materials potassium titanyl phosphate and lithium triborate for second harmonic generation and sum-frequency mixing respectively. For conversion to 266 nm, an overall efficiency of > 18 % was obtained using the nonlinear materials KTP and BBO for two step second harmonic generation.

In the experimental investigations of the all-solid-state lithium triborate optical parametric oscillator pumped at 355 nm a low oscillation threshold was obtained in the type II non-critical phase matching geometry (around 0.2 mJ) and pump depletions of 50 % were obtained at around six times threshold. This device could be temperature tuned (20 - 200 °C) from 457 to 481 nm (signal wave) and 1.6 to 1.35 μm

(idler wave). Optimised focusing conditions corresponding to the theory of Guha et al were approached in the type I phase matching geometry, and despite the existence of a 1° walkoff angle, the minimum oscillation threshold was measured to be around 0.3 mJ. Generally, pump depletions of about 35 % were obtained, at around four times threshold. These devices could be angle tuned (through crystal internal angle 14°) from 457 to 666 nm (signal wave) and 1.6 μm to 768 nm (idler wave). (The whole of the range 420 nm to 2.3 μm could be covered with such a device given additional mirror sets). The all-solid-state type II geometry lithium triborate optical parametric oscillator was also pumped at 266 nm, when it was temperature tunable (20 - 200 °C) from 306 to 314 nm (signal wave) and 2.03 to 1.75 μm (idler wave). Pump depletions of 25 % were demonstrated with this device at pump energies of four times threshold.

In addition to the above experimental investigations, the thesis addresses the issues of (i) choice of nonlinear material for optical parametric oscillators in terms of appropriate figures of merit, and (ii) optimisation of pump and resonated wave focusing parameters. Reviews of the appropriate theoretical background to phase matching geometries and optical parametric interaction are included.

Table of Contents

CHAPTER 1

Introduction

This thesis describes the development and experimental demonstration of optical parametric oscillators (OPO) pumped by Q-switched sources, and based on noncritical phase matching (NCPM) and critical phase matching (CPM) geometries in lithium triborate (LiB_3O_5, LBO) in all-solid-state schemes. The principal goal of this work was to investigate the feasibility of operation of low threshold compact OPO devices using only modest pump energies from diode pumped, Q-switched Nd:YAG lasers, as well as investigating the newly developed nonlinear material lithium triborate as an OPO gain medium operating and tuning in the ultraviolet (UV), visible and near infrared (~IR) bands. Essential to the operation of such devices, was the optimization of frequency doubling, tripling and quadrupling schemes, in order to provide all-solid-state UV pump sources. All these aspects are discussed in this thesis.

1.1 The concept of the "all-solid-state optical parametric oscillator"

Recently the meaning of "Holosteric" (i.e. all-solid-state) has become well known in the field of laser physics, but at the start of this thesis it is still worthwhile emphasising the concept again, which will be useful to our further discussion.

"All-solid-state" means that all radiation generation processes are carried out entirely within the solid-state phase[1].

An example of such a device is the UV pumped, holosteric optical parametric oscillator shown as in figure (1-1)[2].

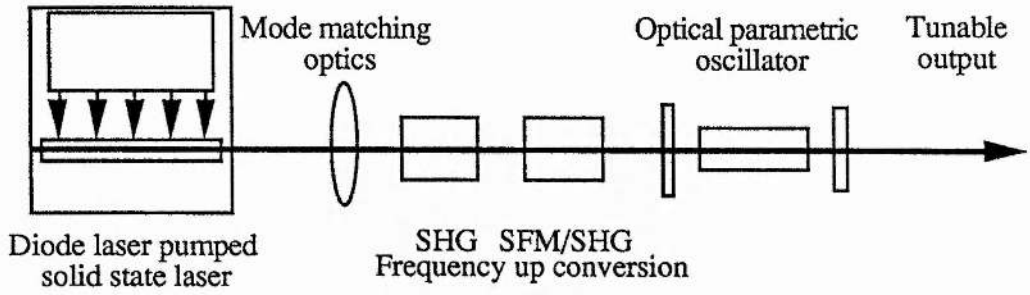

Fig. 1-1 Configuration of an all-solid-state optical parametric oscillator for the generation of radiation in the UV, visible and near infrared regions of the spectrum.

Here an infrared solid-state laser (Nd:YAG, λ = 1.064 μm) is pumped using diode lasers (GaAlAs semiconductor diode laser) and the radiation generated is then frequency shifted (by either frequency tripling or frequency quadrupling) into the ultraviolet so as to be suitable for pumping a solid-state optical parametric oscillator with an output tunable in the UV, visible and near infrared regions of the spectrum.

1.2 Brief historical review and contemporary developments

As continuously tunable coherent light sources, optical parametric oscillators have already been of interest for a number of years now in many applications. The advantages of OPO's compared to normally tunable lasers, such as dye laser and solid-state vibronic lasers, which have long been regarded as convenient sources, is the very much greater tuning bandwidth.

In recent years many new opportunities have arisen for the development of optical parametric oscillators with broad tuning ranges throughout the UV and mid-IR. Optical parametric oscillators are likely to play a role as versatile and practical sources of widely tunable coherent radiation. Specifically in the scheme of a diode pumped solid-state laser used as the pump source, the optical parametric oscillator has many advantages

such as compactness, longevity, high efficiency and better stability. Such devices have been demonstrated for sometime. The first publication in this area was perhaps from Byer et al, where a monolithic MgO:$LiNbO_3$ optical parametric oscillator pumped by the second harmonic of an amplified single mode diode pumped Nd:YAG laser was described[3]. The first demonstration of optical parametric oscillation tunable in the visible and the UV band with an all-solid-state scheme was carried out by our research group[2].

In reality, all-solid-state optical parametric oscillators have greatly benefited from the advances in two different technologies which are nonlinear optical materials and diode lasers. Those technologies have developed in parallel for more than 30 years together with the technique of optical parametric oscillation itself. However, studies of the holosteric or all-solid-state OPO in which these three technologies are combined began just a few years ago, and since then progress has been rapid. A comparison of the tuning ranges addressed by optical parametric oscillators compared with other tunable sources is shown in figure (1-2).

Early work with optical parametric oscillators showed some potentially troublesome problems. Firstly the nonlinear optical materials then available showed either too low a nonlinear coefficient or damage threshold[4][5][6]. Secondly difficulty was encountered in building a suitable pump source, particularly in the ultraviolet, mainly due to the lack of a suitable nonlinear optical material for frequency up conversion[7]. So, it is understandable why in the past operation of OPO's has been confined primarily to infrared spectral regions; and why there has previously been limited interest in the OPO for generation of tunable radiation in the near ultraviolet and visible spectral regions. After Franken's first experiment[8], and despite considerable effort over 20 years, only a handful of nonlinear materials were commonly available until the early 1980's.

Now times have changed. The development of new nonlinear materials and improvement in the techniques used to grow crystal and in the degree of purity of the raw materials used in these processes, has led to a general availability of material with higher nonlinear coefficient, high damage threshold and high optical quality. The nonlinear crystal compounds attracting the most interest today are $KNbO_3$(KN), $KTiOPO_4$(KTP), $KTiOAsO_4$(KTA), d-LAP, β-BaB_2O_4(BBO), LiB_3O_5(LBO) and $AgGaSe_2$[9]. They have an impressive performance for the generation of intense UV,

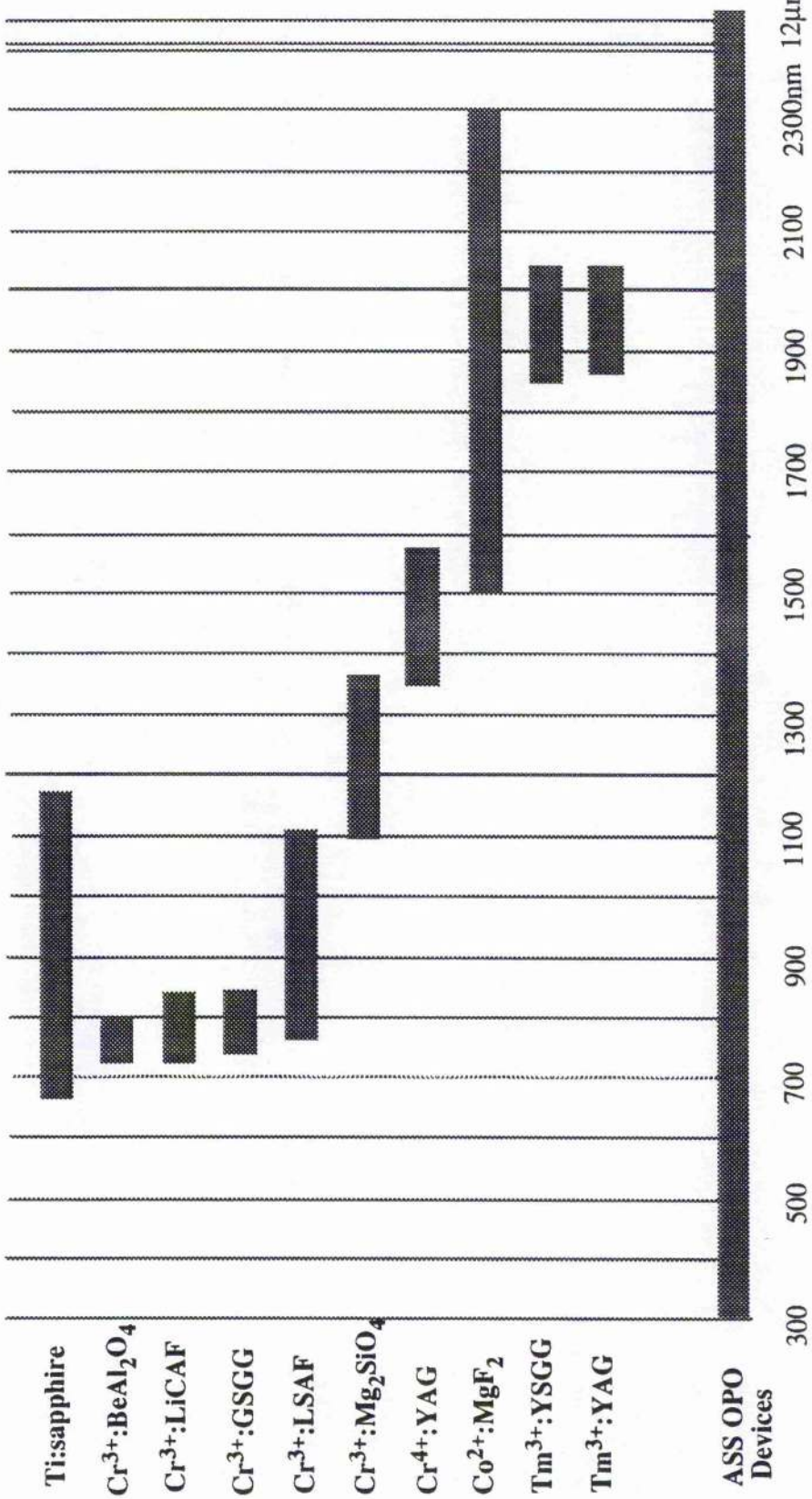

Fig. 1-2 Tuning range of solid-state laser devices.

visible and near-infrared radiation, and may replace the more established nonlinear crystal such as $LiNbO_3$. $LiIO_3$, KB5, lithium formate and urea, as well as KDP and its isomophs in most frequency conversion applications. Based on those newly developed materials, optical parametric oscillator devices are now commercially available[10]. After the first demonstration of the OPO in 1965[11][12], it is only now that for the first time OPO devices have really found a place in the tunable coherent light source market.

The diode laser was invented in the early 1960's[13], but the development of reliable commercial devices only occurred from the early 1980's onwards. In recent years, the semiconductor diode laser spectrum has been extended to cover most of the band from visible red to mid-IR (630 nm - 27 μm). Very recently a blue green band (490 nm) laser diode has been demonstrated using II-VI materials[14]. Unfortunately the output beam quality of diode lasers is generally poor. Output powers in most cases are not sufficient, particularly with regard to the peak power capability and energy capacity of the diode laser to supersede the well developed solid-state lasers, even looking into the long term future. As a result its applications are limited in many cases. However, as a highly efficient pump source GaAlAs diode lasers with a wavelength around 810 nm have been well developed[15]. For long-pulse (quasi-CW) operation GaAlAs lasers at 2.4 kW peak power, 200 μs pulse width, 100 pps repetition, and for CW monolithic GaAlAs diode laser arrays at 20 W output level, are already commercially available. The life-time for these lasers has been demonstrated to be more than 10^9 pulse and 3×10^4 hours respectively[16]. The maximum output power has been demonstrated to be as high as 120 W for CW devices using a diamond heat-sink to dissipate generated heat[17].

It is well known that the use of diode lasers to pump solid state lasers leads to many favourable performance characteristics. Firstly, some of the advantages of diode lasers are directly transfered to the diode pumped solid state lasers; these are longevity, compactness and improved stability. Secondly, the diode laser wavelength can be selected and adjusted, and can be exactly matched to the peak absorption band of the solid-state laser medium, which means that a much greater fraction of the pump radiation is utilised in excitation of the transition, hence making devices much more efficient. Thirdly, accompanying the highly efficient conversion, thermal loading problems are significantly reduced, which greatly improved the output beam quality of diode pumped solid-state lasers. Together with flexibility in design, diode pumped

solid-state lasers have very quickly grown more popular. In the near future in low and even in the medium power devices, the diode lasers will replace the flashlamp as a highly efficient pump source.

It is interesting to note that the trivalent rare earth ions are natural candidates for resonant pumping due to their sharp absorption lines. Some of these ions Nd^{3+}, Dy^{3+}, Er^{3+}, Tm^{3+} and Yb^{3+} have strong absorption lines around the 800 nm region and the laser action is found in 1-3 μm band with relatively high conversion efficiency[18]. Based on those diode pumped solid-state lasers, and highly efficient frequency up shifting techniques, the all-solid-state optical parametric oscillator covering the frequency tuning range from 300 nm to 12 μm becomes practicable. Although, the use of diode pumped, Q-switched, frequency up converted Nd:YAG laser for OPO's operating in the visible generally results in some reduction in overall system efficiency, because of the additional frequency conversion processes, the high efficiency associated with every link still results in a high overall efficiency compared to the cases of normal ion lasers or excimer lasers used as the pump sources. Marshall et al have demonstrated an eye-safe laser based on all-solid-state OPO technology, and they have observed 2 % total wall-plug efficiency with adequate useful output at 1.61 and 1.54 μm[19].

The field of all-solid-state OPO's is moving rapidly. The author believes that this review is reasonably topical at the time of writing, although clearly there will be advances in the field before completion of this thesis.

1.3 UV pumped optical parametric oscillator

The UV pumped optical parametric oscillator (pump wavelength ≤ 355 nm) providing output wavelengths tunable in the UV, visible and near infrared was limited before 1984 due to a lack of nonlinear optical materials that can be phase matched in the UV, have a high nonlinear coefficient, and high optical damage threshold.

However the deficiency was filled first by urea introduced in 1984[20]. An OPO using urea as the nonlinear medium and pumped by 355 nm radiation from a frequency tripled Nd:YAG laser, was first demonstrated by Tang et al[20][21] with a tuning range from 498 nm to 1.23 μm and 20 % optical to optical conversion efficiency. A few years

later, an ever higher conversion efficiency was demonstrated by Ebrahimzadeh et al[22] with a urea OPO pumped at 308 nm by an excimer laser. A 66% conversion efficiency were demonstrated over a narrow wavelength range 537-720 nm close to noncritical phase matching condition. Although crystalline urea has a very high single-shot optical damage threshold, it suffers from long term optical damage problems and was soon superseded by the new nonlinear optical crystal β-barium borate[23], which is comparatively easy to grow and has superior crystal properties.

UV pumped β-barium borate OPO's were reported by many authors from 1988 onwards. A representative result for a BBO OPO pumped at 355 nm is that of Byer et al[24]. They demonstrated a 140 mW average output power at the signal wavelength and 24 % total conversion efficiency. This device can continuously tuned from 412 nm to 2.55 μm. A BBO OPO pumped at 266 nm, using a quadruped Nd:YAG laser, was reported by Bosenberg et al[25]. Their OPO generated continuously tunable light over the range 330 nm to 1.37 μm. BBO OPO's pumped at 308 nm by excimer lasers have also been investigated by some authors. Ebrahimzadeh et al[26] have demonstrated tunable radiation over the entire spectral range from 354 nm to 2.37 μm and energy conversion efficiencies of great than 10 %. High pump depletions (70 % in a double-pass pump geometry[27]) and external conversion efficiency (32 % with the use of dual crystal geometries[28]) have been reported in the last year. BBO has been identified by many experiments as a superior nonlinear material in the ultraviolet, but, due to BBO's larger Poynting vector walkoff angle and relatively small angular acceptance it is not suitable for operation at lower pump powers, where tightly focussing the pump laser is not helpful.

BBO's disadvantage was overcame by the more recently developed nonlinear optical crystal lithium triborate[29]. The nonlinear crystal LiB_3O_5 was recently developed in China, and has a number of advantages compared with β-BaB_2O_4. The transmission extends further into the UV, it is not hygroscopic, and optical damage threshold are reported as high as two times that of BBO[30]. Although LBO has a smaller nonlinear coefficient, and a smaller birefringence, implying a smaller tuning rate, this leads to an inherently narrow linewidth and larger acceptance angles and pump bandwidths than BBO. This make LBO an interesting material for broadly tunable, line-narrowed optical parametric oscillators, pumped by the modest energy from recently developed diode pumped solid-state lasers with tight focussing. An LBO OPO pumped by 308 nm radiation from an excimer laser with type II noncritical phase matching, as

well as critical phase matching configurations has been demonstrated in this laboratory. In the former case, 40 % pump depletion and 30 % external efficiency has been achieved when a signal wavelength of 385 nm and idler wavelength of 1.54 μm is parametrically generated[31]. In the later scheme, tuning ranges of 355-497 nm in the ultraviolet/blue spectral region, and 809 nm - 2.34 μm in the near infrared have been obtained with a pump depletion of 28 %[32]. A type II NCPM LBO OPO pumped at 355 nm was first reported by Hanson et al[33]. They demonstrated a temperature tunable OPO around 470-487 nm blue band with 12.5 % conversion efficiency at room temperature. A type I CPM LBO OPO pumped at 355 nm was first demonstrated by Chen et al[34] with tuning from 435 nm to 1.92 μm and an overall conversion efficiency 14 %.

Table (1-1) possibly lists all the published experimental investigation results of UV pumped optical parametric oscillators.

However, these particular noncritical and critical geometries had not been pumped with an all-solid-state pump source before the present studies. Successfully operating such devices with modest energy from recently developed diode pumped solid-state lasers requires two basic pre-conditions to be fulfilled: firstly high conversion efficiency in frequency up conversion to the UV; and secondly, low threshold for optical parametric oscillation.

In reviewing the UV pumped OPO's which we have demonstrated in the past few years, there are a number of important findings. The first is the demonstration of low pump energy thresholds for the OPO in LBO for both NCPM and CPM geometries, which is significant for the development of both an all-solid-state, highly efficient, temperature tunable coherent blue light source, and a widely angle-tunable OPO in the visible and in the near infrared bands. The second is the demonstration of a OPO pumped at 266 nm, using a type II NCPM geometry in LBO to generate tunable output in the near ultraviolet. The third is the demonstration of narrow inherent linewidths in NCPM geometries, indicating that LBO could be used to build line narrowed OPO devices, especially in the deep blue and UV bands, which is of interest to many research areas. These results give further confidence in the schemes towards which the work in this thesis was directed.

Table 1-1 Performance of some UV pumped optical parametric oscillator

Pump wavelength (μm)	Material	Tuning Range (μm)	Pump Threshold	Characteristics†	Ref.
0.355	KDP	0.96-1.16			[35]
0.35	KDP	0.53 1.06			[36]
0.266	ADP (OPG)††	0.42-0.73		100kW(Peak) 25%, 2ns Line width 5Å	[37]
0.266	ADP	0.458-0.638		Limited by optical damage	[38]
0.347 Single mode	$LiIO_3$(17mm) Cut at 45°	0.415-2.1	1-4MW/cm^2	10kW (peak) 8%, 5ns	[39]
0.355	Urea(12.7mm) 90° Phase match	0.5-0.51 1.17-1.22	4.5mJ, 7ns 0.388MW/cm^2	91kW (peak) 6mw (Average) 20%	[20]
0.355	Urea(23mm) 90° Phase match	0.498-0.640 0.79-1.23	1.4mJ, 7ns	23% Line width 1.2Å	[21]
0.355	BBO(11.5mm) Cut at 30°, Type I	0.45-1.68	8ns 130MW/cm^2	1.4mJ 9.4%	[40]
0.355	BBO(12mm) Cut at 35° and 45° Type I	0.412-2.55	2-5mJ 15-36MW/cm^2	4.7mJ 140mW(Average) 24%	[24]
0.308	BBO(7mm) Cut at 36°, Type I	0.422-0.477	2mJ, 12ns	0.7mJ 10%	[41]
0.266	BBO(20.5mm) Cut at 39.1°, Type I	0.33-1.37	4.5mJ 23MW/cm^2	Limited by optical damage	[25]
0.308 Injection seeded	Urea(15mm) 90° phase match	0.537-0.720	4-5mJ 16-20MW/cm^2	3.8mJ(Signal) 37%	[42]
0.308	Urea	0.537-0.72		11mJ 66%	[22]
0.355	BBO (11.5+9.9mm) Cut at 30.2° and 29.3°	0.42-2.3	1.7mJ 27MW/cm^2	32% Line width 0.3Å with grating	[28]

0.308 Injection seeded	BBO(12mm) Cut at 32°, Type I	0.354-2.37	4.5mJ-10mJ 0.125-0.28J/cm^2 12.5-28MW/cm^2	2mJ 10%	[26]
0.355	BBO(17+10mm) Cut at 37°, Type II	0.48-0.63 0.81-1.36	2.4mJ 38MW/cm^2	12% Line width 0.5-3Å	[43]
0.355	LBO(16.4mm) Cut at 45.4°, Type I	0.54-1.03	2.4mJ 12MW/cm^2	14% at 0.674	[34]
0.355 Injection seeded	LBO(16mm) Type II NCPM	0.480-0.487		12% Line width 0.2Å	[33]
0.355	BBO(10mm) Cut at 29.7°,Type I	0.415-2.411	13mJ 10MW/cm^2	41% 70%*	[27]
0.308	LBO(16mm) Type II, NCPM	0.385	17ns 0.3J/cm^2	40%* at 0.385	[31]
0.266	LBO(16mm) Type II, NCPM	0.314-0.311 1.74-	0.5mJ, 10ns	25%* 7%	[44]
0.355 All solid state scheme	LBO(16mm) Type II, NCPM	0.481-0.457 1.355-1.590	0.42mJ 0.18J/cm^2 15MW/cm^2	50%* 27%	[1]
0.308	LBO(15mm) Cut at 40°, Type I	0.355-0.497 0.809-2.34	17ns 0.45J/cm^2	28%*	[32]
0.355 All solid state scheme	LBO(15mm) Cut at 40°, Type I	0.457-0.666 0.768-1.590	0.3mJ, 10ns	35%*	[45]
0.355 All solid state scheme	LBO(16mm) Type II, NCPM	0.481 1.355	0.19mJ, 10ns 0.6J/cm^2 60 MW/cm^2	50%*	[2]
0.266 All solid state scheme	LBO(16mm) Type II, NCPM	0.314-0.306 1.74-2.03	0.48mJ, 10ns	25%*	[2]

† % figures are conversion efficiency; starred values are internal, others are external.

†† Optical parametric generation only and not oscillation.

1.4 Research programme

The programme of work is outlined in figure (1-4), which is divided into three parts. One part is to construct a diode laser pumped, Q-switched Nd:YAG laser, one is to set up a highly efficient UV pump source using frequency up-conversion techniques, and the last development of OPO itself for tuning in the UV, visible and near infrared bands.

In order to allow the development of frequency up conversion techniques and optical parametric oscillator to proceed from the start of the project, the initial nonlinear optical experiments were carried out using a flashlamp pumped Nd:YAG laser (restricted to low pulse energy operation). The diode laser pumped solid-state laser was developed simultaneously, and subsequently combined with the nonlinear optical devices in the latter stages of the project.

1.5 Thesis outline

The remaining six chapters of this thesis are as follows. Chapter 2 gives the necessary theoretical background for the discussion of the performance of optical parametric oscillators. Chapter 3 reviews nonlinear optical materials suitable for UV pumped OPO's, and then goes on to describe in more detail the properties of the newly developed nonlinear optical material lithium triborate which has been mainly used in these experiments as the OPO gain medium. Chapter 4 gives a description of the pump sources, including the flashlamp and diode pumped Q-switched Nd:YAG lasers, and the doubling, tripling, and quadrupling configurations. Performances are characterised and some results are discussed. Chapter 5 describes the experiments with type II noncritically phase matched LBO OPO's pumped by the 355 nm and 266 nm UV sources. Chapter 6 details the experimental results of the type I critical phase matched LBO OPO pumped at 355 nm. Also the type II critical phase matched LBO OPO is discussed in this chapter. Then in Chapter 7, I briefly describe the conclusions of this project and the possible future investigations. Theoretical considerations in frequency doubling and tripling are briefly discussed in Appendix I. Optical properties of commercially available nonlinear optical materials are summarised in Appendix II, and phase matching in the nonlinear materials of interest are reviewed in Appendix III.

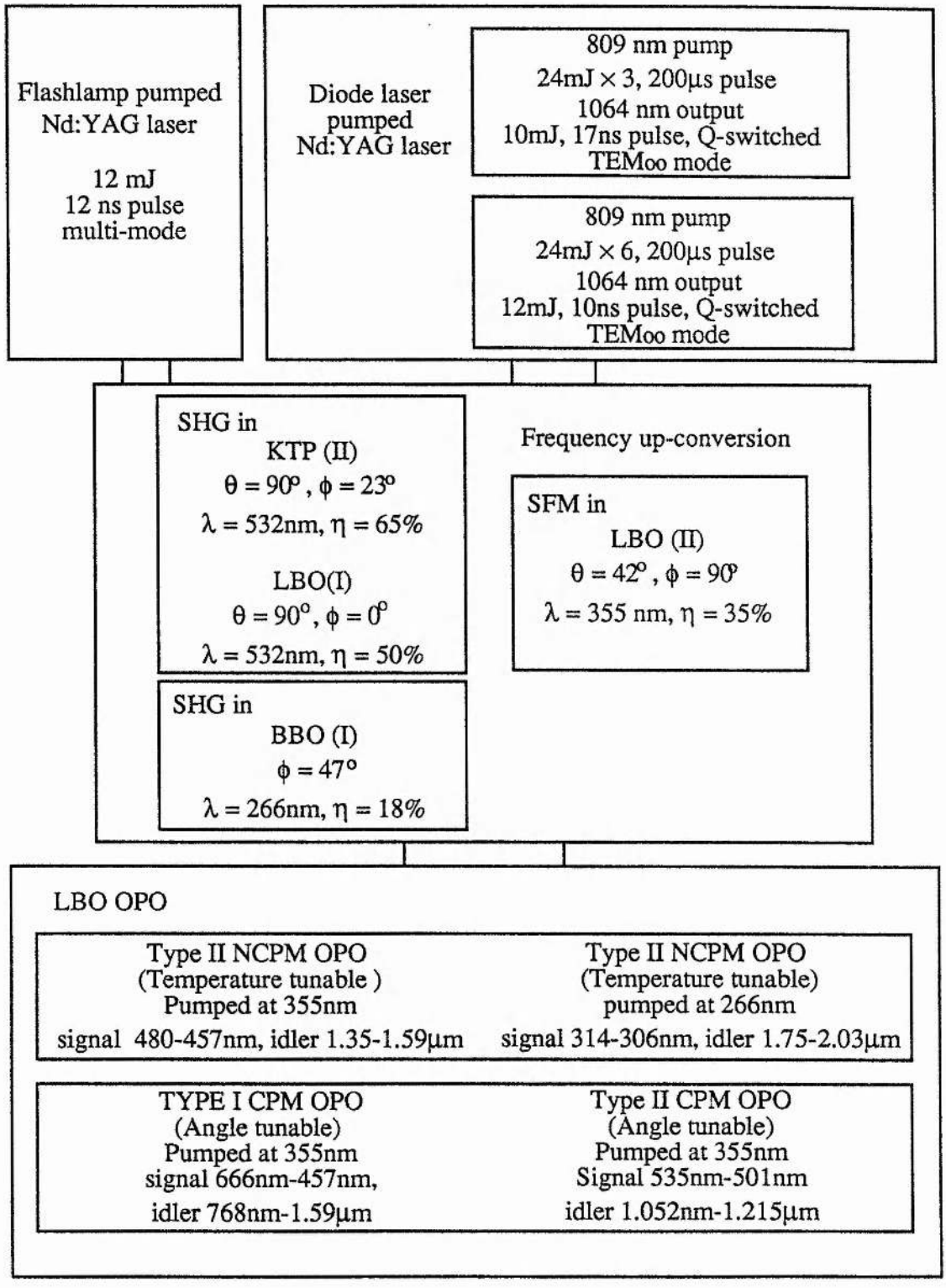

Fig. 1-3 Frame-work of the experiment organisation and some main results.

References

(1) Y. Cui, M. H. Dunn, C. J. Norrie, W. Sibbett, B. D. Sinclair, Y. Tang and J. A. C. Terry
Opt. Lett. **17**(9), 646, 1992

(2) Y. Cui, M. H. Dunn, C. J. Norrie, W. Sibbett, B. D. Sinclair, Y. Tang and J. A. C. Terry
in Conference on Lasers and Electro-Optics (Anaheim, California, USA) OSA Technical Digest Series, **12**, Paper CTuR1, 1992

(3) W. J. Kozlovsky, E. K. Gustafson, R. C. Eckardt, and R. L. Byer
Opt. Lett. **13**(12), 1102, 1988

(4) R. L. Byer
in "Quantum Electronics : a traties", edited by H. Rabin and C. L. Tang, (Acadamic, NewYork) Vol. **1**, Pat B, 587-702, 1975

(5) S. E. Harris
Proc. IEEE **57**(12), 2096, 1969

(6) R. G. Smith
in "Lasers", edited by A. K. Levine and A. J. DeMaria, (Dekker, New York), 189, 1976

(7) R. Pixton
Laser Focus, **14**(7), 66, 1978

(8) R. A. Franken et al
Phys. Rev. Lett. **7**(4), 118, 1961

(9) T. H. Higgins
Laser Focus World **28**(1), 125, 1992

(10) W. Bosenberg, D. Guyer, D. D. Lowenthal and S. E. Moody
Laser Focus World **28**(5), 165, 1992

(11) C. C. Wang and G. W. Racette
Appl. Phys. Lett. **6**(8), 169, 1965

(12) J. A. Giordmaine and R. C. Miler
Phys. Rev. Lett. **14**(24), 973, 1965

(13) R. N. Hall, G. E. Fenner, J. D. Kingsleg, T. J. Soltys, and R. O. Carlson
Phys Rev. Lett. **9**(9), 366, 1962

(14) M. A. Haase, J. Qiu, J. M. Depuydt, and H. Cheng
Appl. Phys. Lett. **59**(11), 1272, 1991

(15) W. Streifer, D. R. Scifres, G. L. Harnagel, D. F. Welch, J. Berger and M. Sakamoto
IEEE J. Quantum Electron. **24**(6), 883, 1988

(16) D. W. Hughes and J. R. M. Barr,
J. Phys. D: Appl. Phys. **25**(4), 563, 1992

(17) M. Sakamoto, J. G. Endriz and D. R. Scifres
IEE Electron. Lett. **28**(2), 197, 1992

(18) T. Y. Fan and R. L. Byer
IEEE J. Quantum Electro. **24**(6), 895, 1988

(19) L. R. Marshall, A. Kaz, R. L. Burnham
in Conference on Lasers and Electro-Optics (Anaheim, California, USA)
OSA Technical Digest Series, **12**, Paper CWQ2, 1992

(20) W. R. Donaldson and C. L. Tang
Appl. Phys. Lett. **44**(1), 25, 1984

(21) M. J. Rosker and C. L. Tang
J. Opt. Soc. Am. B**2**(5), 691, 1985

(22) A. J. Henderson, M. Ebrahimzadeh, and M.H. Dunn
J. Opt. Soc. Am. B**7**(8), 1402, 1990

(23) Chen C. T., Wu B. C., Jiang A. D., and You G. M.
Scientia Sinica(b), **28**, 235, 1985

(24) Y. X. Fan, R. C. Eckardt and R. L. Byer, J. Nolting and R. Wallenstein
Appl. Phys. Lett. **53**(21), 2014, 1988

(25) W. R. Bosenberg, K. L. Cheng and C. L. Tang
Appl. Phys. Lett. **54**(1), 13, 1989

(26) M. Ebrahimzadeh, A. J. Henderson and M.H. Dunn
IEEE J. Quantum Electron. **26**(7), 1241, 1990

(27) Y. P. Wang et al
Appl. Phys. Lett. **58**(14), 1461, 1991

(28) W. R. Bosenberg, W. S. Pelouch and C. L. Tang
Appl. Phys. Lett. **55**(19) 1952, 1989

(29) C. T. Chen, Y. C. Wu, A. D. Jiang, B. C. Wu, G. M. You, R. K. Li, and S. J. Lin
J. Opt. Soc. Am. B**6**(4), 616, 1989

(30) FC CASTECH Inc. Trade Literature on LBO
June 1991

(31) G. Robertson, A. Henderson and M. H. Dunn
Opt. Lett. **16**(20), 1584, 1991

(32) G. Robertson, A. Henderson and M. H. Dunn
Appl. Phys. Lett. **60**(3), 271, 1992

(33) F. Hanson and D. Dick
Opt. Lett. **16**(4), 205, 1991

(34) Z. Y. Xu, D. Q. Deng, Y. P. Wang, B. C. Wu and C. T. Chen
in Conference on Lasers and Electro-Optics (Anaheim, California, USA)
CLEO 1990, OSA Technical Digest Series, Paper CWE6, 1990

(35) Khoklov,
JETP Lett. **3**, 241, 1966

(36) S. A. Akhmanov et al
Modern Optics, **17**, Polytechnic Press. New York, p 343

(37) J. M. Yarborough and G. A. Massey
Appl. Phys. Lett. **18**(10), 438, 1971

(38) R. W. Wallace
IEEE J. Quantum Electron. **7**(6), 307, 1971

(39) G. Nath and G. Pauli
Appl. Phys. Lett. **22**(2), 75, 1973

(40) K. L. Cheng, W. R. Bosenberg and C. L. Tang
Appl. Phys. Lett. **53**(3), 175, 1988

(41) H. Komine
Opt. Lett. **13**(8), 643, 1988

(42) M. Ebrahimzadeh, M. H. Dunn and F. Akerboom
Opt. Lett. **14**(11), 560, 1989

(43) W. R. Bosenberg and C. L. Tang
Appl. Phys. Lett. **56**(19), 1819, 1990

(44) Y. Tang, Y. Cui and M. H. Dunn
Opt. Lett. **17**(3), 192, 1992

(45) Y. Cui, D. E. Withers, C. F. Rae, C. J. Norrie, Y. Tang, B. D. Sinclair, W. Sibbett, and M. H. Dunn
Opt. Lett. **18**(2), 122, 1993

CHAPTER 2

Theoretical background

The nonlinear interaction among three electromagnetic fields has been described by Armstrong et al. in 1962[1] and later by many other authors[2]-[5]. Therefore, the theoretical analysis of three wave interactions in nonlinear optical materials is not discussed in detail in this thesis. However, those aspects of linear and nonlinear optical theory required for the analysis of the nonlinear materials used are summarised here. MKS units were used throughout.

2.1 The optical parametric interaction process

It is well known that when a strong electromagnetic wave propagates through a nonlinear medium, a nonlinear polarisation field is induced. This process lead to many different effects in the optical spectral band, such as second harmonic generation, sum-frequency mixing, and parametric interactions in the case of second order nonlinear effects. The parametric interaction of particular interest here is the following. In this process a strong, high frequency pump wave (frequency ω_p and wave vector $\mathbf{K}_p$) is incident on a nonlinear crystal, and interacts via the nonlinear response of the medium with two lower-frequency electromagnetic waves at ω_s and ω_i ($\omega_s > \omega_i$), which are referred to as the signal and idler waves respectively, where

$$\omega_p = \omega_s + \omega_i \qquad 2\text{-}1$$

and

$$\mathbf{K}_p = \mathbf{K}_s + \mathbf{K}_i \ , \qquad 2\text{-}2$$

$\mathbf{K}_s$ and $\mathbf{K}_i$ being the wave vectors of signal and idler respectively. As a result of this interaction, there is a power flow from the strong pump wave to the weak signal and idler fields. If the nonlinear medium is enclosed within a resonator which is resonant at either the signal or idler wavelengths separately (single resonant) or at both simultaneously (doubly resonant), oscillation can take place. Such a device is known as an optical parametric oscillator, and has been extensively studied both theoretically and experimentally[6]-[11]. It is important that the momentum conservation (i.e. the phase matching) condition given by (2-2) be satisfied for effective operation of the oscillator.

2.2 Phase matching theory and relevant parameters

2.2.1 Phase matching

Deviation from the phase matching condition is measured by the phase mismatching parameter $\Delta\mathbf{K}$, defined by

$$\Delta\mathbf{K} = \mathbf{K}_p - \mathbf{K}_s - \mathbf{K}_i \qquad 2\text{-}3$$

(The condition $\Delta\mathbf{K} = 0$, corresponds to phase matching) The parametric gain is critically dependent on the magnitude of this parameter. As $\Delta\mathbf{K}$ increases, a reduction in gain occurs. Using the relation $\mathbf{K} = k\mathbf{K}_o = (\omega/c)n\mathbf{K}_o$, (2-2) can be written as

$$n_p \cdot \omega_p = n_s \cdot \omega_s + n_i \cdot \omega_i \qquad 2\text{-}4$$

Where n_p, n_s and n_i are the refractive indices at pump, signal and idler wavelengths respectively. From (2-4), we see that phase matching depends on the values of the refractive indices of the material as a function of wavelength.

From crystal optics, it can be shown that for a given wave vector $\mathbf{K}$, in an anisotropic medium, propagation is described by two eigenvectors corresponding to two linearly and orthogonally polarised waves experiencing different refractive

indices[2]-[4]. Using n_a and n_b to represent the refractive indices of the two eigenvectors, and with $n_a < n_b$, from the Fresnel equation[12] we get

$$n_a = \frac{\sqrt{2}}{(-B+(B^2-4C)^{1/2})^{1/2}} \qquad 2\text{-}5$$

$$n_b = \frac{\sqrt{2}}{(-B-(B^2-4C)^{1/2})^{1/2}} \qquad 2\text{-}6$$

where

$$B = [\, -K_x^2 (n_y^{-2} + n_z^{-2}) - K_y^2 (n_x^{-2} + n_z^{-2}) - K_z^2 (n_x^{-2} + n_y^{-2}) \,] \qquad 2\text{-}7$$

$$C = [\, K_x^2 n_y^{-2} n_z^{-2} + K_y^2 n_x^{-2} n_z^{-2} + K_z^2 n_x^{-2} n_y^{-2} \,] \,, \qquad 2\text{-}8$$

where n_x, n_y and n_z are the refractive indices of crystal principal axes, and K_x, K_y and K_z are the cosine vectors of **K** measured relative to the principal optical axes. If we use "θ" to denote the polar angle between **K** and the principal axis z, and ϕ to denote the azimuthal angle from the x axis in the principal plane defined by the x and y axes, then

$$\begin{aligned} Kx &= \sin\theta\cos\phi \\ Ky &= \sin\theta\sin\phi \\ Kz &= \cos\theta \end{aligned} \qquad 2\text{-}9$$

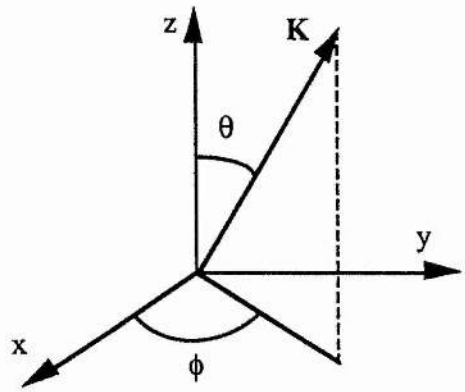

Fig. 2-1 Definitions of the angles θ and ϕ describing the propagation direction of **K** relative to the mutually orthogonal x, y, z axes.

In a normal dispersive and anisotropic medium there exist three possible phase matching process, which are given by

$$n_{p,a} \cdot \omega_p = n_{s,b} \cdot \omega_s + n_{i,b} \cdot \omega_i \qquad 2\text{-}10$$

$$n_{p,a} \cdot \omega_p = n_{s,a} \cdot \omega_s + n_{i,b} \cdot \omega_i \qquad 2\text{-}11$$

$$n_{p,a} \cdot \omega_p = n_{s,b} \cdot \omega_s + n_{i,a} \cdot \omega_i \qquad 2\text{-}12$$

Usually these conditions are called type I, type II, and type III phase matching conditions respectively.

In a uniaxial crystal the indices are such that $n_x = n_y = n_o$ and $n_z = n_e$. If $n_o > n_e$, it is called a negative uniaxial crystal, and if $n_o < n_e$, it is called a positive uniaxial crystal. For both of them one eigenvector of a given wave vector **K** must be an ordinary wave, where the other one is usually an extraordinary wave. The eigen-refractive-indices for both negative or positive uniaxial crystals are listed in table I.

Using table I and the expressions (2-10), (2-11) and (2-12), it can be seen that in a negative crystal, phase matching can in principle be achieved with an extraordinary pump and either one or both of the signal and idler being ordinary wave, whereas in a positive uniaxial crystal the pump must be an ordinary wave, and either the signal or the idler or both of them must be extraordinary.

In a biaxial crystal where $n_x < n_y < n_z$, then for a wave vector with a general propagation direction, both the two eigenvectors may be extraordinary. This is more complicated to analyse. Usually, only the three principal planes are used for phase matching (The following discussions on effective nonlinear coefficient, walkoff angle, and acceptance angle apply only to this condition). In this case only one eigenvector is extraordinary, the other being an ordinary wave. The eigen-refractive-indices for propagation in the principal planes of a biaxial crystal are listed in the table II. From table II and formula (2-10), (2-11), and (2-12), it can be seen that in a biaxial crystal, if a wave vector **K** is orthogonal to the z axis, or the y axis with $\theta < \theta_o$, the phase matching can be achieved in a way similar to a negative uniaxial crystal; while if a wave vector **K** is orthogonal to the x axis, or y axis with $\theta > \theta_o$, the situation is similar to a positive uniaxial crystal. The angle θ_o is defined by

$$\tan \theta_o = \pm \left(\frac{n_y^2 - n_x^2}{n_z^2 - n_y^2} \right)^{1/2} \frac{n_z}{n_x} \quad .$$

Table I Eigen refractive indices of uniaxial crystal

Crystal	n_a	n_b
Negative uniaxial crystal	$\left(\frac{\sin^2\theta}{n_e^2} + \frac{\cos^2\theta}{n_o^2} \right)^{-1/2}$	n_o
Positive uniaxial crystal	n_o	$\left(\frac{\sin^2\theta}{n_e^2} + \frac{\cos^2\theta}{n_o^2} \right)^{-1/2}$

Table II Eigen refractive indices of biaxial crystal

Crystal orientation	n_a	n_b
$\mathbf{K} \perp z$ (**K** is on xy plane)	$\left(\frac{\sin^2\phi}{n_x^2} + \frac{\cos^2\phi}{n_y^2} \right)^{-1/2}$	n_z
$\mathbf{K} \perp x$ (**K** is on yz plane)	n_x	$\left(\frac{\sin^2\theta}{n_z^2} + \frac{\cos^2\theta}{n_y^2} \right)^{-1/2}$
$\mathbf{K} \perp y$ $(\theta < \theta_o^*)$ (**K** is on xz plane)	$\left(\frac{\sin^2\theta}{n_z^2} + \frac{\cos^2\theta}{n_x^2} \right)^{-1/2}$	n_y
$\mathbf{K} \perp y$ $(\theta > \theta_o^*)$ (**K** is on xz plane)	n_y	$\left(\frac{\sin^2\theta}{n_z^2} + \frac{\cos^2\theta}{n_x^2} \right)^{-1/2}$

* The definition of θ_o, please see text.

2.2.2 Effective nonlinear coefficient

For a given phase matching condition the effective nonlinear coefficient is determined by crystal symmetry and the direction of wave propagation within the crystal. The phase matching direction in a crystal should be chosen in such a way as to maximise the value of effective nonlinear coefficient d_{eff}.

Boyd and Kleinman[12] have defined the effective nonlinear coefficient d_{eff} to cover all the cases of three wave interaction processes. In the parametric interaction process this is given by

$$d_{eff} = \sum_{i\xi} U^{(p)}_i \, d(2\omega)_{i\xi} \, (U^{(i)}U^{(s)})_\xi \qquad (i = 1, 2, 3;\ \xi = 1, 2, \text{------}\ 6) \qquad 2\text{-}13$$

where, $d(2\omega)$ is the second order nonlinear polarization tensor of the material; $\mathbf{U}^{(i)}$, $\mathbf{U}^{(s)}$ and $\mathbf{U}^{(p)}$ are the unit vectors of the polarization direction of the electric fields at frequencies ω_i, ω_s and ω_p respectively in the crystal; $U^{(p)}_i$ is the ith component of the $\mathbf{U}^{(p)}$; $(U^{(i)}U^{(s)})_\xi$ is the symmetrized column vector which has the components,

$$(U^{(i)}U^{(s)})_\xi = (U^{(i)}_j U^{(s)}_k + U^{(i)}_k U^{(s)}_j)(1 - \tfrac{1}{2}\delta_{jk}) \qquad (j, k = 1, 2, 3) \qquad 2\text{-}14$$

$\xi = \xi(jk)$ is the condensed notation. The relation between the values of j, k and ξ are given by

ξ :	1,	2,	3,	4,	5,	6,
jk :	11,	22,	33,	23, 32,	13, 31,	12, 21,

δ_{jk} is a delta function.

The unit vectors (cosine vectors) of the electric field of a monochromatic plane wave propagating in the direction **K**, can be easily derived from Maxwell's equations and can be expressed as[13]

$$\cos\alpha = \frac{K_x}{n^2 - n_x^2}\left[\left(\frac{K_x}{n^2 - n_x^2}\right)^2 + \left(\frac{K_y}{n^2 - n_y^2}\right)^2 + \left(\frac{K_z}{n^2 - n_z^2}\right)^2\right]^{-1/2}$$
$$\cos\beta = \frac{K_y}{n^2 - n_y^2}\left[\left(\frac{K_x}{n^2 - n_x^2}\right)^2 + \left(\frac{K_y}{n^2 - n_y^2}\right)^2 + \left(\frac{K_z}{n^2 - n_z^2}\right)^2\right]^{-1/2} \qquad 2\text{-}15$$

$$\cos\gamma = \frac{K_z}{n^2-n_z^2}\left[\left(\frac{K_x}{n^2-n_x^2}\right)^2 + \left(\frac{K_y}{n^2-n_y^2}\right)^2 + \left(\frac{K_z}{n^2-n_z^2}\right)^2\right]^{-1/2}$$

Now the cosine vectors of the electric field of a monochromatic plane wave propagating in the crystal can be written as

$$\mathbf{U}_{\omega_m,i} : \cos(\alpha_{\omega_m,i}),\ \cos(\beta_{\omega_m,i}),\ \cos(\gamma_{\omega_m,i}) \qquad 2\text{-}16$$

where m could be i, s, or p, referring to the frequency ω_i, ω_s, ω_p, and the subscript i could be a or b, referring to the two possible values of the eigen-refractive-index in the propagation direction **K**. The column vector for type I geometry is

$$(\mathbf{U}^{(i)}\mathbf{U}^{(s)}) = \begin{vmatrix} \cos(\alpha_{\omega_i,b})\ \cos(\alpha_{\omega_s,b}) \\ \cos(\beta_{\omega_i,b})\ \cos(\beta_{\omega_s,b}) \\ \cos(\gamma_{\omega_i,b})\ \cos(\gamma_{\omega_s,b}) \\ \cos(\gamma_{\omega_i,b})\ \cos(\beta_{\omega_s,b}) + \cos(\gamma_{\omega_s,b})\ \cos(\beta_{\omega_i,b}) \\ \cos(\gamma_{\omega_i,b})\ \cos(\alpha_{\omega_s,b}) + \cos(\gamma_{\omega_s,b})\ \cos(\alpha_{\omega_i,b}) \\ \cos(\alpha_{\omega_i,b})\ \cos(\beta_{\omega_s,b}) + \cos(\alpha_{\omega_s,b})\ \cos(\beta_{\omega_i,b}) \end{vmatrix} \qquad 2\text{-}17$$

For type II phase matching, the ω_i and ω_s waves are orthogonally polarized and the column vector is

$$(\mathbf{U}^{(i)}\mathbf{U}^{(s)}) = \begin{vmatrix} \cos(\alpha_{\omega_i,a})\ \cos(\alpha_{\omega_s,b}) \\ \cos(\beta_{\omega_i,a})\ \cos(\beta_{\omega_s,b}) \\ \cos(\gamma_{\omega_i,a})\ \cos(\gamma_{\omega_s,b}) \\ \cos(\beta_{\omega_i,a})\ \cos(\gamma_{\omega_s,b}) + \cos(\beta_{\omega_s,b})\ \cos(\gamma_{\omega_i,a}) \\ \cos(\alpha_{\omega_i,a})\ \cos(\gamma_{\omega_s,b}) + \cos(\alpha_{\omega_s,b})\ \cos(\gamma_{\omega_i,a}) \\ \cos(\alpha_{\omega_i,a})\ \cos(\beta_{\omega_s,b}) + \cos(\alpha_{\omega_s,b})\ \cos(\beta_{\omega_i,a}) \end{vmatrix} \qquad 2\text{-}18$$

For both type I and type II

$$\mathbf{U}^{(p)} = \left|\cos(\alpha_{\omega_p,a})\ \cos(\beta_{\omega_p,a})\ \cos(\gamma_{\omega_p,a})\right| \qquad 2\text{-}19$$

2.2.3 Double refraction and walkoff angle

The optimum phase matching directions for an optical parametric processes can be determined from the calculations of the phase matching angle and the effective nonlinear coefficient. However, double refraction will prevent full use of the nonlinear optical properties of a crystal, because for a plane wave the direction of the wave vector and the Poynting vector do not generally coincide inside the crystal. In this case the energy of the generated wave walks off at a finite angle from that of the incident wave, limiting the effective volume over which efficient interaction of the three waves may take place.

In an anisotropic medium, for an extraordinary wave there is an angle of deviation ρ, called the double refraction angle, between the Poynting vector **S** and the wave propagation direction **K**, and also between the electric field **E** and the electric displacement vector **D**. The value of ρ depends on the birefringence of the materials, the frequencies and the propagation directions of the interaction waves. The relation between **E**, **D**, **K**, and **S**, is shown in figure (2-2), where, all the four vectors are in the same plane and are orthogonal to the magnetic field **H**.

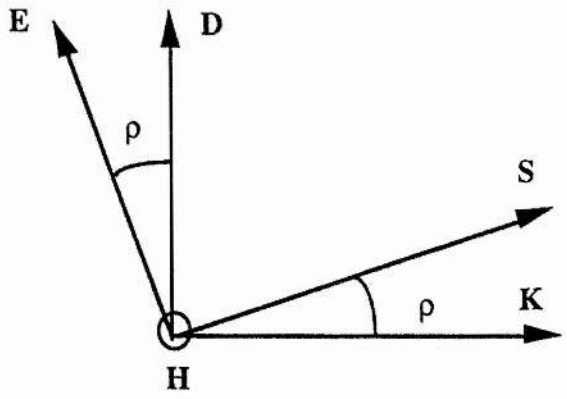

Fig. 2-2 Relation between the wave propagation direction **K** and the Poynting vector **S**, and between the electric field **E** and electric displacement vector **D** in an anisotropic medium.

It is clear from figure (2-2), the double refractive angle ρ is generally

$$\tan \rho = \frac{\mathbf{E_o} \cdot \mathbf{K_o}}{\mathbf{E_o} \cdot \mathbf{D_o}} \quad , \qquad 2\text{-}20$$

where $\mathbf{E}_o$, $\mathbf{D}_o$ and $\mathbf{K}_o$ are the unit vectors of **E**, **D**, and **K** respectively. Starting from Maxwell's equation, and after a few steps of derivation, we can get[14]

$$\tan \rho = \frac{\mathbf{E}_o \cdot \mathbf{K}_o}{\mathbf{E}_o \cdot \mathbf{D}_o} = n^2 \left[\left(\frac{K_x}{n^{-2}-n_x^{-2}}\right)^2 + \left(\frac{K_y}{n^{-2}-n_y^{-2}}\right)^2 + \left(\frac{K_z}{n^{-2}-n_z^{-2}}\right)^2 \right]^{-1/2} , \quad 2\text{-}21$$

where n is the refractive index in the direction $\mathbf{K}_o$ given by (2-5) and (2-6), and n_x, n_y and n_z are the refractive indices of the principal axes. This allows the calculation of the double refraction angle ρ between the energy flow and the direction of the wave propagation $\mathbf{K}_o$ (K_X, K_y, K_Z).

In the parametric interaction processes, the maximum angle w overall between the Poynting vector associated with the three waves is called the walkoff angle. By the calculation (2-21) we know that, if two eigenwaves at frequencies ω_1 and ω_2 have same polarisation direction, then the high frequency eigenwave has a bigger double refraction angle ρ than the low frequency eigenwave. Therefore, in a uniaxial crystal, or in a biaxial crystal in which the pump wave propagates with the restricted conditions given by section (2.2.1) i.e. the pump wave polarisation is orthogonal to any one of the principal axes, one eigenwave vector must be ordinary and the walkoff angle will be the double refraction angle of the extraordinary eigenwave with the highest frequency. In a biaxial crystal, if the pump wave vector is not orthogonal to any of the principal axes, then all three eigenwave vectors will be extraordinary, and there will be three double refraction angles. The Poynting vectors associated with signal and idler waves lie in the plane containing the wavevectors **K** (all collinear), and the pump Poynting vector lies in a plane orthogonal to this plane but also containing **K** (see figure (2.3)). The walkoff angle w is defined as biggest angle difference between the energy flow's unit vectors, they are lie in two orthogonal planes which intersect in the propagation's unit vector $\mathbf{K}_o$. For an example figure (2-3) shows the relations between double refraction angles under the type I phase matching conditions. In this case the walkoff angle w is given by

$$\cos w = \cos\rho_{pa} \cdot \cos\rho_{sb} \qquad 2\text{-}22$$

The detailed behaviour of wave propagation in a nonlinear biaxial crystal has been thoroughly discussed in reference [15].

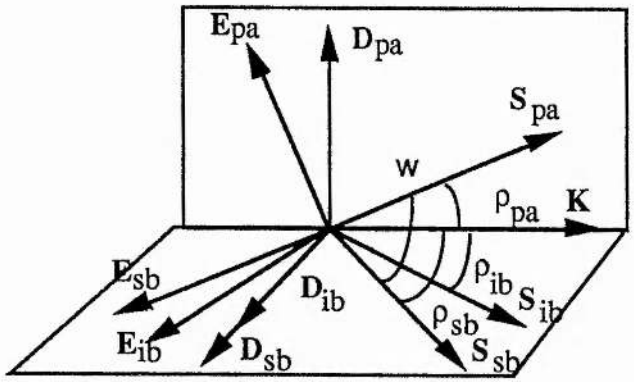

Fig. 2-3 The double refractive walkoff angle in the biaxial crystal (type I geometry) when the pump wave vector is not orthogonal to any of the principal axes.

2.2.4 Acceptance angle and temperature bandwidths

An important parameter in relation to the application of nonlinear optical materials is the acceptance bandwidth, which gives the allowable variation of the pump wavelengths, the pump beam propagation directions, and the temperature of the nonlinear medium.

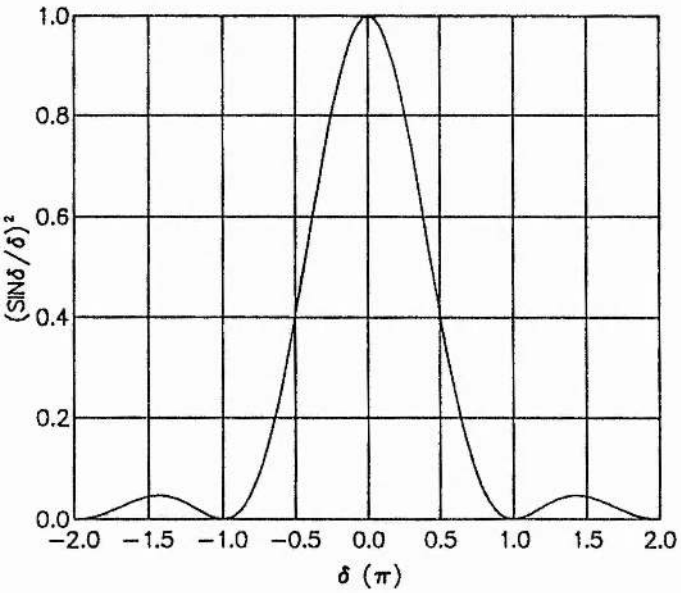

Fig. 2-4 The function $\mathrm{sinc}^2(\delta)$, where $\delta = \frac{1}{2}\Delta kL$.

It is well known that in the three wave parametric interaction processes (in the plane wave approximation) the small signal parametric gain is directly proportional to the function $\text{sinc}^2(\frac{1}{2}\Delta kL)$, which shown in figure (2-4). In practice there are two definitions of the acceptance bandwidth. One is based on the maximum allowable wave vector mismatch being $\Delta k = \pm \pi/L$[16][17], at which the conversion efficiency drops to approximately 0.4 ($\text{sinc}^2(\frac{1}{2}\Delta kL) = 0.4$) that of the peak conversion efficiency. The other definition is based on the maximum allowable wave vector mismatch being $\Delta k = \pm 2\pi/L$, at which the conversion efficiency drops to zero. We prefer to use the second definition throughout our analysis, and the calculation of the angular and temperature acceptance bandwidths are based on this basic definition. (The spectral acceptance bandwidth is not discussed in this thesis.) Assuming α is the most significant parameter determining Δk in a specific case, and that the optimum phase matching is at $\alpha = \alpha_o$, then expanding Δk in a Taylor series at $\alpha = \alpha_o$ we obtain.

$$\Delta k = \Delta k|_{\alpha=\alpha_o} + \frac{d\Delta k}{d\alpha}|_{\alpha=\alpha_o}\,\delta\alpha + \frac{1}{2}\frac{d^2\Delta k}{d\alpha^2}|_{\alpha=\alpha_o}\,(\delta\alpha)^2 + \text{---} = \pm\frac{2\pi}{L} \qquad 2\text{-}23$$

The parameter α could be the phase matching angle θ or ϕ, or the phase matching temperature T. Normally expansion to second order in the Taylor series gives sufficient resolution for most applications. Therefore, the remaining problem is how we solve this quadratic equation. It is necessary to mention that acceptance bandwidths are calculated individually assuming optimum values of the other parameters.

Angular acceptance

The angular acceptance is defined as the planar angle over which the magnitude of the wave vector mismatch for the parametric generation process is no greater than $2\pi/L$. Since two angles are needed to specify the direction of propagation with respect to the crystallographic axes, two acceptance angle will be defined. For sake of simplicity, the wave vector mismatch will be expanded as a function of one angle at a time. In other words we consider $\delta\theta$ and $\delta\phi$ individually .

As an example, in order to define an acceptance angle in the θ direction, a Taylor Series may be written as

$$\Delta k = \Delta k|_{\theta=\theta_o} + \frac{d\Delta k}{d\theta}|_{\theta=\theta_o}\,\delta\theta + \frac{1}{2}\frac{d^2\Delta k}{d\theta^2}|_{\theta=\theta_o}\,(\delta\theta)^2 = \pm\frac{2\pi}{L} \qquad 2\text{-}24$$

It is easy to see that the first term of this expansion is zero when the angle θ is equal to the optimum phase matching angle θ_o, and the solution is then

$$\delta\theta_i = \{ -\frac{d\Delta k}{d\theta} \pm \left(\left(\frac{d\Delta k}{d\theta}\right)^2 + 4 \frac{d^2\Delta k}{d\theta^2} \frac{\pi}{L} \right)^{1/2} \} / \left(\frac{d^2\Delta k}{d\theta^2} \right) \qquad 2\text{-}25$$

$$i = 1,\ 2 \ (\text{at } \theta = \theta_o)$$

$$\delta\theta = \min (\delta\theta_1, \delta\theta_2)$$

Generally in the non-critical phase matching case, the first order term is negligible, because the phase matching angle is at either zero or ninety degrees. Hence the acceptance angle can be written as

$$\delta\theta = 2 \{ \left(\frac{\pi}{L}\right) / \left(\frac{d^2\Delta k}{d\theta^2} \right) \}^{1/2} \qquad (\text{at } \theta = \theta_o) \qquad 2\text{-}26$$

In the critical phase matching situation the first order term is normally much bigger than the second order term, which can therefore be neglected. Much of the data given in the literature, particularly for critically phase matched SHG, is based on this approximation. In this case the acceptance angle is given by

$$\delta\theta = \left(\frac{2\pi}{L}\right) / \left(\frac{d\Delta k}{d\theta}\right) \qquad (\text{at } \theta = \theta_o) \qquad 2\text{-}27$$

Now we can by using the definitions of Δk and θ and taking the derivatives of the functions B (2-7) and C (2-8) with respect to θ given in section (2.2.1), now we can solve for $\frac{d\Delta k}{d\theta}$, and hence obtain solutions for $\delta\theta$.

Temperature acceptance

Different nonlinear optical materials possess different thermal sensitivities, measured by the parameter $\frac{dn}{dT}$ (called the temperature dependence of refractive index). For a temperature change ΔT from the optimum phase matching temperature T_o($T = T_o + \Delta T$), the change Δk is given by

$$\Delta k = \frac{d\Delta k}{dT}\Big|_{T=T_o} \delta T + \frac{1}{2}\frac{d^2\Delta k}{dT^2}\Big|_{T=T_o} (\delta T)^2 + \text{------} \qquad 2\text{-}30$$

The temperature acceptance band width is defined as that change δT leading to a value for Δk of $\pm 2\pi/L$. So that, from (2-30) we obtain

$$\delta T = \{ -\frac{d\Delta k}{dT} \pm \left(\left(\frac{d\Delta k}{dT} \right)^2 + 2\frac{d^2\Delta k}{dT^2}\frac{\pi}{L} \right)^{1/2} \} / \left(\frac{d^2\Delta k}{dT^2} \right) \qquad 2\text{-}31$$

$$i = 1,\ 2 \quad (\text{at } T = T_o)$$

$$\delta T = \min (\delta T_1, \delta T_2)$$

The first-order approximation is

$$\delta T = \left(\frac{2\pi}{L}\right) / \left(\frac{d\Delta k}{dT}\right)$$

In most cases $\left(\frac{dn}{dT}\right)$ is nearly a constant and is independent of the pump wavelength, so that the above may be simplified to

$$\delta T = \frac{1}{L} / \left(\frac{1}{\lambda_p}\frac{dn_p}{dT} - \frac{1}{\lambda_s}\frac{dn_s}{dT} - \frac{1}{\lambda_i}\frac{dn_i}{dT} \right) \qquad 2\text{-}32$$

Therefore, δT can be found readily, provided that the $\left(\frac{dn}{dT}\right)$'s are known.

Recently as the result of precise measurement of refractive indices of the new nonlinear materials, accurate Sellmeier equations have been deduced for them, and this information has now been widely published in the literature. It is now possible to calculate refractive indices to 1 part in 10^{+5}[18]. Such information is required to evaluate the above expressions in specific situations. Detailed information and calculations for the materials of interest here are given in Appendices II and III.

2.3 Parametric gain and pump threshold

We now consider parametric gain and pump powers necessary to reach oscillation threshold. Generally, obtaining low thresholds enable high conversion efficiencies to be reached.

In a singly resonant optical parametric oscillator, when a signal frequency at ω_s is incident on the parametric gain medium, the single pass power gain is[11]

$$G(L) = \frac{|E_s(L)|^2}{|E_s(0)|^2} - 1 = \Gamma^2 L^2 \frac{\sinh^2(gL)}{(gL)^2} \qquad 2\text{-}33$$

where

$$\Gamma^2 = 2\omega_i\omega_s d_{eff}^2 I_p / n_i n_s n_p \varepsilon_o c^3 \quad , \qquad 2\text{-}34$$

$$g^2 = \Gamma^2 - (\frac{\Delta K}{2})^2 \quad . \qquad 2\text{-}35$$

I_p is the pump power intensity, ε_o is the permittivity of free space, and c is the speed of light in vacuum. For the small gain and perfect phase matching ($\Delta K = 0$) case, the gain is thus $\sinh^2(\Gamma L)$, and can be approximated as $\Gamma^2 L^2$. As in a laser oscillator, threshold is reached when the parametric gain equals the loss, namely

$$\Gamma^2 L^2 = \delta_s \quad , \qquad 2\text{-}36$$

where δ_s is the round-trip power loss of the signal wave. The pump power required to reach threshold is then

$$\frac{\delta_s}{P_{th}} = \pi K_o L^2 \quad , \qquad 2\text{-}37$$

Where K_o is defined as

$$K_o = \frac{2\omega_i\omega_s d_{eff}^2}{\pi\varepsilon_o n_i n_s n_p c^3} \quad (W^{-1}) \qquad 2\text{-}38$$

However, this is a simple analysis for the plane wave approximation. In practice, there are many options and conditions, for instance, considering the nonlinear medium geometry, there are both type I and type II phase matching, and both CPM and NCPM etc. An optimisable parameter for the three wave interaction process is the focusing. An optimised focusing parameter can be selected, which significantly reduces the pump threshold and increases the conversion efficiency. But, an accompanying problem is crystal damage. It is clear that there is a watershed in the theoretical analysis. If the available pump energy or power is high enough then optical parametric oscillation does

not require tight focusing, in this case it is appropriate to use the plane wave approximation; if the available pump energy or power is not adequate, and optical parametric oscillation requires resort to tight focusing of the pump wave to reach the pump threshold, then we use the Boyd and Kleinman theory. However, here the limiting condition is crystal damage.

Boyd and Kleinman (1968)[12] have shown that the pump power threshold of second harmonic generation, sum-frequency mixing and optical parametric oscillation can be accurately described as a function of two parameters. One is the focusing parameter ξ, which is defined as the radio of the crystal length L to the confocal beam parameter b in the crystal, namely

$$\xi = \frac{L}{b} \qquad 2\text{-}39$$

For Gaussian beam profiles the confocal parameter is given in terms of the beam waist w_o as follows

$$b = 2z_o = kw_o^2 = \frac{2\pi n}{\lambda} w_o^2 \qquad 2\text{-}40$$

The other parameter is the walkoff parameter B. In the optical parametric oscillator, this is defined by

$$B = \frac{\rho}{2} (Lk)^{1/2} \left(\frac{n_p}{n_o}\right)^{1/2} \qquad 2\text{-}41$$

where

$$n_o = \frac{1}{2} (n_s + n_i) \qquad 2\text{-}42$$

and ρ is defined as the double refraction walkoff angle. For a given pump beam waist w_o, this walkoff limits the effective nonlinear interaction length in the crystal.

The original Boyd and Kleinman theory is valid in situations involving: CW pumping, doubly resonant oscillation of signal and idler wavelengths, and operation near degeneracy. Another assumption in the theory was that pump, signal and idler beam shared the same confocal parameter, and the consequences of them having different confocal parameters was not investigated. Following Boyd and Kleinman,

Fischer et al (1977)[19] first theoretically derived the threshold conditions for singly resonant OPO's with tightly focused pumps. However in their derivations the other assumptions are exactly the same as the Boyd and Kleinman's, including the condition of pump and signal sharing the same confocal parameter. In 1982, Guha, Wu and Falk theoretically extended the analysis to express the consequences of unequal confocal parameters[20]. Their conclusion was that lower thresholds can be generally achieved with unequal confocal parameters. They developed Boyd and Kleinman's theory, and derived singly resonant and doubly resonant OPO threshold formulae with unequal confocal parameters. Their results can be used to describe steady-state operation of pulsed, as well as CW optical parametric oscillators.

Consider an interaction under conditions of type I phase matching, where the pump is an extraordinary ray and signal and idler are ordinary rays then the reciprocal pump threshold can be written as

$$\frac{\delta_s}{P_{th}} = K\, L\, h(\xi, B) \qquad 2\text{-}43$$

where

$$K = K_o\, L\, k_{ps} \quad , \quad (W^{-1}) \qquad 2\text{-}44$$

$$k_{ps} = \frac{k_p k_s}{k_p + k_s} \quad , \qquad 2\text{-}45$$

and $h(\xi,B)$ is a function containing all of the dependence of the generated signal upon the optimisable parameters[12][20]. The $h(\xi,B)$ function can be numerically calculated using a computer. In the general case, Guha's results shows that $h(\xi,B)$ is maximised with unequal confocal parameters and that for certain values of ξ_p and ξ_s, $h(\xi,B)$ can be increased appreciably over its value for $\xi_p = \xi_s$. For example if $\xi_p = 0.1$, $h(\xi,B)$ is increased by nearly a factor of two if the signal focusing parameter is increased from 0.1 to 0.5.

A theoretical derivation of the OPO threshold conditions for a type II phase matching geometry with a tightly focused pump has not appeared in the literature. However, a few papers have discussed type II second harmonic generation using Boyd and Kleinman's theory[21][22]. Deriving the optimum threshold condition for a type II phase matching geometry is more complicated than the type I situation. Since now in the general case two double refraction angles result. Fortunately in most OPO cases, the pump wave propagation in the nonlinear crystal is parallel or orthogonal to a crystal

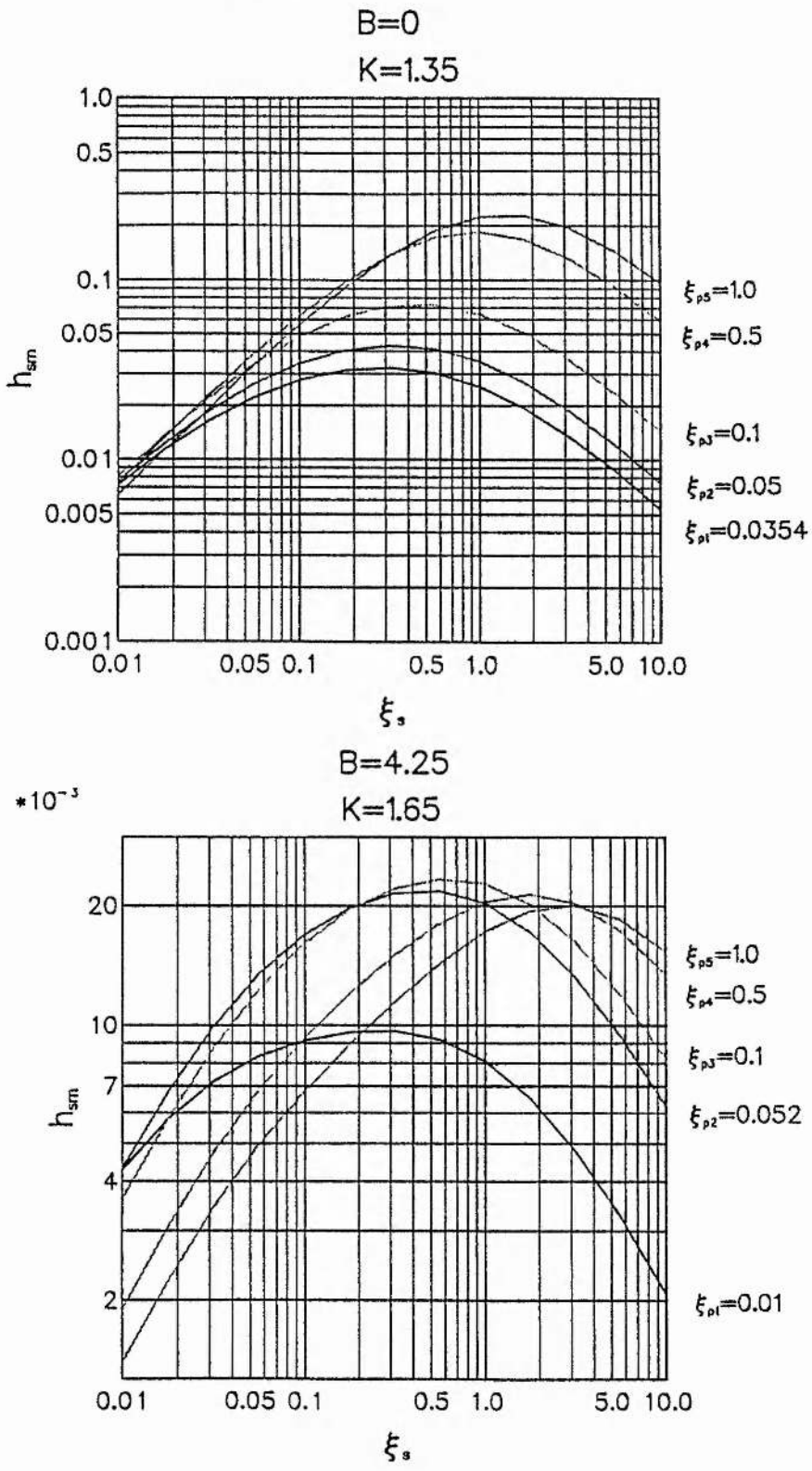

Fig. 2-5 Theoretical calculation results of the optimized h_m curve as a function of signal focussing parameter ξ_s under the different conditions of $k = k_p/k_s$ and ξ_p.

principal axis, so that one or other of the signal/idler waves is an ordinary wave. Further in the non-critical phase matching geometry, the Poynting vector walkoff is eliminated (B=0). In this case the type I and type II geometries have the same optimised universal h_m curve. Following Guha, Wu and Falk, we have predicted the optimum h_m curves suitable for our situations (see figure (2-5)), where $k = k_p/k_s = 1.35$, $B = 0$, for noncritical phase matching geometry, and $k = k_p/k_s = 1.65$, $B = 4.25$ for type I ($e \rightarrow o + o$) critical phase matching geometry. These curves can be used to calculate the steady state pump threshold, the optimum crystal length, the optimum pump beam spot size, and the optimum signal wave spot size in the OPO cavity, the latter determining the optimum radius of curvature of the OPO cavity mirrors. These aspects we will fully discuss in the following chapters.

2.4 Conversion efficiency

The power conversion efficiency in an optical parametric oscillator can be considered in a similar way to the analysis of pump threshold, namely for either uniform-plane waves or Gaussian beams. These also have been discussed by many authors[10][11][23]-[27]. For simplicity, some conclusions which are useful to illustrate our experimental results are summarised below.

Let I_p be the incident pump intensity, I_{th} be the oscillation threshold intensity, I_p' be the intensity of pump beam transmitted through the oscillator, and I_s and I_i be the intensities of the signal and idler beams respectively. For the singly resonant optical parametric oscillator, we have

$$I_s + I_i = I_p - I_p' \qquad 2\text{-}46$$

The internal conversion efficiency, or pump depletion, defined as the fraction of the pump power/intensity going into the signal and idler fields, is given by

$$\eta_{int} = \frac{P_s+P_i}{P_p} = 1 - \frac{I_p'}{I_p} \quad , \qquad 2\text{-}47$$

where P is defined as pump power, and the subscripts are defined in a similar way to those for intensity I. P or I can be obtained by solving the coupled wave equations with given boundary conditions. For the singly resonant optical parametric oscillator

under steady-state conditions and for the plane-wave, the internal conversion efficiency is given by

$$\eta_{int} = [\ 1 - (\frac{\Delta k}{2\beta})^2\ ] \sin^2(\beta L) \quad , \qquad 2\text{-}48$$

where β is defined by

$$\frac{\sin^2(\beta L)}{(\beta L)^2} = \frac{P_{th}}{P_p} \frac{\sin^2(\Delta k L/2)}{(\Delta k L/2)^2} \quad , \qquad 2\text{-}49$$

for $I_p > I_{th}$ (when $I_p < I_{th}$, of course, $I_p' = I_p$). In the case of perfect phase matching, where Dk = 0, the above equations reduce to the following

$$\eta_{int} = \sin^2(\beta L) \qquad 2\text{-}50$$

and

$$\frac{\sin^2(\beta L)}{(\beta L)^2} = \frac{I_{th}}{I_p} \qquad 2\text{-}51$$

The Gaussian beam solution is obtained by integration of (2-50), subject to (2-51), over the pump beam cross section, thus,

$$\frac{P'}{P_p} = \frac{P_{th}}{P_p} + \int_0^{\ln(P/Pth)} e^{-x} \cos^2(\beta L) dx \quad , \qquad 2\text{-}52$$

where

$$\frac{\sin^2(\beta L)}{(\beta L)^2} = \frac{P_{th}}{P_p} e^x \quad . \qquad 2\text{-}53$$

Equations (2-50) - (2-53) were solved by Kreuzer[23] and Bjorkholm[24] by numerical integration on a computer. The results showed that for a uniform plane-wave pump, total depletion and 100 percent conversion efficiency occurs for $P_p/P_{th} = (\pi/2)^2$, while for a Gaussian pump beam, maximum efficiency is about 71 percent and occurs for $P_p/P_{th} = 6.5$.

The external efficiency for the non-resonant wave is given by the frequency ratios times the internal efficiency, which is

$$\eta_{ext} = \frac{\omega_{(non\text{-}resonated)}}{\omega_p} \eta_{int} \qquad 2\text{-}54$$

and for the resonant wave which is

$$\eta_{ext} = \frac{\omega_{(resonated)}}{\omega_p} \frac{T_r}{T_r+\delta_s} \eta_{int} \quad , \qquad 2\text{-}55$$

where T_r is the resonated wave output coupling loss and δ_s is the total parasitic round trip loss for this wave.

In practice, the conversion efficiency of the optical parametric oscillator is generally limited by other restrictions. One is the pump beam quality, since conversion efficiency can be markedly decreased if the pump beam optical quality is non-uniform. The other is the build-up time of the coherent resonated wave power. In pulsed operation, the steady-state condition is achieved only after a finite build up time. Thus the energy conversion efficiency is less than the power conversion efficiency by approximately that fraction of the pumping time that the oscillator is below threshold. Detailed discussion can be found in the given references[11][25][27].

2.5 Frequency tuning

Frequency tuning is an important feature of the optical parametric oscillator. The OPO tuning range is dependent upon the crystal's transparency range, phase matching conditions and the variation of the effective nonlinear coefficients with angle. The tuning rate is much more critically dependent upon the crystal birefringence. There are many frequency tuning methods. The most popular are temperature and angular variation of the extraordinary eigen-refractive-index. We already know from section (2.2) that using the Sellmeier equation and the phase matching theory we can predict OPO tuning curves. But in some cases comparison of the tuning rate may be necessary, particularly in the case where linewidth and frequency stability need be considered.

If ζ denotes any variable which may be used to vary the refractive index, and if we assume the pump frequency is fixed, then for collinear phase matching the rate of signal frequency tuning with ζ is given by

$$\frac{d\omega_s}{d\zeta} = \frac{1}{s}\left(\frac{d\Delta k}{d\zeta}\right) \qquad 2\text{-}56$$

where

$$s = \frac{dk_s}{d\omega_s} - \frac{dk_i}{d\omega_i} \qquad 2\text{-}57$$

Which is called the dispersive constant[28]. The half-power gain linewidth was shown to be determined approximately by the condition $|\Delta kL| = 2\pi$. Noting that $\Delta\omega_i = -\Delta\omega_s$, then $\Delta k = s\Delta\omega_i$. Thus the full half-power gain linewidth in Hz is

$$\Delta\nu = \frac{1}{sL} \qquad 2\text{-}58$$

From these formulae it is seen that materials with small s in general have large tuning rates, but correspondingly large linewidths. Also, near degeneracy where the linewidth of an oscillator is large, it will in general, tune much more rapidly than when far from degeneracy[9].

References

(1) J. A. Armstrong, N. Bloembergen, J. Ducuing, and P. S. Pershan
Phys. Rev. B**127**(6), 1918, 1962

(2) Max Born and Emil Wolf
"Principles of Optics : Electromagnetic Theory of Propagation, Interference and Diffraction of Light"
Pergamon Press, Oxford, 1965

(3) H. Rabin and C. L. Tang
"Quantum Electronics : A Treatise, Vol. 1 Nonlinear Optics"
Academic Press, New York, 1975

(4) A. Yariv and P. Yeh
"Optical Waves in Crystals : Propagation and Control of Laser Radiation"
New York, 1984

(5) Y. R. Shen
"The Principles of Nonlinear Optics"
New York, 1984

(6) W. H. Louisell, A. Yariv and A. E. Siegman
Phys. Rev. **124**(6), 1646, 1961

(7) C. C. Wang and G. W. Racette
Appl. Phys. Lett. **6**, 169, 1965

(8) J. A. Giordmaine and R. C. Miller
Phys. Rev. Lett. **14**, 973, 1965

(9) S. E. Harris
Proc. IEEE **57**, 2096, 1969

(10) R. G. Smith
in "lasers", edited by A. K. Levine and A. J. DeMariar
Vol. 4, Marcel, Dekker, New York 1976

(11) R. L. Byer
in "Quantum Electronics : A Treatise", edited by H. Rabin and C. L. Tang
(Acadamic, NewYork) Vol. **1**, Part B, 587-702, 1975

(12) G. D. Boyd and D. A. Kleinman
J. Appl. Phys. **39**, 3597, 1968

(13) B. Wyncke and F. Brehat
J. Phys. B : At. Mol. Opt. Phys. **22**, 363, 1989

(14) F. Brehat and B. Wyncke
J. Phys. B : At. Mol. Opt. Phys. **22**, 1891, 1989

(15) T. A. Maldonado and T. K. Gaylord
Appl. Opt. **30**, 2465, 1991

(16) N. P. Barnes and V. J. Corcoran
Appl. Opt. **15**, 696, 1976

(17) J. Q. Yao and T. S. Fahlen
J. Appl. Phys. **55**, 65, 1984

(18) D. Eimerl
Ferroelectrics, **72**, 95, 1987

(19) R. Fischer, C. Tran-ba' and L. W. Wieczorek
Sov. J. Quantum Electron. **7**, 1455, 1977

(20) S. Guha, F. J. Wu, and J. Falk
IEEE J. Quantum Electron. **18**, 907, 1982

(21) Jean-Jacques Zondy
Opt. Commun. **81**, 427, 1991

(22) K. Asaumi
Appl. Phys. B. **54**, 265, 1992

(23) L. B. Kreuzer
in"Proc. Joint Conf. on Lasers and Opto-electronics",
(Univ. of Southampton, IERE, London), 53, 1969

(24) J. F. Bjorkholm
IEEE J. Quantum Electron. QE-**7**, 109, 1971

(25) J. E. Pearson, U. Ganiel and A. Yariv
IEEE J. Quantum Electron. QE-**8**, 433, 1972

(26) T. F. Ewanizky
IEEE J. Quantum Electron. QE-**14**, 962, 1978

(27) S. J. Brosnan and R. L. Byer
IEEE J. Quantum Electron. QE-**15**, 415, 1979

(28) R. L. Byer and S. E. Harris
Phys. Rev. **168**, 1064, 1968

CHAPTER 3

Nonlinear optical materials

Recently new developments in nonlinear optical materials such as the discovery and development of $KNbO_3$ (KN), $KTiOPO_4$ (KTP), β-BaB_2O_4 (BBO), LiB_3O_5 (LBO) etc, have given investigators much choice in selecting a nonlinear optical material for their applications. This has greatly invigorated the field of nonlinear optics in general, and optical parametric oscillator in particular. However, these nonlinear materials have many different features such that some are better suited to a particular application than others. The task of the optical designer is to strike a balance between the physical limitations of the crystal and the demands of the application.

3.1 Figure of merit of a material

In attempting to classify the many materials available for specially designed applications it is imperative that materials be compared with well defined terms of reference. Defining a figure of merit based on relevant nonlinear optical parameters is a convenient method for choosing a material. This allows a semi-quantitative comparison to be made of the gain available from different crystals, without resort to complicated calculations. General considerations of figures of merit have normally been based on frequency conversion efficiency in SHG, where we have $\eta_{SHG} \propto M$ (figure of merit), and have been discussed by many authors[1]. The actual form most commonly used is

$$M \text{ (figure of merit)} = d_{eff}^2/n_1n_2n_3 \qquad 3 - 1$$

However, this figure of merit formula does not address all the issues. In addition to the effective nonlinear coefficient, the following parameters are also important in comparing crystals, normally the crystal damage power threshold, the available maximum crystal length and the double refractive walkoff angle etc. In some cases, comprehensively considering these parameters together and stressing a particular parameter is very useful. Based on the above considerations we have defined three different figures of merit and we now discuss there.

In the last chapter we mentioned that if the pump power is high enough, so that focusing is not required, then theoretically we can use the plane wave approximation. In this case the parametric gain coefficient can be written as

$$G = \Gamma^2 L^2 = \frac{2\omega_1\omega_2 d_{eff}^2 L^2}{n_1 n_2 n_3 \varepsilon_o c^3} I_p$$
$$= \left(\frac{8\pi^2}{\varepsilon_o c}\right)\left(\frac{d_{eff}^2 L^2}{n_1 n_2 n_3 \lambda_1 \lambda_2} I_p\right) \qquad 3-2$$

If we further assume that the available pump intensity is high enough, so as to approach the crystal damage threshold, then using I_D to represent this parameter, the second part of the right hand side of formula (3-2) can be used to defined a crystal damage limited figure of merit, which is

$$M \text{ (figures of merit)} = \frac{d_{eff}^2 L^2}{n_1 n_2 n_3 \lambda_1 \lambda_2} I_D \qquad 3-3$$

Where L represent the available crystal length. In this case a crystal with a high optical damage threshold is generally considered to be superior. However, the material's figure of merit as defined above does not depend on this parameter only. For example, LBO has a high damage threshold (~10 GW/cm^2) which is twice that of BBO's (~5 GW/cm^2), but, if we consider both crystals used under similar conditions, due to BBO's larger effective nonlinear coefficient, the figure of merit of BBO is larger than LBO's (please see table (3-1)).

If we take into account the effect of walkoff, then using the simple relations given by

$$A = \pi w_o^2$$
$$w_o \approx \rho L \quad , \qquad 3-4$$

the figure of merit formula (3-3) can be rewritten as

$$M \text{ (figures of merit)} = \frac{d_{eff}^2}{\pi\rho^2 n_1 n_2 n_3 \lambda_1 \lambda_2} P_p \quad , \qquad 3 - 5$$

where P_p is assumed to be the available pump power. The formula (3-5) is the walkoff limited figure of merit. In this case the crystal length for a given pump beam radius is restricted by the walkoff angle of the crystal. Further comparison of the properties of BBO and LBO crystals under similar conditions to above, and assuming that the pump power is limited so as not to approach the crystal damage threshold, then we can see that due to the larger walkoff angle of BBO the figure of merit given by formula (3-5) is then a few times smaller than that of LBO.

Actually Gaussian beams are usually used in frequency conversion processes. In this case, according to the Boyd and Kleinman theory[2], the parametric gain can be written as

$$\begin{aligned} G &= \frac{2\omega_1\omega_2 d_{eff}^2 L}{\pi n_1 n_2 n_3 \varepsilon_o c^3} P_p k_3 \, h(\xi,B) \\ &= \left(\frac{8\pi^2}{\varepsilon_o c}\right)\left(\frac{d_{eff}^2 L \, 2h(\xi,B)}{n_1 n_2 \lambda_1 \lambda_2 \lambda_3} P_p\right) \quad , \qquad 3 - 6 \end{aligned}$$

where the parameters have been defined in Chapter 2. Under optimised conditions and in the absence of walkoff effects, the focusing factor $h(\xi,B)$ has a maximum value ($h(2.84, 0) = 1.068$[2]), and the figure of merit formula can hence be written as

$$M \text{ (figures of merit)} = \frac{d_{eff}^2 L(2.14)}{n_1 n_2 \lambda_1 \lambda_2 \lambda_3} P_p \qquad 3 - 7$$

The figure of merit defined by (3-7) is called the crystal length limited figure of merit. It is clear that under given conditions, a longer crystal length can compensate for a poorer nonlinear coefficient. However, when walkoff effects are taken into account in the presence of a Gaussian beam, formula (3-6) becomes more complicated due to the variation in the parameter $h(B,\xi)$. However, it has been shown that the conditions when the birefringence walkoff aperture length is greater than the crystal length ($L_a = \pi^{1/2} w_o/\rho > L$), and the focusing parameter $\xi < 1$, the gain in the parametric interaction process can be approximated by[2]

$$G = \frac{2\omega_1\omega_2 d_{eff}^2}{\pi n_1 n_2 n_3 \varepsilon_o c^3} \frac{LL_a}{w_o^2} P_p$$

$$= \left(\frac{8\pi^2}{\varepsilon_o c}\right)\left(\frac{d_{eff}^2 L}{\pi^{1/2} n_1 n_2 n_3 \lambda_1 \lambda_2 \rho w_o} P_p\right) \qquad 3 - 8$$

and the figure of merit associated with a Gaussian beam under walkoff limited conditions can be written as

$$M \text{ (figures of merit)} = \frac{d_{eff}^2 L}{\pi^{1/2} n_1 n_2 n_3 \lambda_1 \lambda_2 \rho w_o} P_p \qquad 3 - 9$$

If we change the conditions as given above, so that the walkoff aperture length equals the crystal length L and use the relation between L, ρ, w_o given by (3-4), then the walkoff limited figure of merit formula (3-9) is similar to (3-5). Hence, we do not need to particularly emphasise whether the pump radiation is Gaussian or plane wave in the application of the figures of merit formulae for selecting the nonlinear optical materials.

We have defined three different figures of merit, i.e. crystal damage limited, crystal length limited, and walkoff limited figures of merit. They appropriately reflect the intrinsic properties of the crystals and are very useful in selecting the nonlinear medium for a particular design application. The figures of merit of BBO and LBO are calculated based on the above analysis, and are listed in table (3-1). The key parameters describing these nonlinear materials under conditions appropriate to our studies are summarised in table (3-2). Although the figures given in these tables refer to the specific conditions therein stated with regard to such parameters as crystal length, pump wavelength, available pump energies, etc., they are in general a good indication of the relative properties of these two materials. In comparing the two materials when used in the critical type I phase matching geometry, which offers the wide angle tuning range, it can be seen that BBO has the higher effective nonlinear coefficient but also the larger walkoff angle and the lower optical damage threshold. LBO has in addition to its critical phase matching geometry, a non-critical phase matching geometry where the nonlinear coefficient is comparable to that of the critical geometry, but where the walkoff angle now is zero. It is also clearly shown that the figure of merit with common definition is not always fit to use in comparing the material properties. Under certain conditions the conclusion can be completely different.

Table 3.1 The figures of merit of BBO and LBO crystals with different restrictions.

			BBO (CPM)	LBO (CPM)	LBO (NCPM)
Common	$M = \frac{d_{eff}^2}{n_1 n_2 n_3}$	$(10^{-24}\frac{m^2}{V^2})$	0.89	0.14	0.24
Damage limited	$M = \frac{d_{eff}^2 L^2}{n_1 n_2 n_3 \lambda_1 \lambda_2} I_D$	$(10^{-4}\frac{W}{V^2})$	175.8	55.31	94.81
Walkoff limited	$M = \frac{d_{eff}^2}{\pi\rho^2 n_1 n_2 n_3 \lambda_1 \lambda_2} P_p$	$(10^{-4}\frac{W}{V^2 rad^2})$	0.2	0.67	------
Crystal length limited	$M = \frac{d_{eff}^2 L(2.14)}{n_1 n_2 \lambda_1 \lambda_2 \lambda_3} P_p$	$(10^{-4}\frac{W}{V^2})$	-------	------	173.6

Table 3.2 The parameters used in calculations.

	BBO (CPM)	LBO (CPM)	LBO (NCPM)
d_{eff} † (pm/V)	2	0.75	1
I_D (GW/cm^2) (10 ns pulses at 355 nm)	5	10	10
P_p (MW) (3 mJ, 10 ns pulses)	0.3	0.3	0.3
ρ (Degrees)	4.5	1	0
L_{max} (cm)	2	2	2
L (cm)	1.6	1.6	1.6
n ††	1.65	1.60	1.60

† Typical over OPO tuning range.
†† Average over OPO tuning range.
††† λ_1, λ_2 and λ_3 are 0.48, 1.35 and 0.355 μm respectively.

In the above discussions it has been assumed that the pump power is always higher than the pump threshold for any nonlinear materials used in the OPO's. But, in practice, the situation is not always like that. Sometimes, particularly when low power diode-pumped solid-state lasers are used as pump sources, the pump power may be adequate to reach the pump threshold only in a particular nonlinear material, but not in others. At the end of day, the whole issue addressed by these of figures of merit is the minimisation of the threshold pump power. The material with the lowest threshold pump power under the given conditions is the superior material. A comparative analysis of threshold pump power (or energy) embracing all possible condition can be carried out based on Boyd and Kleinman theory as subsequently developed by Guha et al[3]. This we have carried out for both critical and non-critical phase matching geometries in LBO and BBO. The results are shown in figure (3-1)[4].

Based on the theory of Guha et al. (please see Chapter 2 section 2.3), a computer programme has been developed in collaboration with Y. Tang to calculate ultraviolet pump energy and energy densities appropriate to threshold for a range of focusing conditions in both critical and non-critical phase matching geometry for the two nonlinear materials. The data used in the programme are summarised in table (3-2), and in addition cavity round trip losses have been assumed to be 0.35 (and the BBO crystal length used in this calculation is 2 cm). Mean energy density (J/cm^2) is plotted on the vertical axis and pump energy on the horizontal axis. Each of the parallel diagonal lines across the graph corresponds to a particular value of the pump beam spot size in the crystal, and the coordinates of the intersection of such a line with one of the three curves describing either LBO or BBO give the pump energy and associated pump energy density required to reach oscillation threshold for that spot size and in that material and phase matching geometry.

Figure (3-1) clearly illustrates the figures of merit of the two nonlinear materials in relation to their use in optical parametric oscillators. When high pump pulse energies are available, such as in the case of pumping with excimer lasers or large frame frequency up-converted Nd:YAG lasers, the operating conditions lie towards the bottom right-hand part of the graph. In this case oscillation threshold can be reached with large pump beam spot sizes (conditions tending to the plane wave case), the effects of beam walkoff become insignificant, and the relative merits of the different materials/phase matching geometries are determined largely by their effective nonlinear coefficient for the parametric process. This part corresponds to that previously described by either the common or damage limited figure of merit (please see table (3-

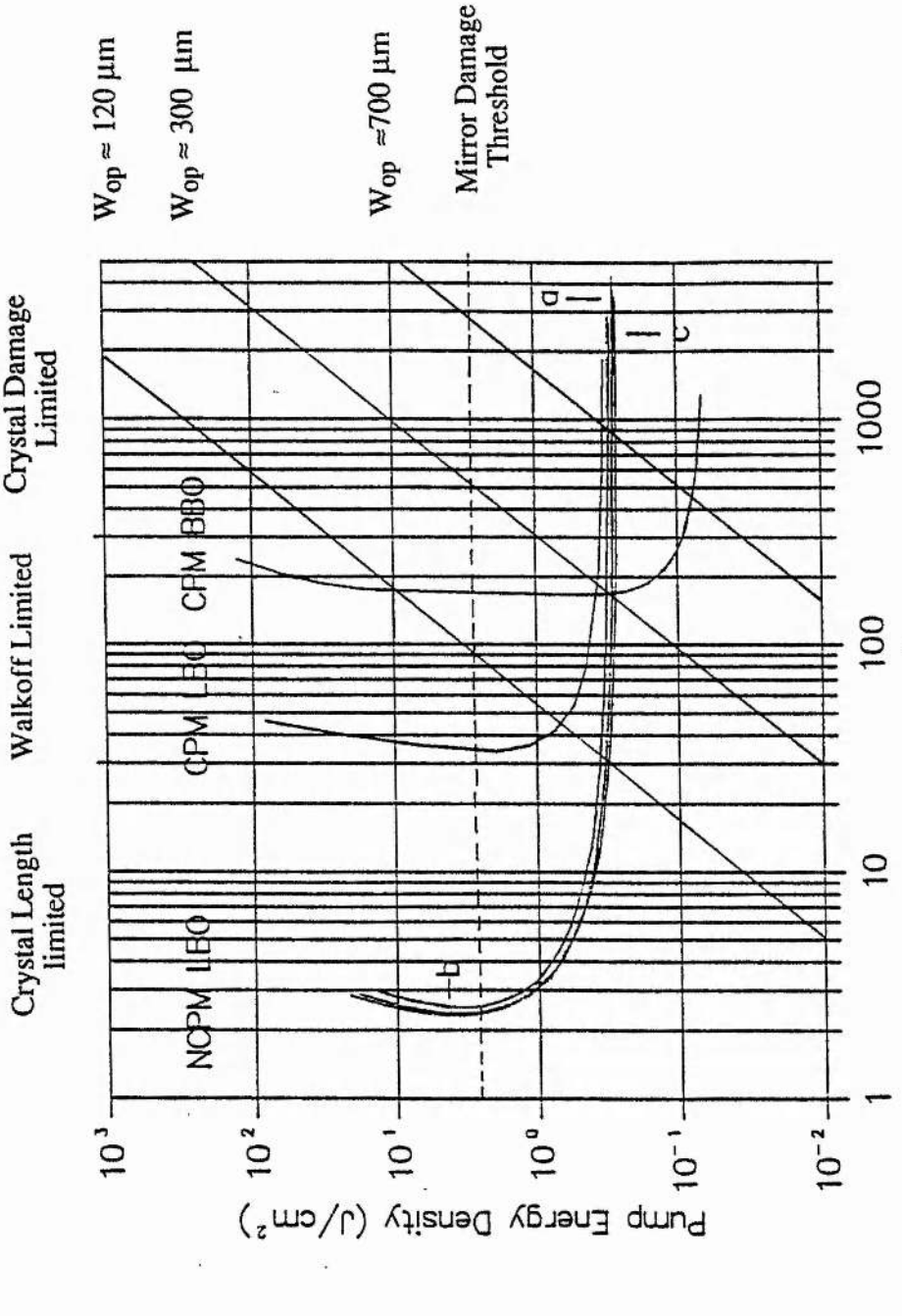

Fig. 3-1 The optimised threshold curves of NCPM LBO, CPM LBO and CPM BBO optical parametric oscillators. Where a, b and c denote that NCPM LBO are pumped at 308 nm, 355 nm and 266nm. The others are pumped at 355 nm.

1)). In this regime of operation, BBO is clearly the superior material possessing the highest value of d_{eff}. However, as the pump pulse energy available becomes less, it is apparent that tighter focusing is required in order to reach oscillation threshold, and eventually a pump spot size is reached at which the effect of Poynting vector walkoff causes the threshold pump energy density to rise rapidly. First to experience this rapid rise is critically phase matched BBO, which has a large walkoff angle, and is hence sensitive to pump beam spot size. Second to experience this rapid rise is critically phase matched LBO, which has a smaller walkoff angle than BBO, so that the pump energy threshold at the retracing point on the pump threshold energy curves is one order of magnitude lower than BBOs case. For this pump energy regime, the operating conditions lie towards the bottom centre of the graph, and correspond to those previously described by the walkoff limited figure of merit. The non-critically phase matched LBO, in which walkoff does not occur retains a low threshold energy density until much smaller pump spot size. The threshold energy density ultimately rises in this last case for pump beam spot size smaller than 100 μm because of the effects of pump beam divergence on phase matching, and intensity variation of the pump in the nonlinear medium along the propagation direction. Significantly, in this non-critical phase matching geometry the crystal length is a dominant parameter, and can be used to compensate for the other parameters. When the operating conditions lie towards the bottom left-hand part of the graph, the conditions correspond to those described by the crystal length limited figure of merit.

In the figure (3-1) it is apparent that for pulse energies below around ~2 mJ, oscillation threshold cannot be reached in BBO, no matter how tight the focusing. However because of the lower walkoff angle associated with LBO, oscillation threshold can still be reached in this material in both critically phase matched and non-critically phase matched geometries at pump energies below the 1 mJ level. In devices required to operate at low pump pulse energies (less than a few mJs), such as here, it is apparent that LBO is the suitable nonlinear material. An upper limit to the pump energy density that can be employed is determined by mirror or crystal damage. This limit is indicated in figure (3-1) by the horizontal lines. Since OPOs must be operated at several times the threshold pump energy in order to attain reasonable conversion efficiencies, it is apparent that crystal/mirror damage can also limit the minimum pump energy required for the successful operation of a practical device. This point we will further discuss in Chapter 6.

Obviously, the figures of merit formulae we have discussed above do not include all of the material's intrinsic natural properties. It is clear that in many applications we have also to consider such parameters as the pump wave velocity dispersion, the material intrinsic linewidth, the material thermal characteristics etc. Hence, when choosing a nonlinear medium for a specific usage, it is necessary to consider other issues in addition to the those addressed by the figures of merit[5].

3.2 An overview of nonlinear material for use in the UV

As we have described in the Introduction, we are interested in nonlinear materials that are useful for optical parametric oscillators pumped at wavelengths equal or shorter than 355 nm. This restricts the available nonlinear optical materials to the following: lithium triborate (LBO)[6], barium borate (BBO)[7], urea[8], lithium iodate ($LiIO_3$)[9], deuterated L-arginine phosphate (d-LAP)[10], potassium dihydrogen phosphate (KDP)[11], and its isomophs. Unfortunately some excellent nonlinear crystals such as KTP[12], $KNbO_3$[13] are not included due to limitation in transparency and potential for phase matching. The transmission cutoff wavelength for KTP and $KNbO_3$ are 350 nm and 400 nm respectively. It is appropriate to briefly mention other possible materials, such as potassium penta borate tetrahydrate (KB5)[14] and $BeSO_4 \cdot 4H_2O$[15]. About 10 years ago, KB5 was the only material used for generating vacuum UV (VUV 100 nm - 200 nm) coherent radiation by sum frequency mixing. However, because of its small nonlinear coefficient ($d_{31} = 0.046$ pm/V) it has recently been completely replaced by BBO and LBO. The nonlinear optical crystal $BeSO_4 \cdot 4H_2O$ was developed in the 1970s, and more recently has been investigated and mentioned by Kato again last year, for frequency doubling from 532 nm to 266 nm[16]. $BeSO_4 \cdot 4H_2O$ has not been well characterised, but due to its small nonlinear coefficient ($d_{36} = 0.24 \pm 0.25$ pm/V) it has attracted little interest.

KDP:

Potassium dihydrogen phosphate (KDP)[11] is a negative uniaxial crystal, belonging to tetragonal system with point group $\bar{4}2m$. It has found wide-spread use in the frequency doubling of ultra-high power 1 μm lasers (as used in plasma fusion experiments), as it is one of the few nonlinear crystal that can be grown with a large enough aperture size. While KDP does possess a high damage threshold (8.4 GW/cm^2 for 1.3 ns pulses at 1.053 μm[17]), it has a nonlinear coefficient of only 0.39 pm/V. Furthermore, it can only transmit wavelengths in the range 0.2-1.5 μm. Therefore the

tuning range of a parametric oscillator based on this material is very limited in the infrared part of the spectrum. This is the reason that while parametric oscillation has been demonstrated using this material, its use has not been wide-spread. KDP shortest SHG phase matchable wavelength is 0.259 μm, and the shortest SFM phase matchable wavelength is 0.218 μm.

$LiIO_3$:

Lithium iodate ($LiIO_3$)[9] is a negative uniaxial crystal belonging to the hexagonal system with symmetry point group 6. The transparency range in this material is 0.3-5.5μm and the nonlinear coefficient at d_{31} is eleven times that of d_{36} of KDP ($d_{31}(LiIO_3) = 4.1 \pm 0.2$ pm/V). Unfortunately, the optical damage threshold of $LiIO_3$ is relatively low, being about 0.5 GW/cm^2. Also the absorption in lithium iodate crystals is generally high, of the order of 10 %/cm in the UV. Metal impurities, especially iron, increase this absorption considerably even when present in concentrations of a few ppm. High birefringence and large walkoff angle are another two features. Its use an OPO gain medium is marginal, with optical damage generally occurring close to oscillation threshold.

Urea:

Urea[8] is a positive uniaxial crystal of point group 42m. It has a nonlinear coefficient of 1.4 pm/V, about 4 times that of KDP and a high damage threshold of up to 5 GW/cm^2 (1.3 ns pulses at 1.064 μm, single shot). Urea has high transparency in the 200 nm to 1.4 μm band and is consequently of use in the ultraviolet, it e.g. can be used to frequency quadruple the output of a Nd:YAG laser and to pump optical parametric oscillators tunable in the visible spectrum band. Until barium borate became available, it was the dominant material for this use.

d-LAP:

d-LAP[10] is a potentially promising nonlinear optical material. It is easily obtainable in large sizes (70 x 70 x 40 mm^3) and has a relatively high nonlinear coefficient ($d_{\beta\beta\beta}$ = 0.92 pm/V) and high optical damage threshold. The damage threshold of this material was found to be twice as high as for the best quality commercially available KDP crystals. Its use in optical parametric oscillators is also limited by its transparency range, which is only from 250 nm to 1.3 μm. High absorption in the UV is another problem, being 4 %/cm and 12 %/cm at 355 nm and 266 nm respectively.

BBO:

Barium borate (BBO)[7] is a recently developed material that is of great utility in the ultraviolet, as it transmits wavelengths down to 190 nm. However, BBO is also of use in the near infrared, as it can transmit wavelengths as long as 3.5 μm. BBO has a large nonlinear coefficient (d_{11} = 2.2 pm/V[18]) comparing well with the other materials that transmit into the ultraviolet. BBO possesses a high damage threshold of 10 GW/cm^2. It is fair to say that the direct doubling of wavelengths shorter than 630 nm is now almost exclusively achieved using BBO crystals. The major disadvantage with BBO is the large walkoff over the majority of its tuning range, making it unusable for low power applications. BBO's shortest SHG phase matchable wavelength is 205 nm, and the shortest SFM phase matchable wavelength is 190 nm.

One property that has not been mentioned so far is resistance to atmospheric water vapour. Urea, lithium iodate, KDP and its isomophs, are highly hygroscopic and must therefore either be permanently heated, or mounted in index matching cells. BBO is slightly hygroscopic and therefore should not be left exposed to the atmosphere for any appreciable length of time. If possible the crystal should be maintained at a temperature slightly above room temperature to prevent condensation forming on the crystal[5].

LBO:

LBO is a recently newly developed nonlinear material[6]. It has a high transmission in the range from 160 nm to 2.6 μm, and a relatively high nonlinear coefficient (about 3 times that of d_{36} of KDP). It does however, possess a remarkably high damage threshold for Q-switched pulse (18 GW/cm^2), and can be phase matched in all three principal planes. It has a sufficient thermal variation of the birefringence to enable it to be temperature tuned to achieve non-critical phase matching. This along with the high damage threshold allows a high conversion efficiency to be achieved by tightly focusing the pump wave despite the small nonlinear coefficient. As it has, unlike BBO, appropriate birefringence with corresponding small walkoff angle and large angular acceptance band width, it is the only material suitable for an OPO tunable in the UV, visible and near infrared when pumped with modest UV powers.

3.3 Selection of the optical parametric oscillator gain medium

We have already described in Chapter 1 that one of the essential purposes of this project is investigating the properties of the nonlinear optical crystal lithium triborate as

used for an OPO medium. LBO is not only a new nonlinear material, but is also better suited in general to OPO applications compared to other nonlinear materials. For pump sources only providing a few of milli-joules of pump energy in the UV, so that for pumping an OPO tight focusing schemes are required for reaching oscillation threshold and achieving good conversion efficiency, then lithium triborate may be the only feasible material.

There are three key parameters that should be considered, and these are: crystal transmission range, effective nonlinear coefficient and walkoff angle. The first parameter limits our discussion to just a few crystals. However, because potentially wide tuning ranges are being sought, only two crystals, BBO and LBO, are acceptable. The second and third parameters need to be considered together, and primarily decide the pump threshold and the conversion efficiency. We have calculated the figures of merit of these materials. The results and the parameters used in the calculations are listed in tables (3-1) and (3-2) respectively. From these results, the conclusions are that: in the high pump power situation BBO is the superior material, due to its larger effective nonlinear coefficient; but in the low pump power situation, the advantages of LBO are significant. LBO has a small walkoff angle, and consequently, the figure of merit is then larger than BBO's. Particularly in the non-critical phase matching geometry, when the effective nonlinear coefficient reaches its maximum value, and the walkoff effect is eliminated, the figure of merit of LBO is as high as one hundred times that of BBO.

The pump energy threshold curves given in figure (3-1) also clearly illustrate this point. It can be seen that if the available pump energy is high enough (higher than ~4mJ) then BBO is the superior material for an OPO. However, if the pump energy is lower than ~2 mJ, then optical parametric oscillation with BBO is not possible, However, this pump energy is around ~5 times that required to reach threshold in a critically phase matched LBO optical parametric oscillator, and ~10 times that required to reach threshold in a non-critically phase matched LBO optical parametric oscillator.

Since in these studies of all-solid-state devices we are limited to pump energies in the ultraviolet below 3 mJ, it is clear that LBO is the only viable nonlinear material. In the next section we will thoroughly discuss the intrinsic properties of this superior nonlinear crystal -lithium triborate.

3.4 Lithium triborate (LBO) crystal

Lithium triborate is a new nonlinear optical material recently developed by the Fujian Institute on Structure of Matter, in China[6]. LBO crystals have excellent properties such as high transparency in the near-infrared, visible and UV, high optical damage threshold, relatively high nonlinear coefficient, large acceptance angle, small walkoff angle, non-hygroscopic, and moderate temperature sensitivity etc. All of these have been discussed by many authors in the past two years. This section summarises the properties of lithium triborate that are relevant to its use as the medium in an OPO. The pump wavelength used during the investigation of the LBO OPO, as described in Chapter 1, was 355 nm and 266 nm. Consequently, all values quoted in this section for phase matching etc., pertain to these wavelengths.

Crystallographic structure

LBO is an negative biaxial crystal belonging to the orthohombic system with point symmetry mm2, whose indicatrix axes x, y, z (ordered according to increasing refractive index $n_z > n_y > n_x$) correspond to the crystallographic a, c, b. (a = 8.4473 Å, b = 7.3788 Å, c = 5.1395 Å[19])

Transmission

The transmission range of lithium triborate first reported by Chen et al[6], extended from 160 nm in the ultraviolet to about 2.6 μm in the infrared. Later this parameter was measured again by Kato[20] and Zhao et al[21] individually. Their results indicate that the long wavelength cutoff is around 3.2 μm. More recently Xie et al[22] have given another transmission range which is from 160 nm to 3.5 μm. Unfortunately they didn't provide any information about the experimental measurement process, and this figure could be due to a typing mistake.

The absorption coefficient of lithium triborate was first measured by Kato[20], using a Hitachi FPS-3T spectrophotometer. He reported that there is no measurable absorption from 187 nm to 1.7 μm. However, because LBO is grown from a high temperature flux, there is concern about the possible presence of impurities and inclusions in the crystal. Consequently, more recently absorption coefficients have been carefully measured again at some typical wavelengths. Velsko at al[23] have measured the absorption at 1.064 μm and 355 nm using a Calorimetric method. It was found to

be 0.035 %/cm at 1.064 μm and 0.31 %/cm at 355 nm. Despite the relative newness of LBO, these results compare very favourably with similar measurement in the established material KD*P. There is indication that LBO is a material appropriate for high power applications.

Effective nonlinear coefficient

The nonlinear optical coefficients of lithium triborate LiB_3O_5, have been measured by Chen et al[6][24] using the Maker Fringe method at 1.079 μm, as well as by Velsko et al[23] using the SHG and THG phase matching method at 1.064 μm. It is known that the LBO crystal with point group mm2, has five non-zero coefficients, namely d_{31}, d_{32}, d_{33}, d_{15}, and d_{24} in the piezo-electric axes system. From Kleinman symmetry d_{15} and d_{24} are equal to d_{31} and d_{32} respectively, so in practice, only three parameters are independent. The experimentally determined nonlinear coefficients for LBO crystal are listed in table (3-3). They are slightly different, but the values agree to within experimental uncertainties.

Table 3-3 The nonlinear optical coefficients of lithium triborate (tensor elements)

	Chen et al[6] pm/V	Chen et al[24] pm/V	Velsko et al[23] pm/V
d_{31}	+ 1.07 (1±0.031)	+ 0.98 (1±0.04)	
d_{32}	± 1.16 (1±0.031)	± 1.05 (1±0.05)	0.83 ±0.05
d_{33}	± 0.06 (1±0.004)	± 0.06 (1±0.04)	0.00 ±0.10
d_{15}		+ 0.89 (1±0.09)	0.71 ±0.05
d_{24}		± 0.98 (1±0.08)	

The original nonlinear tensor coefficients given by Chen et al[6][24] were relative to d_{36} for potassium dihydrogen phosphate (KDP), and CGS units were used in his paper.

Angular behaviour

The optically nonlinear material LBO has a number of phase match options, and it can be phase matched in all three principal planes. In particular, the x-y plane provides a type I critical phase matching geometry which is rapidly angular tunable and the tuning range is comparable to BBO[7] (When it is pumped at 355 nm, it is potentially

tunable from 405 nm to 2.6 μm[25]). This broadly tunable type I geometry has been extensively studied by others, as well as in this laboratory in all-solid-state schemes.

Figure (3-1) gives three dimensional diagrammatic curves of phase mismatch, signal and idler tuning range, effective nonlinear coefficients, walkoff angle, and acceptance angle, for the type I LBO optical parametric oscillator pumped at 355 nm.

The type II critical phase matching geometry in LBO is also of interest, although the tuning rate is not as rapid as in the type I geometry, and the tuning range is only from 483 nm to 565 nm (signal) and 1.33 to 0.95 μm (idler) when the device is pumped at 355 nm. However, it should be noted that despite the slow tuning rate the type II geometry has some significant advantages, which are smaller walkoff angle, larger acceptance angle, and intrinsically narrow line width than the type I geometry, consequently the figure of merit is larger than the type I geometry (please see Appendix III). Recently, this geometry has been widely used for frequency up conversion by frequency mixing; for example, frequency mixing of the 1.064 μm and the 0.532 μm waves to 0.355 μm wave.

Non-critical phase matching is another option. It can be seen from Appendix III that, in this case, the effective nonlinear coefficient reaches maximum and walkoff is eliminated. However, the angular tuning range around this non-critical phase matching situation is limited in a few nano-meters. However the material can be temperature tuned (please see below).

Thermal behaviour

The birefringence of LBO has a high thermal dependence, thus making it sensitive to environmental temperature and laser induced heating. However, it also makes it possible to temperature tune. This feature is particularly important when material is used in a non-critical phase match geometry.

The temperature behaviour of lithium triborate has been investigated by several authors. Most of them report only experimentally measured temperature tuning rates. Some experimental results are listed in table (3-4) and table (3-5), where all of the OPO (type II NCPM) wavelength tuning rates were measured in our laboratory.

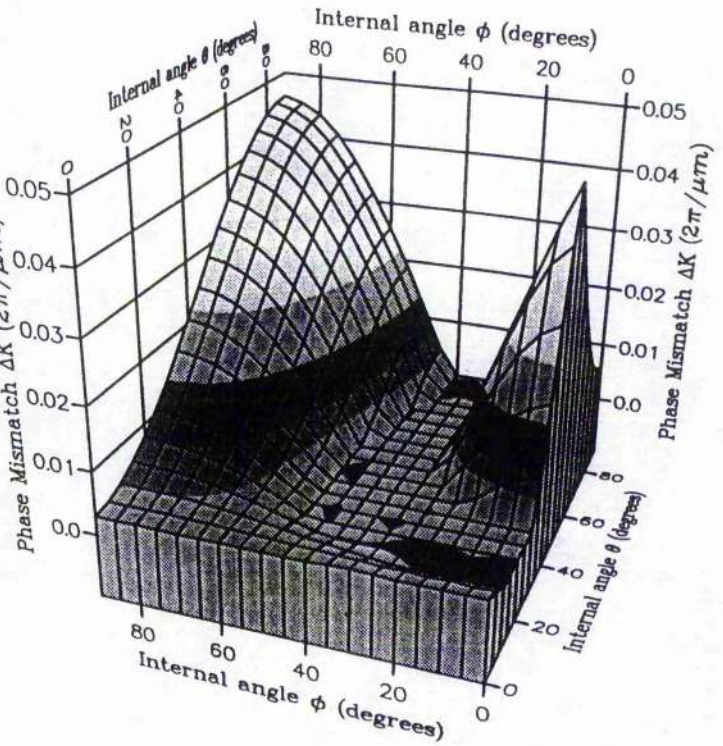

Fig. 3-1(a) Phase matching for type I CPM LBO OPO pumped at 355 nm. The flat area is phase matching area, which corresponding to $\Delta k = k_3 - k_2 - k_1 = 0$. Where wavelength have been chosen so that this condition is satisfied.

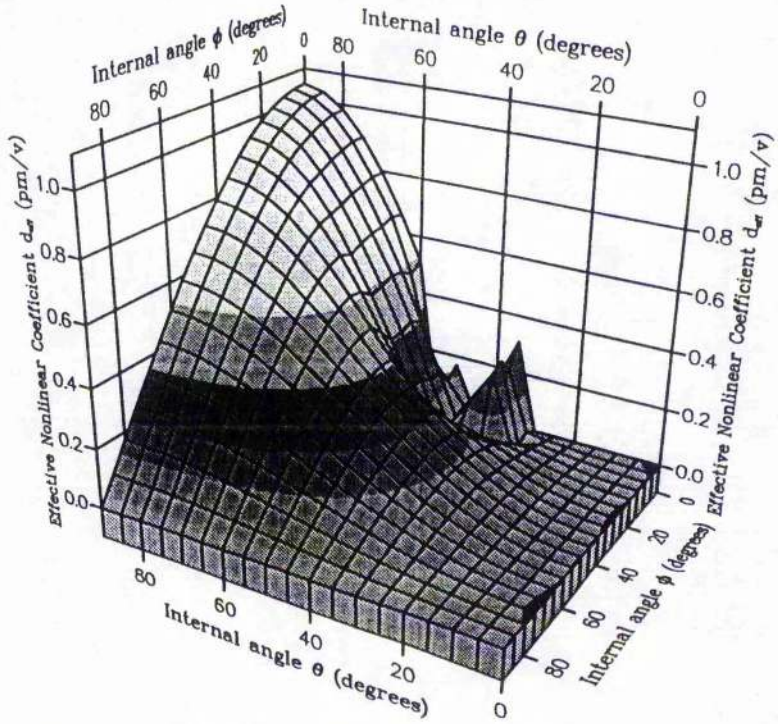

Fig. 3-1(b) Effective nonlinear coefficient (d_{eff}) for type I CPM LBO OPO pumped at 355 nm.

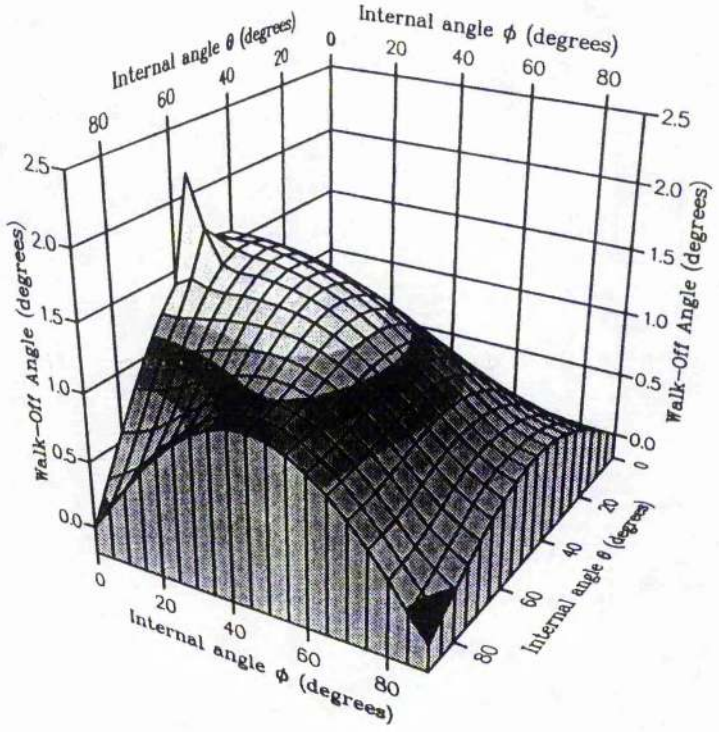

Fig. 3-1(c) Walkoff angle for type I CPM LBO OPO pumped at 355 nm.

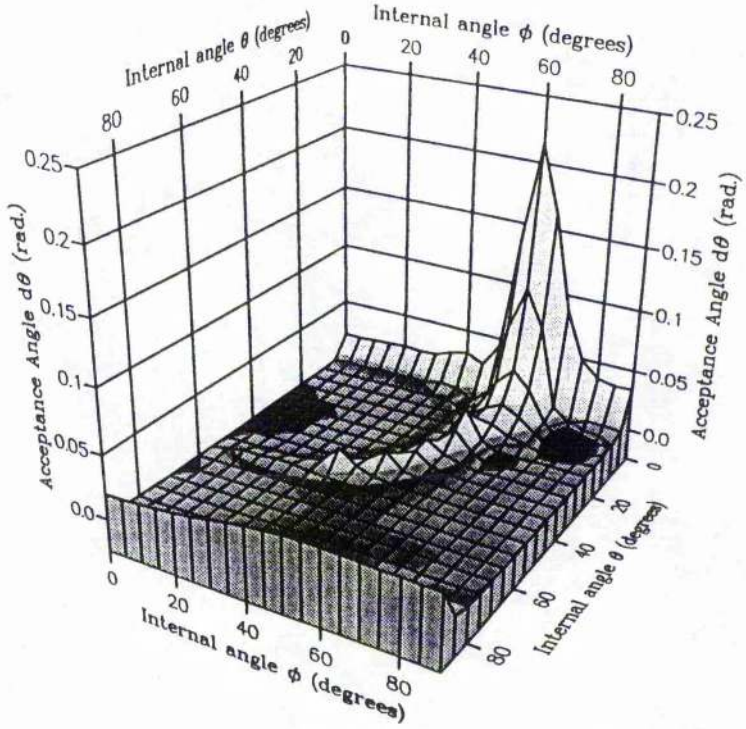

Fig. 3-1(d) Acceptance angle $\delta\theta$ for type I CPM LBO OPO pumped at 355 nm.

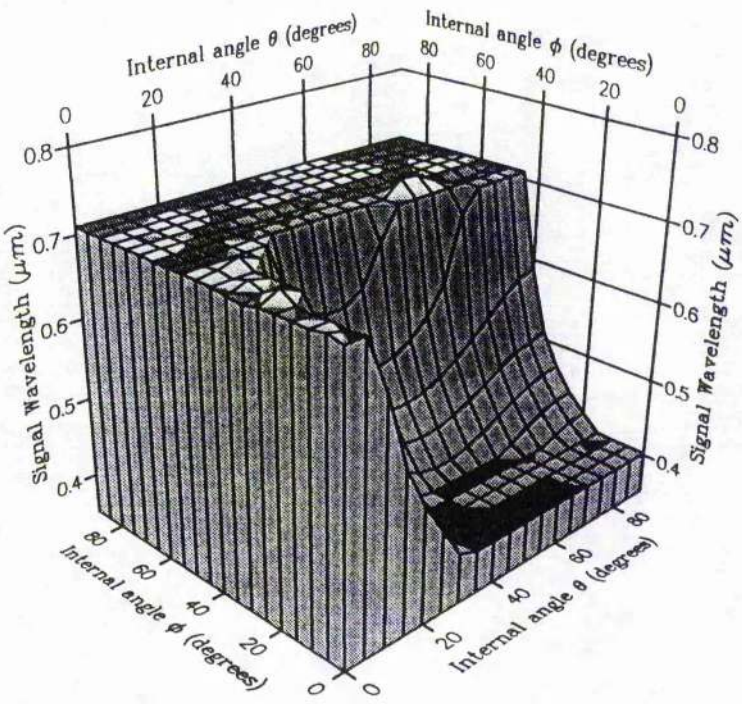

Fig. 3-1(e) Signal wavelength tuning of type I CPM LBO OPO pumped at 355 nm.

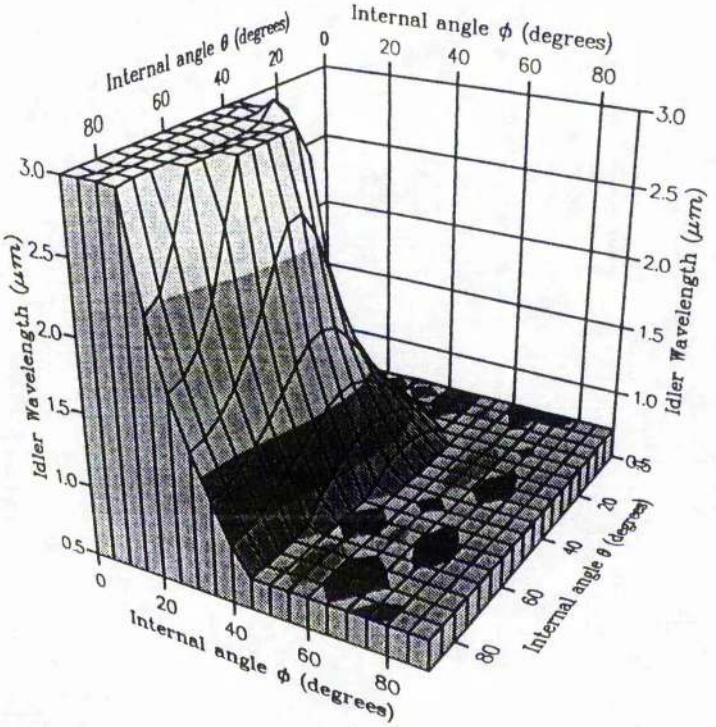

Fig. 3-1(f) Idler wavelength tuning of type I CPM LBO OPO pumped at 355 nm.

Table 3-4 Phase matching temperature of SHG in type I non-critically phase matched LBO(1064-532nm)

	Chen[22]	Huang[26]	Ukachi[27]	Yang[28]	Lin[29]	Ours
Phase matching temperature (°C)	137±	148.5±0.5	148.0±0.5	149.5	149.0	149.0±2
Temperature band width (°C)		1.8	10.1	6.8	0.8	1.8

Table 3-5 Temperature tuning behaviour of the type II non-critical phase matched LBO optical parametric oscillator

Pump wavelength (nm)	355[30]	308[31]	266[32]
Temperature (°C)	20-200	20-60	20-200
Signal tuning range (nm)	480.6-457.0	385.5-383	313.8-306.0
Idler tuning range (μm)	1.355-1.590	1.53-1.57	1.75-2.03
Tuning rate (nm/°C) (at near room temperature)			
Signal	-0.11	-0.07	-0.04
Idler	+0.87	+1.08	+1.30

The dependence of the refractive indexes on temperature (thermal data) has been evaluated by Velsko et al[23], using minimum deviation measurements at several temperatures between 20 °C and 65 °C, and the results are

$$\frac{dn_x}{dT} = \{ -1.8 \pm 0.2 \} \times 10^{-6} \quad \text{(wavelength independent)}$$

$$\frac{dn_y}{dT} = \{ -13.6 \pm 0.1 \} \times 10^{-6} \quad \text{(wavelength independent)}$$

$$\frac{dn_z}{dT} = \{ -6.3 \pm 0.6 + (2.1 \pm 0.8) \lambda \} \times 10^{-6} \quad (\lambda \text{ in } \mu m)$$

However we have found that this thermal data does not fit to our experimentally measured temperature tuning curve when the temperature goes up to more than 100°C.

Optical damage threshold

LBO's highest optical damage threshold has been confirmed by many experiments. Some experimentally measured optical damage threshold powers are listed in table (3-6). The material is also mechanically tough, being harder than SiO_2.

Table 3-6 Optical damage threshold of the LBO crystal

Energy density (J/cm^2)	Power density (GW/cm^2)	Experimental conditions	Ref.
	25	λ=1.064μm Q-switched, 0.1ns pulse	[6]
24.6	18.9	λ=1.054μm Q-switched, 1.3ns pulse	[17]

References

(1) R. L. Byer
in "Quantum Electronics:a treatise", edited by H. Rabin anf C. L. Tang, (Acadamic, New York) Vol. **1**, Part B, 587-702, 1975

(2) G. D. Boyd and D. A. Kleinman
J. Appl. Phys. **39**(8), 3597, 1968

(3) S. Guha, F. J. Wu, and J. Falk
IEEE J. Quantum Electron. **18**(5), 907, 1982

(4) M. H. Dunn, Y. Cui, A. J. Henderson, G. Robertson, Y. Tang, D. E. Withers, W. Sibbett, and B. D. Sinclair
J. Opt. Soc. Am. B. (submitted, Nov. 1992)

(5) A. Guy
Ph. D thesis, Department of Physics, University of Southampton, UK (unpublished)

(6) C. T. Chen, Y. C. Wu, A. D. Jiang, B. C. Wu, G. M. You, R. K. Lin and S. J. Lin
J. Opt. Soc. Am. B6(4), 616, 1989

(7) C. T. Chen, B. C. Wu, A. D. Jiang, and G. M. You,
Scientia Sinica(b), **28**, 235, 1985

(8) J. M. Halbout, S. Blit, W. Donaldson, and C. L. Tang
IEEE, J. Quantum Electron. **15**, 1176, 1979

(9) G. Nath and S. Haussuhi
Appl. Phys. Lett. **14**(5), 154, 1969

(10) D. Eimerl
IEEE J. Quantum Electron. **25**(2), 179, 1989

(11) D. Eimerl
Ferroelectrics, **72**, 95, 1987

(12) F. C. Zumsteg, J. D. Bierlein and T. E. Gier
J. Appl. Phys. **47**(11), 4980, 1976

(13) E. Wiesendanger
Ferroelectrics, **1**, 141, 1970

(14) C. F. Dewey, Jr. W. R. Cook, Jr. R. T. Hodgson and J. J. Wynne
Appl. Phys. Lett. **26**(12), 714, 1975

(15) M. P. Golovi et al
Sov. Phys. Crystllogr. **15**, 651, 1971

(16) K. Kato
IEEE J. Quantum Electron. **26**(9), 1455, 1990

(17) FC CASTECH Inc. Trade Literature on LBO
June 1991

(18) R. C. Eclardt, H. Masuda, Y. X. Fan and R. L. Byer
IEEE Quantum Electron. **26**(5), 922, 1990

(19) H. Konig and A. Hoppe
Z. Allorg. Allg. Chem. **439**, 71, 1978

(20) K. Kato
IEEE J. Quantum Electron. **26**(7), 1173, 1990

(21) S. Q. Zhao, H. W . Zhang, C. E. Huang, Y. C. Lin, W. Lin, Z. W. Hao and Z. Z. Su
J. Synthetic Crystals, **18**(1), 9, 1989

(22) F. L. Xie, B. C. Wu, G. M. You and C. T. Chen
Opt. Lett. **16**(16), 1237, 1991

(23) S. P. Velsko, M. Webb, L. Davis and C. E. Huang
IEEE. J. Quantum Electron. **27**(9), 2182, 1991

(24) S. J. Lin, Z. Y. Sun, B. C. Wu, and C. T. Chen
J. Appl. Phys. **67**(2), 634, 1990

(25) H. -J. Krause and W. Daum
Appl. Phys. Lett. **60**(18), 2180, 1992

(26) J. Y. Huang and Y. R. Shen, C. T. Chen and B. C. Wu
Appl. Phys. Lett. **58**(15), 1579, 1991

(27) T. Ukachi, R. J. Lane, W. R. Bosenberg and C. L. Tang
Appl. Phys. Lett. **57**(10), 980, 1990

(28) S. T. Yang, C. C. Pohakski, E. K. Gustafon and R. L. Byer
Opt. Lett. **16**(19), 1493, 1991

(29) J. T. Lin, J. L. Montgomery and K. Kato
Opt. Commun. **80**(2), 159, 1990

(30) Y. Cui, M. H. Dunn, C. J. Norrie, W. Sibbett, B. D. Sinclair, Y. Tang and J. A. C. Terry
Opt. Lett. **17**(9), 646, 1992

(31) M. Ebrahimzadeh, G. Robertson and M. H. Dunn
Opt. Lett. **16**(10), 767, 1991

(32) Y. Tang, Y. Cui and M. H. Dunn
Opt. Lett. **17**(3), 192, 1992

CHAPTER 4

Pump sources

Successful operation of an optical parametric oscillator requires a pump with sufficient intensity and of high beam quality. In this chapter, we describe how we set up the UV pump source using a diode laser pumped Nd:YAG laser with only modest pump energy of around 10 mJ (at 1.064 μm). The main results of experimental investigations of frequency doubling, tripling and quadrupling the Nd:YAG laser are presented here. The theoretical considerations are discussed in Appendix I.

It is of interest to mention briefly that, a high power coherent UV light source has many promising applications, including laser-Raman spectroscopy, photo-chemistry, atmospheric studies, high speed near-ultraviolet photography, pumping short-wavelength dye lasers, laser medicine, laser processing of semiconductors, as well as pumping optical parametric oscillators. This is particularly so in an all-solid-state configuration, when the device becomes more compact, efficient and stable. Some UV devices are already commercially available, such as excimer lasers, ion lasers and frequency up converted solid-state lasers. The coherent UV source based on an all-solid-state scheme, however, is just beginning to appear on the market[1]. A constraint on the utilisation of such a source is the cost of the diode laser, which is still high. We have recently shown that it is possible using a diode pumped solid-state laser, and employing the newly developed nonlinear optical materials such as KTP, LBO. BBO, to achieve an overall optical-optical conversion efficiency in these geometry of frequency tripling and quadrupling of more than 30 % at 355 nm and 18 % at 266 nm.

4.1 Flash-lamp pumped Nd:YAG laser

The flash lamp pumped Nd:YAG laser used in these investigations is a Quantel YG 481 laser †. It was used only as a simulator pump source at 1.064 μm before the diode pumped Nd:YAG laser was constructed. By theoretical calculations we estimated that the output energy from the diode pumped Nd:YAG laser would be around 10 mJ, so initially the output energy of the flash-lamp pumped Nd:YAG laser was limited to this level.

The cavity configuration of the Quantel YG 481 laser is shown in figure (4-1), and is a plano-concave geometry. The radius of curvature of the curved mirror is 3 m and both mirrors were coated for high reflection at 1.064 μm and were physically separated by around 1.2 m.

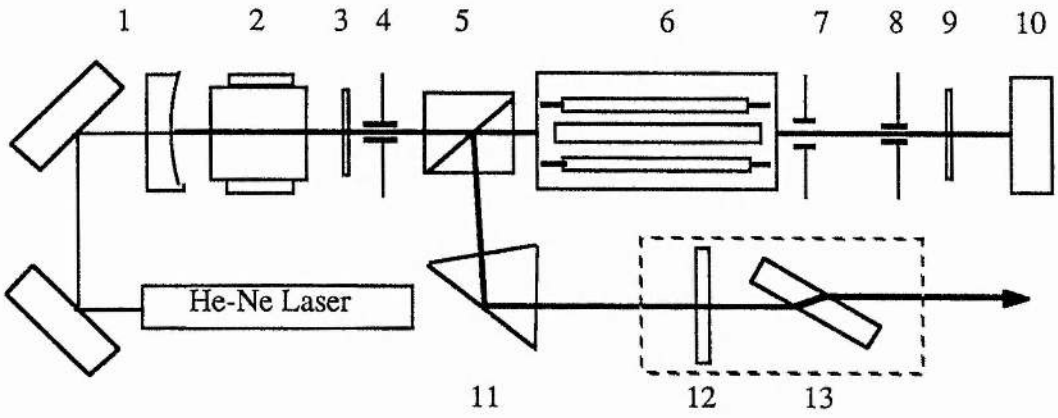

Fig. 4-1 Schematic diagram of flash-lamp pumped Quantel YG 481 Nd:YAG laser. (1) HR Mirror, (2) KD*P EO-Q-switch, (3) Quarter-wave plate, (4) Aperture, (5) Glan-Thomson polarizer, (6) Laser head, (7) Aperture, (8) Aperture, (9) Quarter-wave plate, (10) HR Mirror, (11) HR prism, (12) Half wave plate, (13) Glass plate with Brewster angle.

† Please see Synopsis book of Quantel Model YG 481 laser, March, 1981

The oscillator cavity contains a laser head, a KD*P Pockels cell, two quarter-wave plates, a Glan-Thomson type polarizer, and two apertures to limit high order transverse mode oscillation.

The laser head contains one Nd:YAG rod which is doped to about 1% with neodymium ions, has a diameter of 9 mm, a length of 115 mm and its two optical faces (cut to a 2^{o} angle from the transverse plane) are anti-reflection coated for 1.064 μm wavelength. The laser head also contains two high pressure Krypton flash-lamps for pumping. The length of the discharge gap in there is 101.6 mm (4 inch) and the tube inner diameter is 5 mm. The pump reflector cavity of the laser head is a diffusing reflection glass cavity. The laser head is cooled by de-ionized water with closed-circuit flow.

The Pockels cell is fitted with a KD*P crystal, the optic axis of which is parallel to the light propagation direction as well as to the longitudinal electric field. The optical windows closing the cell are externally anti-reflection coated. There is a liquid for index matching between the faces of the crystal and the internal faces of the windows.

The Glan-Thomson type polarizer was anti-reflection coated at 1.064 μm on all of its optical faces.

The combination of the Pockels cell with the polarizer, a quarter wave plate and the curved cavity mirror formed a switch unit. As long as there is no voltage across the Pockels cell the laser cannot oscillate. The laser cavity is closed by turning the quarter wave plate placed between the Pockels cell and the polarizer so as to form in effect a half wave plate. As soon as the appropriate high voltage (a quarter-wave voltage at 3.3 KV) was applied to the Pockels cell, the laser oscillated and the power extracted from the cavity was optimised by rotating another quarter wave plate placed on the other side of the polarizer.

The output characteristics of this flash-lamp pumped Nd:YAG laser are listed table (4-1).

The output beam profile was measured using a pin-hole-scanning method. The results clearly showed that the output laser beam was not exactly a Gaussian distribution and hence was not a TEM_{oo} mode. This is detrimental to the frequency doubling and tripling processes; this point we will discuss latter. The pulse width was

measured to be 12 ns (FWHM), when the maximum output peak power was 1MW (12mJ, 12 ns).

Table 4-1 The output characteristics of the flash-lamp pumped Nd:YAG laser.

Wavelength	1.064	μm
Output energy	12	mJ
Pulse width	12	ns
Energy stability	± 3.5	%
Repetitions	1, 5, 10	Hz
Mode structure	Lower order mode (Gaussian like)	
Beam divergence	≥ 0.7	mrad
Line width	≥ 0.7	cm^{-1}

4.2 Diode laser pumped Nd:YAG laser

The diode laser pumped Nd:YAG laser was developed in two steps. In the first step three 24 mJ quasi-CW diode laser arrays (total energy 72 mJ at 809 nm) were used as the pump, and in the second step the number of diode laser was doubled, so that the total pump energy was then 144 mJ. The schematic diagram of the triple-diode-laser pumped Nd:YAG laser is shown in figure (4-2).

The pump sources are SDL double stack laser diode bars (Spectra Diode Labs SDL 3230-TA)†. These quasi-CW laser bars emit radiation in pulses of up to 200 μs duration at repetition rates up to 100 pps having a maximum energy of 24 mJ. As usual, the wavelength of the radiation from each laser bar was tuned to the Nd:YAG absorption peak at 809 nm by individually adjusting the heat-sink temperature for each laser bar. Each laser bar was mounted on a copper base plate with soft indium foil providing good thermal contact. Temperature control of each laser bar was provided by individual Peltier thermo-electric stages powered by bipolar stabilisation control units (Photon control) with the temperature of the copper plate monitored by 10 KΩ thermistors. Heat generated at the other side of the Peltier cooler was dissipated using a

† Please see the commercial literature of Spectra Diode Labs. (USA), 1991.

small water cooled copper block. The output power and wavelength of these devices were found to be close to the manufacturers specifications, with operation at 809 nm occurring between 25 °C and 30 °C. The output power and wavelength were found to vary only slightly when the repetition rate was increased from 10 pps to 100 pps, which is indicative of the good thermal engineering within the SDL package and in our heat-sinking arrangement.

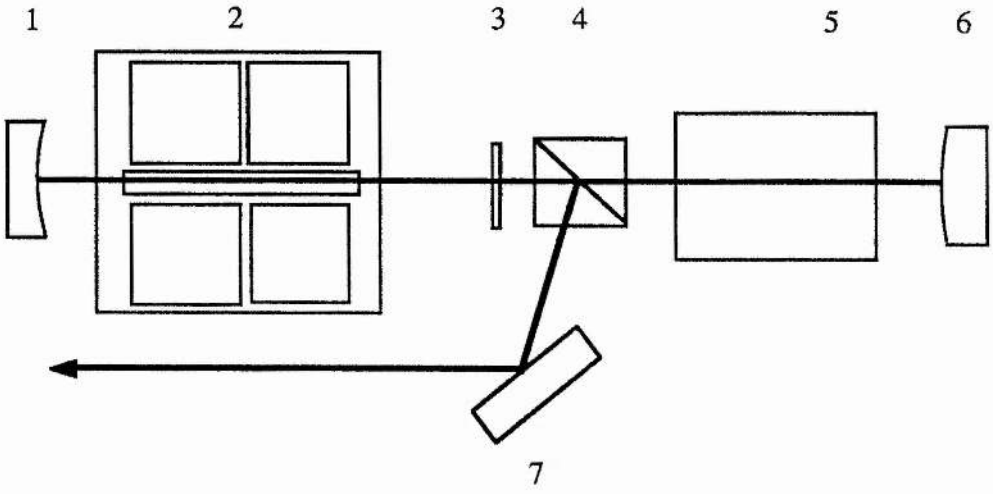

Fig. 4-2 The schematic diagram of the diode pumped Q-switched Nd:YAG laser. (1) HR concave mirror, (2) Triple diode-bar pump module, (3) Quarter-wave plate, (4) Air-spaced Glan-Taylor polariser, (5) KD*P Pockels cell, (6) HR convex mirror, (7) 45 degree HR mirror.

The pumping arrangement consisted of three laser diode bars symmetrically placed around a Nd:YAG rod of 3 mm diameter. No coupling optics were used. In order to reduce Fresnel reflection of the pump light, the barrel of the rod was polished and anti-reflection coated for 810 nm. The pump light that was transmitted through the rod was reflected back into the Nd:YAG by a chromium/gold reflective coating on the rod holder opposite each laser bar. The cross section of the rod holder, and the arrangement of the pump sources is shown in figure (4-3). The combination of the three fold pump symmetry with the back reflectors has been shown to result in a pump distribution that

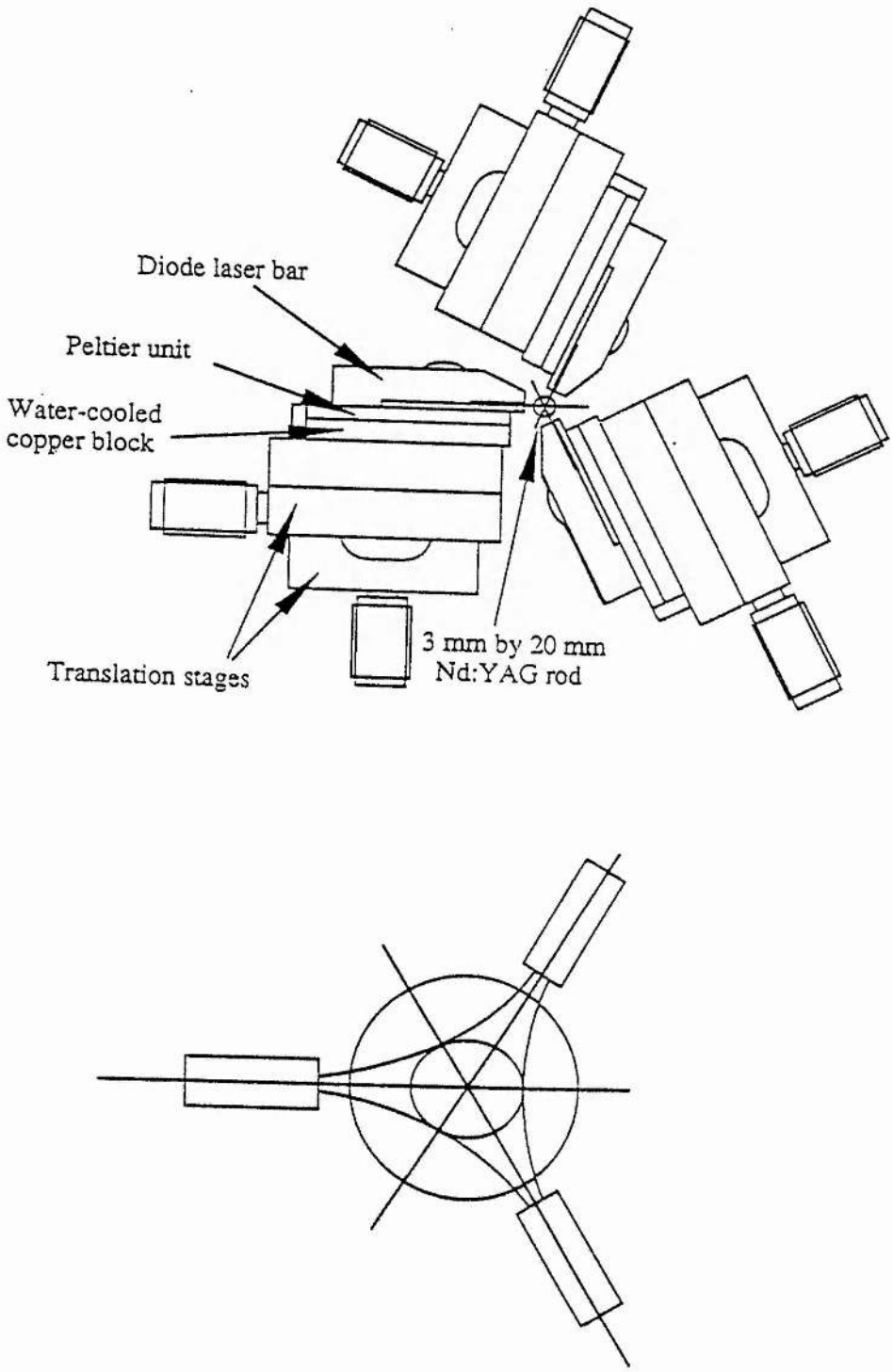

Fig. 4-3 The schematic diagram of the arrangement of diode-laser pump sources.

makes possible the efficient extraction of optical gain in the fundamental transverse mode[2].

The design of the cavity for the Q-switched laser was undertaken with the aim of producing TEM_{oo} pulses with as high a peak power as possible. Thus the cavity was designed to be as short as possible to reduce the Q-switched pulse length meanwhile simultaneously satisfying two other requirements. These were (1) that the $1/e^2$ beam waist within the Nd:YAG rod should be 1 mm to obtain fundamental transverse mode operation with minimum clipping loss and (2) that the peak power within the lithium niobate Q-switch should be less than 300 MW/cm^{-2} to avoid optical damage. The cavity design that best satisfied these requirements was a 30 cm long standing wave cavity with highly reflecting concave and convex mirrors. A rotatable quarter wave plate and an air-spaced polarizer provided optimisation of the output coupling (~20 %) from this cavity. The Q-switching process in this device is the following. When a high voltage is applied to the Pockels cell, the laser cavity has a low Q since the cell then acts as a quarter wave plate. When the high voltage is removed using a Krytron switch, the Pockel cell no longer shown birefringence and the cavity Q increases. The laser emits a beam, extracted from the cavity through the output coupler formed by the polarizer and the quarter-wave plate.

The output Q-switched pulse energies was measured to be 10.7 mJ with 17 ns (FWHM) duration at optimised adjustment. The output beam profile is close to Gaussian and hence a single transverse mode (TEM_{oo}).

The basic design for the six double stack diode laser pumped (144 mJ-input triple-pumped) laser is the same as for the 72 mJ input laser. There are six SDL double-stack laser diode bars mounted in pairs (side-by-side) arranged symmetrically around the 20 mm long by 3 mm the diameter cylindrical Nd:YAG rod. Each pair of diode bars is mounted on the same copper heat sink and consequently the temperature of both is controlled by only one Peltier unit. Also no coupling optics were used between the bars and the rod.

The diode laser pumped Nd:YAG laser was not fully optimised in the latter case. There are some problems which need further consideration and practical improvement. The flexibility of mechanical adjustment of the system is poor, the position of the diode lasers relative to the Nd:YAG rod being virtually fixed. With the previous cavity configuration the intra-cavity energy density was high, which damaged optical

components in the cavity, particularly in the Q-switch. To avoid this damage the $LiNbO_3$ Q-switch was replaced by a KD*P Q-switch. The Q-switched pulse extraction efficiency was low, only 50% compared to the long pulse situations. The stability of the Q-switch high voltage driver is poor, which also affected the output stability. The diode pumped Nd:YAG laser output characteristics are listed in table (4-2).

Table 4-2 The output characteristics of the diode pumped Q-switched Nd:YAG laser

Pump Module (mJ)	Long Pulse Energy (mJ)	Output Energy at 1064nm (Q-Switched) (mJ)	Q-Switched Pulse length (ns)	Output power at 1064nm (MW)	Mode Quality
72	14.6	10.7	17	0.6	TEMoo
144	29.0	12.0	8	1.5	TEMoo

The output pulse-width was measured in the latter case using a vacuum photo-diode (ITL S-1)†, to be 10 ns. This is much shorter than that of the three diode bar pumped case. The maximum output energy was 12 mJ, corresponding to the peak power of 1.5 MW. Although there is clearly scope for improving the efficiency of this laser, particularly when used in Q-switched mode, the pulse power/energy was delivered in TEMoo mode, and as such was adequate for developing the nonlinear optics.

4.3 Second harmonic generation

The second harmonic generation technique has been extensively developed in recent years. Some excellent results for variety of configurations, i.e. Q-switched[3], mode locked[4] and even CW[5], have been reported by many authors. Second harmonic conversion efficiencies of 50 % are now very common when employing the newly developed nonlinear optical materials. Among these materials the type II KTP and the type I LBO have been paid much attention for doubling the 1.064 μm Nd:YAG

†Please see commercial literature of Instrument Technology LTD. (UK), 1991

laser[6][7]. It is well known that KTP has a high effective nonlinear coefficient, and is suitable for use in the low/middle power range, while NCPM LBO with a zero walkoff angle and high damage threshold is suitable for use in high power cases[8]. Both were considered in our original design and were compared in experiment investigations. We are interested in not only the converted green light, but also in the unconverted residual 1.064 μm wave in the next step which is the sum frequency mixing.

The type II phase matched KTP crystal was from Shan-Dong University of China. It was grown by the flux growth method, was 5 mm long, had a 5 x 5 mm^2 optical aperture, and was cut for a phase matching angle of $\phi = 23^o$. The crystal's two optical faces were coated for high transmission at both of 1.064 μm and 532 nm. Unfortunately the coatings turned out to be not as damage resistant as the crystal. Eventually the crystal was repolished but left uncoated to avoid this problem. The KTP crystal was mounted on suitable rotation and translation stages for easy of alignment.

The type I non-critical phase matched LBO crystal was from China as well, and was provided by FC Castech Inc., Fuzhou, China. The LBO crystal was cut at $\theta = 90^o$, $\phi = 0^o$. The pump beam propagated along the optical principal axis x, and was linearly polarised along the y axis. The polarisation direction of the generated green light along the z axis. This LBO crystal had dimensions $y \times z \times x = 3 \times 3 \times 14$ mm^3, and the two optical faces were uncoated. The crystal was fitted into a carefully designed thermally controlled oven to adjust the phase matching temperature. The oven was made of stainless steel and thermally controlled to better than $\pm 0.4\ ^oC$. A holder made of PTFE was used for thermal insulation. A 3 mm diameter hole on both sides of the oven and holder allowed the focused pump and its harmonic to pass through conveniently. The use of a small hole minimised possible thermal gradients on the crystal's optical surfaces. The maximum temperature of the oven was set at 160 °C.

It is well known that compared to the critical phase matching situation the advantages of the non-critical phase matching situations are that Poynting vector walkoff is eliminated and large acceptance angles obtained, thus making the doubling process more easier and more efficient. The disadvantage compared to normal phase matching processes is the need to hold the crystal at an elevated temperature of 150 °C[9]. Over long term operation we have found that the crystal-colour slightly yellows, but without significant loss of conversion efficiency.

The second harmonic generation experiments were carried out using the flash-lamp pumped and the diode laser pumped Nd:YAG lasers. When the KTP crystal was used as the doubler, and with given pump energy around 10 mJ, the SHG conversion efficiency was significantly higher than in the case of LBO. Experimentally, 66 % maximum conversion efficiency was obtained with 12 mJ energy (in the flash-lamp pumped scheme), 12 ns pulse width and 350 μm pump spot size, corresponding to the 260 MW/cm^2 peak power density. Theoretically, a 90 % conversion efficiency is predicted under these circumstances (please see Appendix I). However, the 1.064 μm pump beam was neither accurately Gaussian profile nor a plane wave, and hence was not a TEMoo mode. It was thus different to the theoretical modelling conditions. The multi-mode pump beam has a dephasing effect on the frequency conversion process which decreases the conversion efficiencies[10]. Another reason may be the tolerance in the measurement of the pump spot size. This is a quite an old topic, but until now this technology has not been significantly improved. Burn patterns on thermal paper or exposed polaroid film, or pin-hole-scanning, or the use of a CCD camera, all of them still have some restriction to use particularly in high power/energy cases. During the experimental investigation we observed that with a more tightly focused pump beam in the KTP crystal (using a lens with focal length f = 500 mm instead of the lens with focal length f = 750 mm), the conversion efficiency increased further. There is hence no saturation effect, unlike the theoretical predications, for the case when the focal spot size is smaller than 300 μm (corresponding to the mean power density of 350 MW/cm^2) when the conversion efficiency is expected to saturate. Damage on the coating and in the bulk of the crystal prevented further investigation of tighter focusing.

In the diode laser pumped cases the maximum conversion efficiency obtained was around 60 % with a 8 mJ, 17 ns pulse of 280 μm spot size, corresponding to a mean power density of 165 MW/cm^2. This figure is much closer to the theoretically calculated result (please see Appendix I). It is clear that the improvement in SHG frequency conversion efficiency was due to the improvement in the pump beam quality.

Using the LBO crystal the SHG conversion efficiency approached ~60 % when the pump intensity was over 470 MW/cm^2 (multi-mode). This is poor compared to the performance of KTP. These results can be explained by the different effective non-linear coefficients of KTP and LBO, which are 3.18 pm/V[11] and 0.9 pm/V[12] respectively. A relatively longer LBO crystal (14 mm) somewhat compensated for this. The phase matching temperature for doubling 1.064 μm radiation in this NCPM LBO crystal was found to be 149 ± 2 °C. In these investigations a thermocouple was used

for measurement, a digital meter was used for display, and the temperature reading resolution was estimated to be less than ± 1°C. The measured results are in good agreement with those reported by Ukachi et al[9] and Huang et al[13]. The full width of the temperature tuning curve was found to be around 3.6 °C, corresponding to a temperature acceptance band width ($\Delta T \cdot L$) of 2.5 °C-cm for crystal length 14 mm. Generally we have found that SHG frequency conversion efficiency was higher when the diode laser pumped Nd:YAG laser was used as the pump source. For the case of the diode laser pumped Nd:YAG laser, the agreement between theoretically calculated and experimentally observed second harmonic generation is much better than in the case where a flashlamp laser is used. This is due to the much improved beam quality in the former case. The typical output performance of SHG has been listed in table (4-3).

Table 4-3 The output energy of 532 nm green light and the conversion efficiency from 1.064 μm to 532 nm with different SHG modules.

1064 nm (mJ)	532 nm (mJ)	SHG Medium	η_{eff} (%)
12.0 (low order mode)*	8.0	KTP(II)	66.6 (Max.)
7.8 (TEMoo)**	4.7	KTP(II)	60.2
21.9 (Multi-mode)*	13.3	LBO(I)	60.7

* With flash-lamp pumped Nd:YAG laser source, 12 ns pulsewidth, and ~350 μm spot size.

** With diode laser pumped Nd:YAG laser source, 17 ns pulse width, and ~280 μm spot size.

4.4 Establishment of 355 nm pump source

Theoretically it is well known, that sum frequency mixing in a nonlinear medium can be obtained by meeting the conditions of photon energy conservation and momentum conservation (please see Appendix I). By the energy conservation relations and in particular for the case of frequency mixing of the 1.064 μm infrared wave and its second harmonic wave we know that the optimum ratio of the green light intensities to the infrared light intensities in the mixing crystal should be 2:1. The momentum conservation condition depends upon what type of geometry is to be employed in the

mixing crystals, which further determines the polarisation directions of these two radiations. For efficiently generating the third harmonic wave, other conditions also need to be met as we have discussed in the previous chapter, and there can be summarised in terms of a figure of merit.

A type II frequency mixing geometry has recently been identified in LBO for the generation of 355 nm radiation from incident 1.064 μm and 532 nm radiation[14]. The advantage of the type II geometry compared to the type I geometry is a reduced walkoff angle, and as is apparent from the calculations, a minimum value for the type II geometry of 0.55° is obtained under the phase matching conditions (please see Appendix III). The other advantage of this geometry is the comparatively large angular acceptance bandwidth which is calculated to be 2.5 mrad in the yz phase matching plane, and is, of course infinite, to first order, in the orthogonal plane. The effective nonlinear coefficient has been calculated to be 0.8 pm/V. It is slightly lower than the type I geometry, but, considering all the above parameters we find that the figure of merit of the type II geometry is considerably larger than the type I geometry.

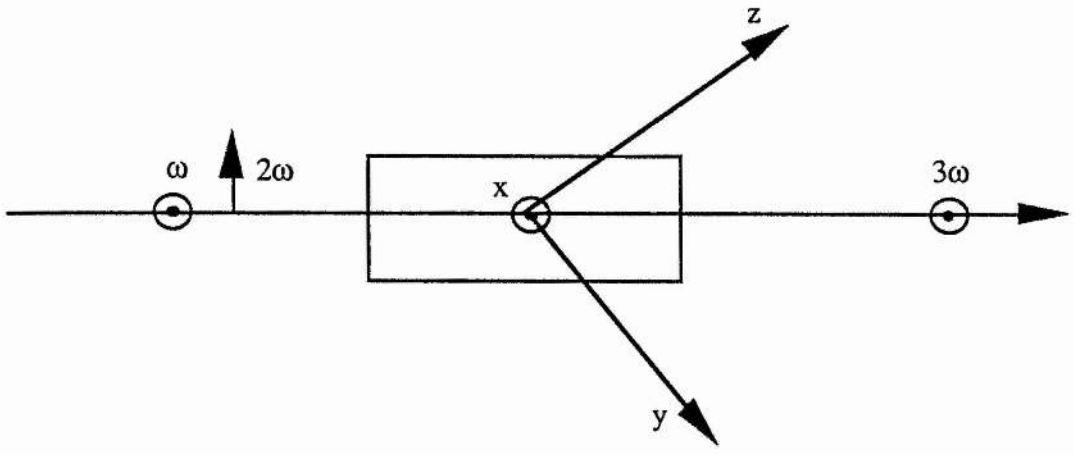

Fig. 4-4 Type II phase matching geometry for sum frequency mixing of 1.064 μm and 532 nm radiation in LBO.

The type II geometry SFM LBO crystal used had dimensions of 5 x 5 x 15 mm^3, and was also supplied by FC Castech Inc., Fuzhou, China. This crystal was cut at θ = 42.2°, ϕ = 90°. The polarisation states of 1.064 μm (ω), 532 nm (2ω), and 355 nm

(3ω) waves are shown in figure (4-4) along with the principal axes of the crystal. The Sellmeier equation coefficients used in this calculation was from Chen et al[15].

For the experimental investigation we have used two different tripling geometries as shown in figure (4-5). These two geometries are believed to be the best selections. The first geometry uses a high efficiency KTP doubling crystal, but the problem is that the second harmonic wave and the residual fundamental wave polarisation directions are not ideal for the following type II frequency mixing crystal. This mismatch reduces the conversion efficiency. The second geometry uses a type I NCPM LBO as a doubling medium. In this alternative frequency tripling geometry the polarisation states of both the generated second harmonic radiation and remaining fundamental radiation are ideally matched to the subsequent sum frequency mixing process in the CPM type II LBO crystal. However, because the doubling efficiency is lower in the LBO crystal at this modest pump level compared to the situation in a KTP, the third harmonic conversion efficiency was not improved. These conclusions are, of course, dependent on the power available at the fundamental frequency, and, as this increases, the LBO may eventually be superior to KTP as a doubler. However, a KTP(II)/LBO(II) frequency tripling geometry has been used to efficiently generate the 355 nm ultraviolet and has been used as an OPO pump source throughout this project.

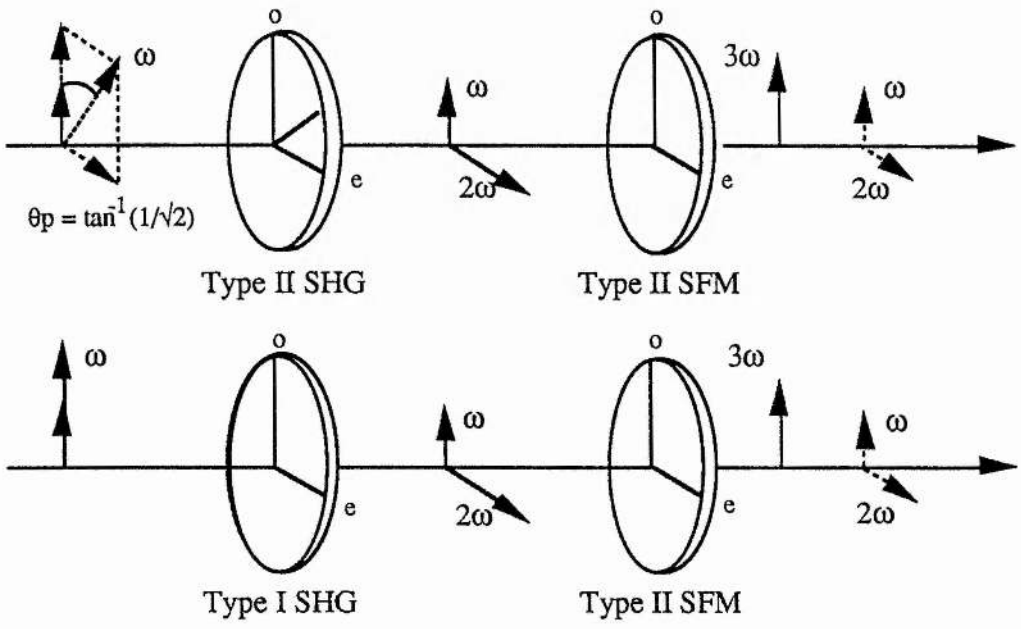

Fig. 4-5 The phase matching configuration with TYPE II (SHG)/TYPE II (SFM) and TYPE I (SHG)/TYPE II (SFM) geometries.

The arrangement of the frequency tripling experiment is shown in figure (4-6). There are no additional optical components for compensating the fundamental and second harmonic polarisation, so that they are orthogonal for optimised frequency mixing.

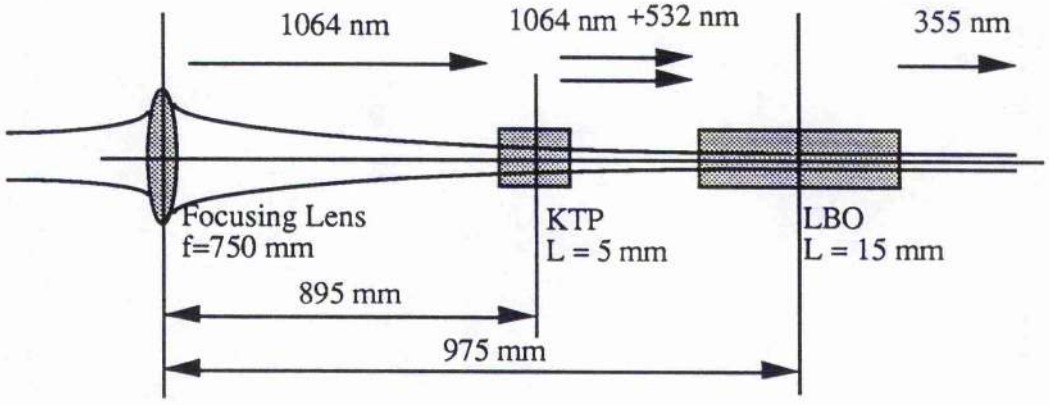

Fig. 4-6 Geometry for frequency tripling.

In the KTP(II)/LBO(II) frequency tripling geometry, the input radiation at 1.064 μm was linearly polarised, and was initially oriented for optimum second harmonic generation, i.e. with its electric vector at 45° to the KTP z-axis. In this case equal number of photons at the fundamental frequency ω are incident in each of ordinary and extraordinary directions, and some fraction of the incident photons combine to form 2ω photons in the e-direction. The remaining radiation at ω emerges as two linearly polarised components of equal magnitude in the o- and e-directions, but only o-photons at ω can frequency mix with e-photons at 2ω (extraordinary) in the following type II geometry tripling crystal. It is easy to see that, in this case the optimum frequency doubling efficiency should be 50 %, and ideally the maximum overall efficiency should be 75 % (please see Appendix I).

However, the residual radiation at 1.064 μm leaving the KTP crystal was generally found to be elliptically polarised, and, as expected, this elliptical polarisation state

changed with the crystal temperature (the KTP is acting as a waveplate). On changing the KTP temperature from around 20 °C to 36 °C, the polarisation state rotated 90°, and underwent changes from elliptical to circular, and to elliptical again. It was never observed to be linearly polarised, and this is believed to be due to slightly inaccuracy in the crystal orientation or in the alignment of the pump beam polarisation. However, as expected, the intensity of the o-component of the residual output at ω did not change. Hence, the subsequent sum-frequency mixing stage is insensitive to the polarization changes discussed above. On increasing the temperature further, the above cycle repeated, so that it was not possible by this means to further increase the component of the electric vector of the fundamental wave in the ordinary direction (KTP z-axis). Throughout the above temperature changes, as expected the polarisation state of the generated radiation at 532 nm stayed constant, namely linearly polarized with electric vector in the xy-plane (extraordinary wave). The above behaviour of the polarisation state of the residual radiation at 1.064 μm has implications for the subsequent step of sum frequency mixing.

An efficient method for further increasing the frequency conversion efficiency with the type II/type II tripling geometry, namely a "polarisation-mismatch" scheme, has been discussed by Craxton[16]-[18]. In this geometry, the incident electric field at ω is linearly polarized at an angle $\theta_p = \tan^{-1}(1/\sqrt{2})$ to the o-direction (KTP z-axis). This ensure that two o-photons are input for every e-photon, and for a suitable choice of doubler thickness the e-photon will combine with the o-photon to give one e-photon at 2ω, leaving one o-photon at ω unconverted. Hence this doubler output is suitably polarized for direct input to a type II tripler. Using this method and taking account of material absorption and pump beam divergence losses, Craxton has proposed that the overall conversion efficiency could be 90 %. However, 80 percent energy conversion efficiency has been demonstrated using this tripling scheme for fusion applications, but with large beam spot size and high pump intensities[4].

Our experimental conditions are very different to reference [4]. In our case the pump energy at 1.064 μm was around 10 mJ, the beam spot size was generally smaller than 300 μm, and the maximum SHG conversion efficiency was ~60 %. Using the "polarization mismatch" scheme in our system, we have demonstrated an overall conversion efficiency of around ~35 % to the UV. In our experiment, the main constraint is low pump energy, and, therefore, in pursuing high conversion efficiency we have to resort to tight focusing, which exacerbates dephasing effects.

Experimentally we found that even using the "polarization-mismatch" scheme, and under the condition of best alignment of the system, only 60 % of the second harmonic radiation takes part in the frequency mixing process.

Some typical experimental results of the SFM conversion efficiencies have been listed in table (4-4). For input energy of the order of 10 mJ, of the order ~3 mJ has been routinely obtained at 355 nm in the ultraviolet, using this type II phase match geometry in LBO, representing an overall efficiency in excess of ~30 % from 1.064 μm to 355 nm. Figure (4-7) shows the efficiency of the optimised tripling as a function of 1.064 μm energy. The maximum overall conversion efficiency was measured to be 33.5 %, and saturation was already beginning at an input energy at 6 mJ. This behaviour to believed to be due to the relatively small pump spot size (~350 μm), which results in large beam divergence and hence large dephasing loss, and thus prevents the conversion efficiency from further increasing. This effect was also been confirmed in the diode pumped situation. In this case the saturation conversion efficiency was found to be around 28 %, corresponding to a spot size in the tripling crystal of ~280 μm; the same power intensity as in the flash-lamp pumped case.

Table 4-4 The output energy of 355 nm ultraviolet and the overall conversion efficiency from 1.064 μm to 355 nm with different frequency tripling modules.

1064 nm (mJ)	355 nm (mJ)	SFM Geometry	η_{eff} (%)
12.0 (low order mode)*	3.5	KTP(II)/LBO(II)	29.1
12.0 (low order mode)*	4.02	KTP(II)/LBO(II)	33.5 (optimized)
7.8 (TEMoo)**	2.2		28.2
10.5 (low order mode)*	3.47	LBO(I)/LBO(II)	33.0 (optimized)

* With flash-lamp pumped Nd:YAG laser source, 12 ns pulsewidth, and ~350 μm spot size.

** With diode laser pumped Nd:YAG laser source, 17 ns pulse width, and ~280 μm spot size.

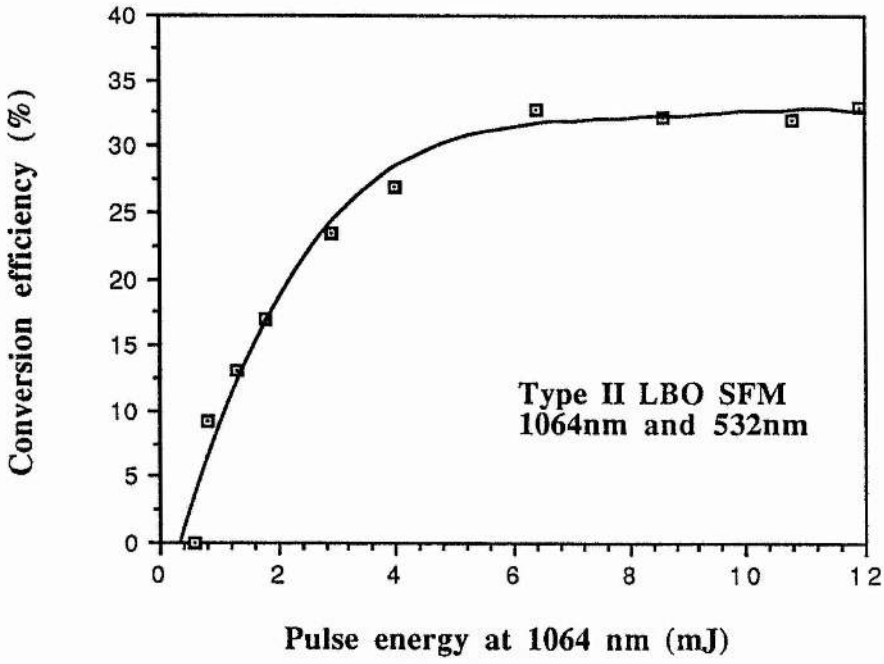

Fig. 4-7 Overall conversion efficiency from 1.064 μm to 355 nm as a function of the pump energy at 1064 nm. These results are for the flash-lamp pumped system.

The pulse width of the converted 355 nm ultraviolet wave has been measured using the vacuum photo-diode to be 8-10 ns (FWHM), and the beam profile as measured by the pin-hole-scanning method was found to be slightly elliptical (see figure (4-8)), but close to the Gaussian distribution.

Clearly, the KTP(II)/LBO(II) third harmonic generation geometry is a remarkably efficient method even for relatively modest pulse energies.

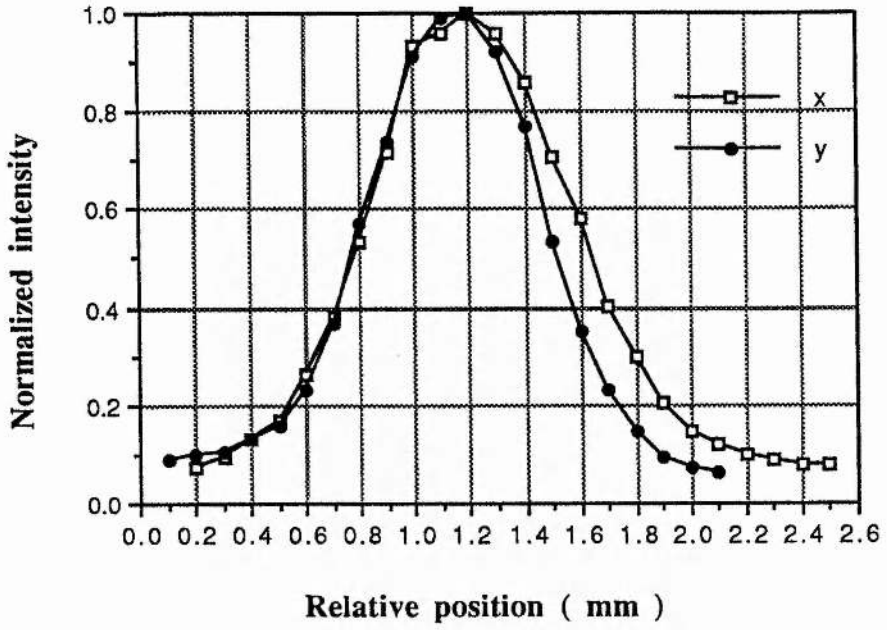

Fig. 4-8 The beam profile of the converted 355 nm ultraviolet wave.

4.5 Establishment of 266 nm pump source

It has recently been shown that the BBO crystal is the best candidate for doubling 532 nm radiation to 266 nm. In our experiment the BBO crystal was cut at $\phi = 47°$ (type I geometry), was 6 mm long, and the two optical faces were not coated. Using the same pump geometry as for frequency tripling, the BBO crystal was placed directly following the doubling crystal, and only a single focusing lens (f = 750 mm) was used to configure the beam through the KTP and the BBO crystals. For this focusing arrangement the beam radius of the 1.064 μm radiation was measured to be 350 μm in the KTP and the BBO crystal. Using this KTP/BBO geometry we have obtained 2.1 mJ of UV radiation of 266 nm with a 5 Hz repetition rate and a 10 ns pulse width (mean power 10 mW). The conversion efficiency was 35 % from 532 nm to 266 nm, and the overall conversion efficiency from 1.064 μm to 266 nm was ~18 % for 12 mJ input pulse energy. When type I NCPM LBO was used as the initial doubler, similar experimental results were obtained. In the latter case the conversion efficiency is ~30 % from 532 nm to 266 nm. We have also found that the 266 nm ultraviolet beam was

significantly non-uniform. It is clear that this is because of BBO's large walkoff angle and small acceptance angle. More tightly focusing the pump wave into the BBO crystal would not improve conversion efficiency but would further reduce the beam quality at 266 nm.

References

[1] The 1992 Buyers Guide
Laser Focus World, 1992

[2] C. J. Norrie
Ph. D Thesis, Dept. Phys. and Astronomy, University of St. Andrews, Scotland, UK, 1991 (unpublished)

[3] Y. S. Liu, D. Dentz and B. Belt
Opt. Lett. **9**, 76, 1983

[4] W. Seka, S. D. Jacobs, J. E. Rizzo, R. Boni and R. S. Craxton
Opt. Commun. **34**(3), 469, 1980

[5] Z. Y. Ou, S. F. Pereira, E. S. Polzik, and H. J. Kimble
Opt. Lett. **17**(9), 640, 1992

[6] J. D. Bierlein and H. Vanherzeele
J. Opt. Soc. Am. B**6**, 622, 1989

[7] S. P. Velsko, M. Webb, L. Davis and C. E. Huang
IEEE J. Quantum Electron. **27**(9), 2182, 1991

[8] F. L. Xie, B. C. Wu, G. M. you, and C. T. Chen
Opt. Lett. **16**(16), 1237, 1991

[9] T. Ukachi, R. J. Lane, W. R. Bosenberg, and C. L. Tang
Appl. Phys. Lett. **58**(15), 1579, 1991

[10] D. Emierl
IEEE J. Quantum Electron. **23**(5), 575, 1987

[11] R. C. Eckardt, H. Masuda, Y. X. Fan, R. L. Byer
IEEE J. Quantum Electron. **26**(5), 922, 1990

[12] J. T. Lin, J. L. Montgomery, and K. Kato
Opt. Commun. **80**(2), 159, 1990

[13] J. Y. Haung and Y. R. Shen
Appl. Phys. Lett. **58**(15), 1579, 1991

[14] B. C. Wu, N. Chen, C. T. Chen, D. Q. Deng, and Z. Y. Xu
Opt. Lett. **14**(19), 1080, 1989

[15] F. L. Xie, B. C. Wu, G. M. You, and C. T. Chen
Opt. Lett, **16**(16), 1237, 1991

[16] W. Seka, S. D. Jacobs, J. E. Rizzo, R. Boni and R. S. Craxton
Opt. Commun. **34**(3), 496, 1980

[17] R. S. Craxton
Opt. Commun. **34**(3), 474, 1980

[18] R. S. Craxton
IEEE J. Quantum Electron. QE-17(9), 1771, 1981

CHAPTER 5

Type II non-critical phase matched lithium triborate optical parametric oscillator pumped at 355 nm and 266 nm

In the demonstration system developed for realisation of the basic concept of all-solid-state which we have described in Chapter 1, the optical parametric oscillator is based on lithium triborate as the nonlinear gain medium, employed in the non-critical phase matching geometry discussed here. The non-critical phase matching geometry in this newly developed LBO crystal was first identified in this laboratory[1][2]. Computation showed that the non-critical phase matching geometry eliminates Poynting vector walkoff while optimising the effective nonlinear coefficient (please see Appendix III). For this reason, it is possible to tightly focus the pump radiation into the crystal, so minimising the pump energy required to reach threshold and ensuring high conversion efficiency.

During the experimental investigations a very low pump energy threshold was demonstrated when this non-critical phase matched LBO optical parametric oscillator was pumped at 355 nm with tightly focused ultraviolet radiation from the frequency tripled diode pumped Nd:YAG laser[3][4]. The threshold was as low as 190 μJ, and after the pump energy reached to two times threshold, the pump depletion reached 40 %. This type II LBO optical parametric oscillator was also pumped at 266 nm wavelength[5][6], which we believe is the first LBO based optical parametric oscillator pumped with this UV radiation. This device generates what we believed is the shortest signal wavelength (306 nm) yet obtained directly from an optical parametric oscillator. This part of the investigation is discussed in section (5.6).

5.1 Pump geometry

The pump geometry used in this investigation is shown in figure (5-1). As we have described in the last chapter, there are two pump sources. One is the flash-lamp pumped Nd:YAG laser, the other is the diode-laser-pumped Nd:YAG laser. The output energy of these pumps have been limited to the same level (i.e. around 10 mJ). The beam quality of these pump waves was different; the former was multimode but of low order, and the latter was TEMoo mode.

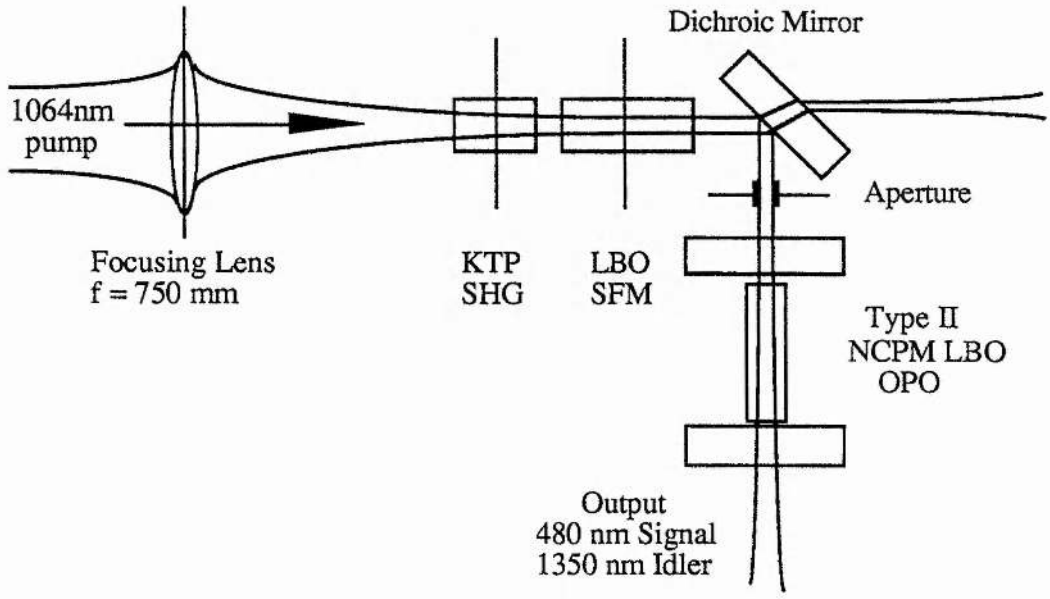

Fig. 5-1 The schematic diagram of the type II NCPM LBO visible OPO pumped by a frequency tripled Q-switched Nd:YAG laser.

The flashlamp pumped Nd:YAG laser was configured for prelase Q-switched operation, as described in Chapter 4. It was operated at a repetition rate of 5 Hz, produced pulses with a full width half maximum (FWHM) of 12 ns, and 12 mJ energy, corresponding to a peak power of 1 MW. The resulting fundamental was frequency tripled with an energy conversion efficiency of 33 % using a 5 mm KTP doubler and a 15 mm LBO tripler, to give up to 4 mJ of 355 nm ultraviolet radiation. The generated UV was then separated from the fundamental and 532 nm green light using a 45° dichroic mirror which gives 99.5 % reflection at 355 nm and 90 % transmission at 532 nm and 1.064 μm. After that, the generated UV was directly used for pumping the optical parametric oscillators. This pump geometry minimised optical loss of the pump radiation by minimising the numbers of optical components used.

The diode pumped Nd:YAG laser has a similar configuration to the flash-lamp pumped Nd:YAG laser. Here, instead of the focusing lens, the 1.064 μm output was inherently focused by the laser cavity configuration, so as to be directly used for harmonic generation and sum-frequency mixing. The diode-laser-pumped scheme results in a more compact and efficient system. However, in order to explore the effects of the beam size on the threshold and generation efficiency, additional focusing optics were used to focus the ultraviolet pump radiation into the OPO cavity. Fuller details of the arrangement are given in section (5.5).

Since some three nonlinear processes are involved in converting the primary radiation from the Nd:YAG laser to tunable output radiation, it is vital to optimise the conversion efficiency at each stage. Optimising the SHG and SFM stages have already been described in the last chapter.

5.2 Type II non-critical phase matching geometry in LBO

The type II non-critical phase match condition in LBO corresponds to the case where $\theta = 0$, $\phi = 0$. The phase matching geometry is illustrated in figure (5-2), where crystal dimensions as used in this experiment are 3 x 3 x 16 mm^3 in the x, y and z directions respectively. The two optical faces were not coated. In this type II scheme, the pump radiation at 355 nm or 266 nm is linearly polarised along the x axis of the crystal, and the signal and idler wave generated are linearly polarised along the y-axis and the x-axis respectively. We have carried out phase match calculations for this geometry using the recently revised Sellmeier equations due to Chen[7], and the

predicted tuning curves for the signal and idler wave are presented in Appendix III, where angle tuning by rotation about both the x-axis and the y-axis are displayed. As described in the Chapter 3, LBO also exhibits temperature tuning, so it is possible to tune the signal and idler wavelength by this means while still maintaining non-critical phase matching.

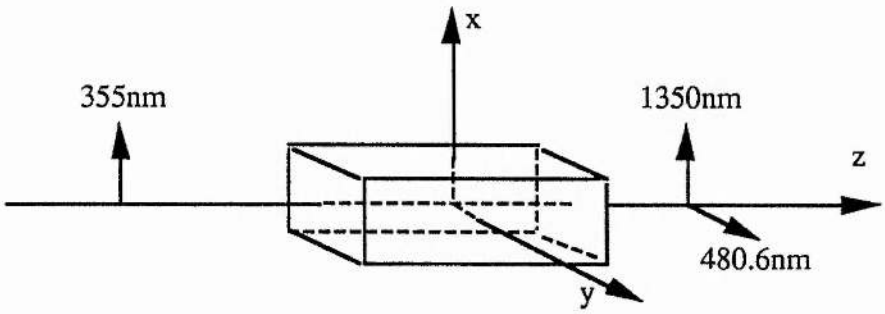

Fig. 5-2 The type II non-critical phase matching geometry in LBO for optical parametric oscillator.

It is well known that non-critical phase matching geometries have some advantages compared to the critically phase matched situations. Firstly, the Poynting vector walkoff is eliminated in this geometry. Secondly, this geometry has a large angular acceptance band which tends to infinity. Thirdly, the effective nonlinear coefficients reaches its maximum values (d_{eff} = 0.89 pm/V). To sum up the advantages above it is clear that this non-critical geometry allows tight focusing of the pump light in the nonlinear crystal, so enabling high energy densities to be obtained at modest pulse energies. In this way it is possible to operate an optical parametric oscillator based on this material at many times threshold, and hence obtain high conversion efficiencies, with pulse energies of the order of 1 mJ.

5.3 Cavity

The OPO cavities used in this experiment were of two types; the simple standing wave cavity formed by plane mirrors and the mode matching cavity formed by curved mirrors. The former one has been used in the investigation of general performance

characteristics such as OPO tuning range, linewidth, and output characteristics. The latter one has been used to investigate the optimum geometry of the OPO cavity when related to the optimum focussing of the pump wave. The Boyd and Kleinman theory has been used through out the analysis[8] (Please see Chapter 2).

5.3.1 Cavity with plane-parallel geometry

The cavity of the optical parametric oscillator in this normal scheme is a simple standing wave cavity formed by two mirrors with reflectivity 95 % at 480 nm (the total output coupling is then 10 % per round trip) which are generally spaced by 18 mm, just slightly longer than the crystal for minimising the pulse build-up time effects. The mirrors are highly transmitting at the pump wavelength of 355 nm, and have only a low residual reflectivity at the idler wavelength of 1.35 μm. The optical parametric oscillator hence operates in singly resonant mode for the signal wave. The radiation generated at 355 nm by the frequency tripling configuration described previously was used to pump the optical parametric oscillator directly without any ancillary focusing optic being introduced. The radius of the 355 nm pump beam at the LBO crystal was measured to be 350 μm in the flash-lamp pumped system, and 280 μm in the diode pumped system.

5.3.2 Cavity with tightly focused pump

As we have described in Chapter 2, for given conditions, including the crystal length, and focused pump spot size, we can calculate the optimum signal spot size (singly resonated OPO) using the theory of Guha et al[9], and from this parameter we can identify the optimum radii of curvature of the cavity mirrors. Also we know from theoretical considerations that for non-critical geometries (B=0), optimum focusing conditions are the same in type I and type II geometries. Therefore, the previously calculated results (which were for a type I geometry) can be used in this analysis.

The curved mirrors used in the experiments were coated the same as the plane mirrors, and among them the smallest radius of curvature of the mirror was 100 mm. The cavity length was generally set up as short as possible to avoid the difficulty of aligning a close to confocal cavity and in order to minimise the pulse build-up loss[10]. The relation between the radius of curvature of the cavity mirrors and the oscillation threshold are discussed in section (5.5).

5.4 Oven and temperature controller

For experimentally investigating the NCPM LBO OPO temperature tuning behaviour, a temperature controlled oven has been used, which is structurally the same as to that used in the type I NCPM LBO SHG experiment; the only difference being that the maximum temperature in the former case was set at 160 °C, and in the later case was set at 210 °C.

The oven's body was made of stainless steel, and had dimensions of ϕ18 x 24 mm. A square hole in the centre of oven was fitted to the size of the LBO crystal (3 x 3 x 16 mm), but with enough free space to avoid mechanical stress on the crystal, even in high temperature situations. A 4 m long nichrome wire with resistance 100 Ω (resistivity = 25 Ω/m) was wound on the outside of the oven's body. Mica was used to separate the wire layers. The oven was insulated by a PTFE holder, with only a 3 mm aperture at each of its ends, sufficient to admit the focused pump wave and to allow the generated signal and idler waves pass through, while minimising the thermal gradients on the crystal's optical surface.

The heart of the thermal controller was supplied by RFL Industries, Inc. (USA), and the system was completed in the Department's electronic shop with the addition of a transformer for safety considerations. A 47 KΩ (at room temperature) thermistor was used as the sensor. However, the curve of oven temperature against the adjustable resistance used to set the oven temperature showed that the linearity was not good enough in the low temperature (~20°C) and high temperature (~200 °C) ranges. Consequently, the resolution in these bands was slightly poor compared to the centre band (50 °C -150 °C). In addition, the stainless steel possesses a low thermal conductivity, so that large thermal gradients were present in the oven's body. The sensor was hence located as close to the crystal as possible. However, when the thermal balance was achieved (generally taking a few minutes), there still existed 1 °C difference between the temperature measured from the sensor and the crystal. Excluding this difference, the reading resolution is estimated to be less than ±1 °C. The average stability of temperature of this thermally controlled oven was ±0.4 °C.

5.5 Performance of type II non-critically phase matched LBO optical parametric oscillator pumped at 355 nm

5.5.1 Pump threshold

The experimental results relating to oscillation threshold are listed in table (5-1).

Table 5-1 The pump threshold versus the pump spot size and the radii of curvature of the cavity mirrors.

	Flash-lamp pumped system				Diode pumped system		
Cavity geometry	Plane	R=3m	R=1.5m	R=0.5m	Plane	Plane	R=0.1m
Pump spot size (μm)	350	350	350	350	280	100	100
Threshold energy (mJ)	(10ns) 0.40	(10ns) 0.36	(10ns) 0.36	(10ns) 0.32	(12ns) 0.42	(10ns) 0.24	(10ns) 0.19
Threshold energy density (J/cm^2)	0.1	0.094	0.094	0.083	0.18	0.79	0.6
Peak power density (MW/cm^2) at threshold	10	9.3	9.3	8.3	15	79	60

The pump power to reach oscillation threshold was investigated as a function of mirror radius of curvature (the two mirrors being maintained identical throughout) and the pump beam spot size. The oscillation threshold was 0.4 mJ for the plane-plane combination, and decreased progressively towards 0.3 mJ as the radius of curvature was decreased to 0.5 m (concave) - this latter value being the minimum observed energy threshold in a flashlamp pumped system and without an added focusing lens after frequency tripling. From the measured pump pulse duration (10 ns, FWHM) and the pump beam spot size (350 μm, half width to the $1/e^2$ point, at the centre of the LBO crystal), the mean threshold energy density and the mean power density for the case of the plane-parallel cavity were determined to be 0.1 J/cm^2 and 10 MW/cm^2 respectively.

The following general observations can be made regarding these results. Firstly, with fixed pump beam spot size, the oscillation threshold in terms of both energy and energy density decreases with decreasing radius of curvature of the cavity mirrors. Secondly, if a plane-parallel geometry cavity is employed, the threshold energy decreases with decreasing pump beam spot size, but the energy density increases rapidly. The conditions appropriate to obtaining low threshold energy can be identified in the table (5-1); namely tight pump beam focusing (100 μm spot) and small radius of curvature mirrors (0.1 m).

However, we can use the Guha theory to analyse these results. If the pump beam spot size is fixed at 100 μm, then we know that the focusing parameter ξ_p at 355 nm wavelength is 0.0354 (L = 16 mm). The optimum focusing parameter ξ_s at the signal wavelength of 480 nm under these conditions is 0.3 (please see figure (2-4)), with a corresponding confocal parameter of b_s = 53 mm. In this case the radius of curvature of the cavity mirrors for a confocal geometry cavity is 53 mm, and the signal wave spot size is 50 μm in the LBO crystal. Under our conditions the radius of curvature of the cavity mirror is fixed at 0.1 m, and hence the focusing parameter ξ_s at the signal wavelength (480 nm) is 0.16 and the signal spot size is 87 μm. However, from the theoretical curve (figure (2-4)) we can see that the optimisable value h_{sm} does not change a great deal when the signal wave focusing parameter ξ_s changes from 0.16 to 0.3, and the signal spot size changes from 87 μm to 50 μm. Hence optimum signal wave focusing was closely approached here.

From the above analysis the conclusions at this stage are that: Firstly, the oscillation threshold obtained in this experiment was close to the minimum value attainable with the restriction that ξ_p = 0.0354; secondly, the oscillation threshold is generally less sensitive to the radius of curvature of the cavity mirrors when the pump beam spot size is relatively large, and more sensitive to the radius of curvature of the cavity mirrors when the pump beam spot size is relatively small, (this is also in agreement to with theoretical analysis); thirdly, decreasing the oscillation threshold further is possible in this particular geometry, which depends upon further tightly focusing the pump radiation into the cavity and carefully designing the radius of curvature of the cavity mirrors accordingly.

5.5.2 Conversion efficiency

The conversion efficiency was investigated as a function of pump energy at 355 nm, and the typical results are plotted in figure (5-3) and (5-4). All of these measurements were carried out with a plane-parallel cavity, and with a pump spot size of 350 μm (10 ns) and 280 μm (12 ns) in the flashlamp pumped system and diode-laser-pumped system respectively.

Experimental investigations in the flashlamp pumped cases have been carried out carefully. Using these results as an example, we now analyse the variation in extraction efficiency for the signal (480 nm) and idler (1.35 μm) waves. For a pulse energy of 3.3 mJ incident on the mirror of the optical parametric oscillator, some 84 % of this energy reached the inside of the nonlinear crystal (the loss being due to mirror absorption/reflection at the pump wavelength and Fresnel losses at the crystal face), and this input energy led to a measured pump depletion of 43 %. Hence the total energy generated in the signal and idler waves internally in the crystal was some 1.2 mJ. On the basis of the ratio of the photon energy at 480 nm to that at 1.35 μm, this energy partitions as 0.9 mJ in the signal wave and 0.3 mJ in the idler wave. The measured energy exiting the optical parametric oscillator in the idler wave was 0.24 mJ, and this represents some 87 % of the generated energy in this wave. Since the idler wave is non-resonant, the only loss it suffers on leaving the crystal is a single pass loss, and this measured extraction efficiency is consistent with the expected single pass losses (Fresnel reflection loss at one face followed by mirror loss at the idler wavelength).The measured energy exiting the optical parametric oscillator in the signal wave (from both ends of the cavity taken together since both mirrors have the same transmission of 5 % at the signal wavelength) was 0.48 mJ, which is 55 % of the internally generated energy in this wave. This lower figure is to be expected since the signal wave is the resonant wave, and the internally generated energy for this wave partitions between the useful output coupling loss of the cavity and any parasitic losses. Parasitic losses, due essentially to Fresnel reflection losses off the crystal faces, are comparable to the useful loss, and so extraction efficiencies for the signal wave of the order observed are to be expected.

Experimental investigations carried out in the context of excimer laser pumped optical parametric oscillators in this laboratory[13], in which the infrared wave (the idler wave) was resonated in the cavity, while the visible wave at 385 nm (the signal wave) exited on a single pass through the cavity (i.e. was non-resonant) showed that

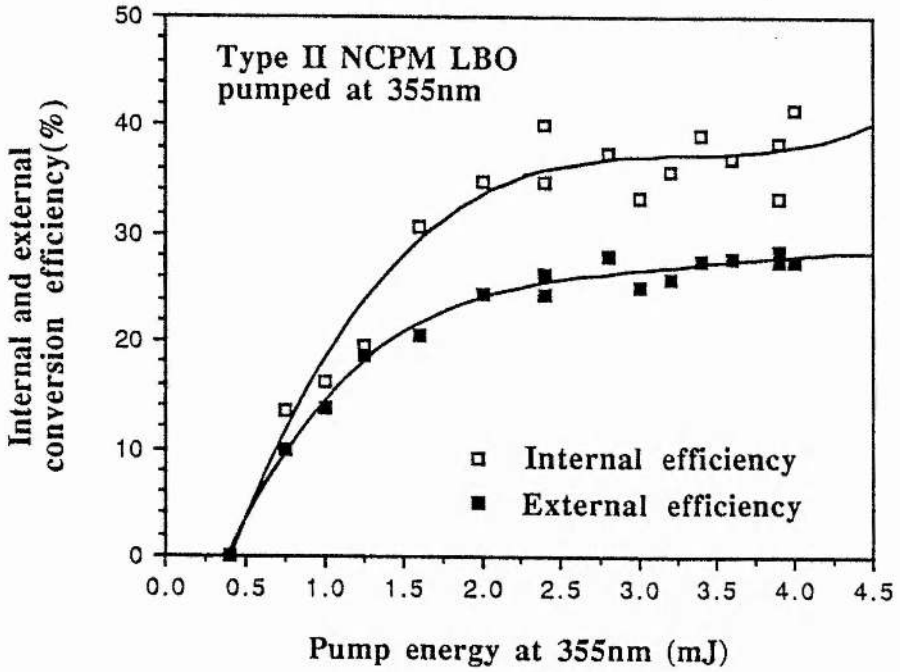

Fig. 5-3 Internal and external conversion efficiency of type II NCPM LBO optical parametric oscillator pumped at 355 nm (flash-lamp pumped scheme).

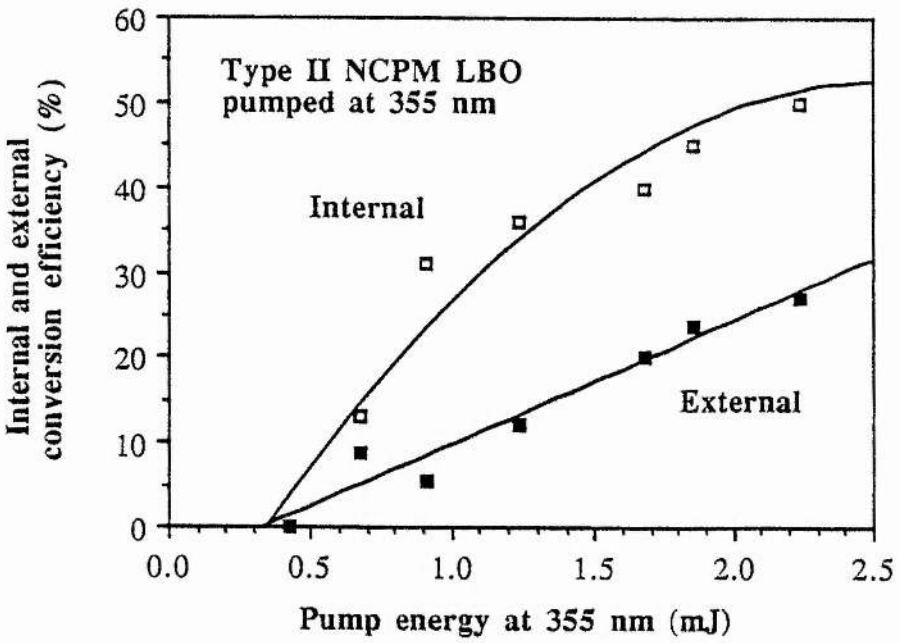

Fig. 5-4 Internal and external conversion efficiency of type II NCPM LBO optical parametric oscillator pumped at 355 nm (all-solid-state scheme).

the extraction efficiency for the signal wave was substantially improved as expected. Through lack of suitable mirrors this configuration could not be explored in the present device pumped at 355 nm. However, the general conclusion is that the wanted wave should be the non-resonant wave in this singly resonant optical parametric oscillator.

The investigation of conversion efficiency with an all-solid-state configuration has yielded similar results to the flash-lamp pumped situation. The oscillation threshold was measured to be 0.42 mJ corresponding to a threshold energy density (mean) of 0.18 J/cm^2, and a threshold power density (mean) of 15 MW/cm^2. When pumping at 5 to 6 times threshold, an internal conversion efficiency of 50 % was observed. The usable outputs at both signal and idler wavelength were measured as 0.39 and 0.22 mJ respectively for a pump energy 2.4 mJ, corresponding to a total external conversion efficiency of 27 %.

However, saturation of the conversion efficiency was found to occur for mean power intensities of ~75 MW/cm^2 in both flash-lamp pumped and diode laser pumped situations, which was around 6 times oscillation threshold, and in this case it is not possible to further improve the conversion efficiency by increasing the pump intensities.

Table 5-2 Saturation intensity with the different pump spot size and cavity geometries.

	Flash-lamp pumped system	Diode pumped system		
Cavity geometry	Plane	Plane	Plane	R=0.1m
Spot size (μm)	350	280	100	100
Saturation energy (mJ)	(10ns) 2.75	(12ns) 2.25	(10ns) 0.70	(10ns) 0.60
Saturation energy density (J/cm2)	0.7	0.91	2.23	1.91
Saturation peak power density (MW/cm 2)	71.5	76.1	223	191
Number of times of threshold	6	6	3	3

The early research work on the conversion efficiency has indicated that for a singly resonant OPO operated under phase matched conditions, an internal conversion efficiency of 100 % at pumping levels of $(\pi/2)^2$ times oscillation threshold may be possible in the uniform plane wave and steady-state limits. However, for a Gaussian intensity profile the maximum conversion efficiency is only 71 %, which may be reached at 6.5 times oscillation threshold[14] (Please see Chapter 2). In our present systems, as we have described previously, the spatial profile of the pumping light in all cases is closely Gaussian. The results presented here exhibit 30 % and 20 % differences from the optimum for the flashlamp pumped and the diode laser pumped situations respectively. However, with pump pulse durations of 10-12 ns, and single pass gains and cavity round trip times of the magnitudes pertaining here, the build up time of the coherent signal and idler waves from noise is a significant fraction of the pump pulse duration, and hence this effect plays a significant role in limiting the total energy depletion of the pump pulse. Figure (5-5) shows, under typical conditions summarised in the figure caption, the variation of the depletion of the pump pulse with time across the pump pulse profile. It is clear that the leading edge of the pulse is undepleted, since during this period the coherent signal and idler waves have not yet built up to intensity levels sufficient to do so. The energy in this region of the pulse is hence unconverted, even though the oscillator is operating above its steady-state oscillation threshold, and, as a result, the average internal conversion efficiency is limited to below that expected for the steady-state case[13]. Conversion efficiency is also limited by high intra-cavity gains, since now back conversion (the signal and idler waves recombined in a sum frequency mixing process) may start to occur in the peak intensity regions before the forward conversion is complete in the lower intensity regions of the spatial Gaussian profile of the pump wave.

The 10 % differences in conversion efficiency between flashlamp pumped and diode laser pumped situations is believed to be due to the difference in beam qualities. In the former case due to the poor beam quality, dephasing loss is more significant, leading to low power conversion efficiency.

5.5.3 Temperature tuning behaviour

The temperature tuning of the OPO has been investigated over the limited range from 22 ^{o}C to 200 ^{o}C (Studies were at this stages confined to the case of the plane cavity geometry). The tuning behaviour of the parametric oscillator was characterised using a MONOSPEX 1000 monochromator and type 931B photomutiplier. The

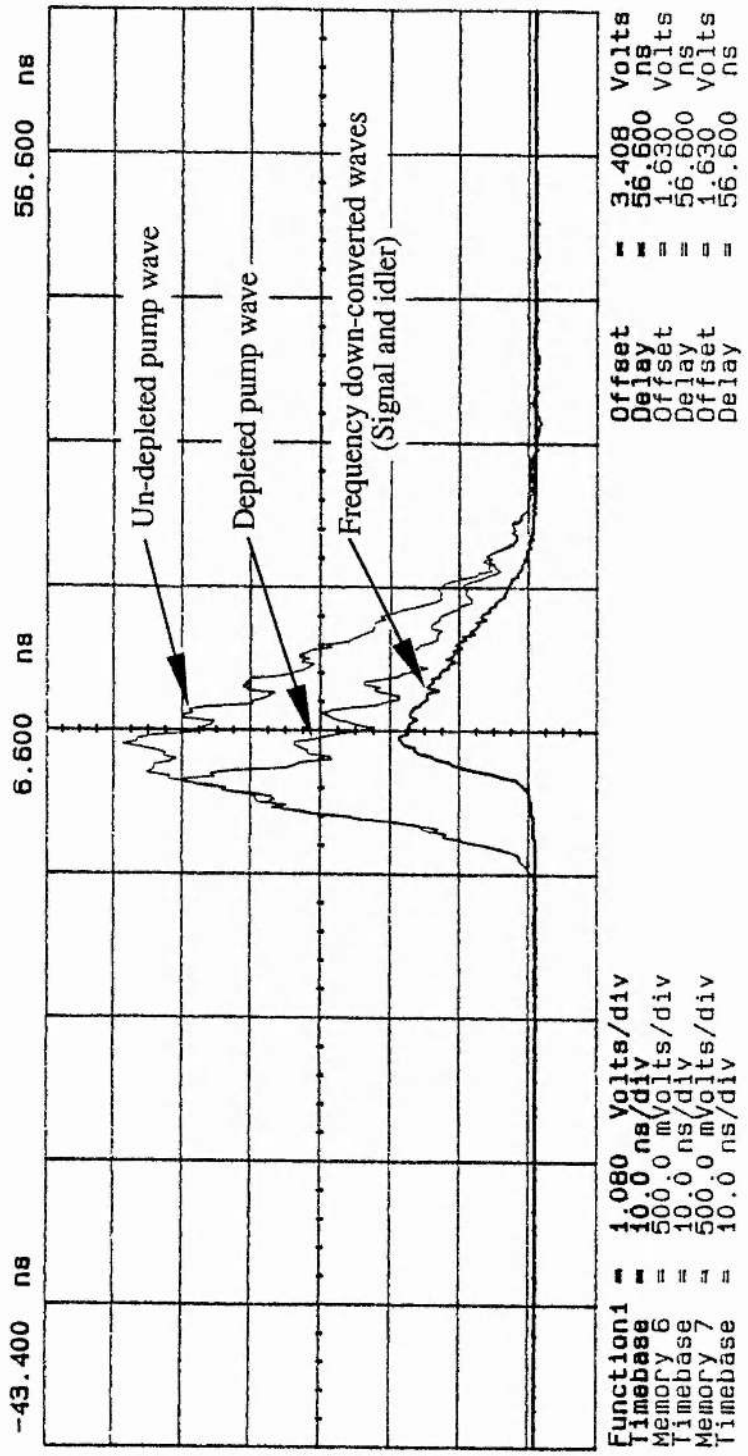

Fig. 5-5 Temporal punp pulse depletion in type II NCPM LBO OPO pumped by a 10 ns 355 nm pulse under conditions corresponding to an internal conversion efficiency of about 30 %.

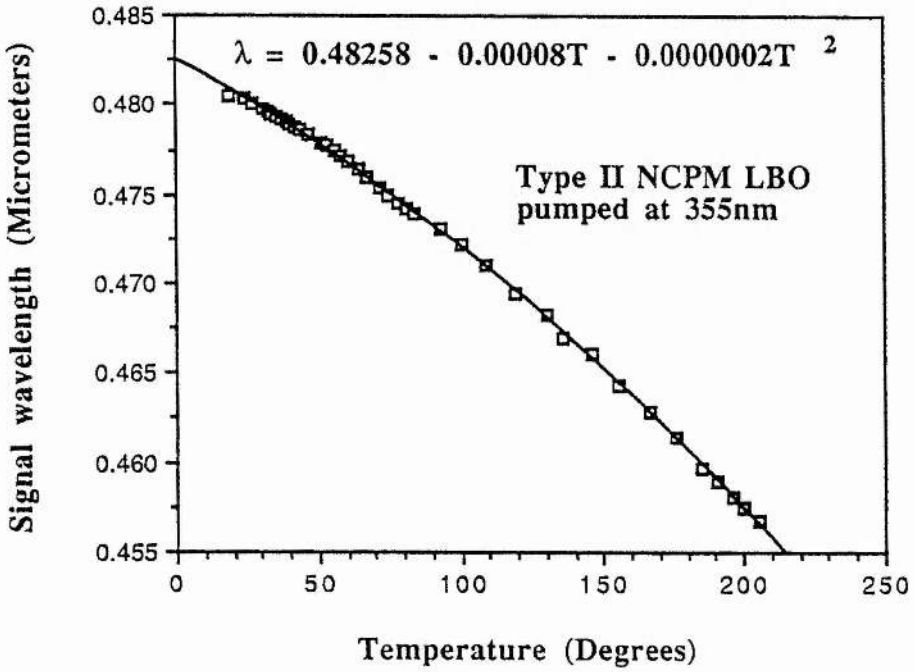

Fig. 5-6 Signal wavelength tuning curve as a function of crystal temperature.

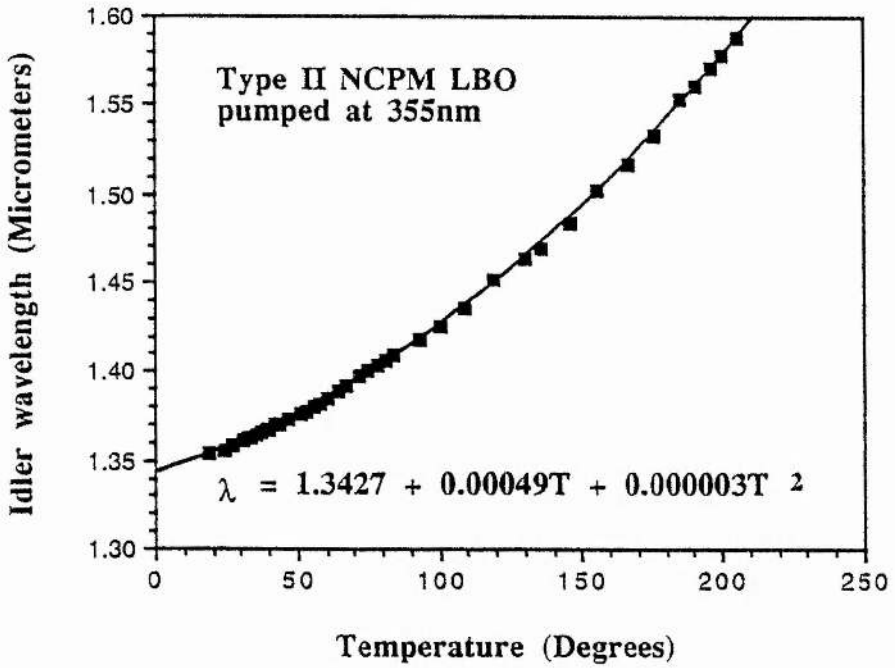

Fig. 5-7 Idler wavelength tuning curve as a function of crystal temperature.

birefringence of the crystal alters with the change of temperature to give non-critical phase matching at different wavelengths. The results for the signal (blue) wavelength are shown in figure (5-5), where the 180 °C change in temperature results in a shift from 480 nm to 457 nm, a rate of some -0.11 nm/°C (the negative sign indicating decrease in the signal wavelength with increasing temperature) around room temperature, and with a complementary tuning rate for the idler wave in the infrared of +0.87 nm/°C. The idler wavelength likewise is expected to change from 1.35 μm to 1.59 μm under the same conditions. At 20 °C we measured the signal wave wavelength to be 480.6 nm ±0.2 nm, close to the value of 481 nm expected from the Sellmeier equations given by Chen[7]. The temperature tuning range was limited by the band width of the dielectric coatings of OPO cavity mirrors, as well as by the pump energy. The threshold was significantly higher on the short signal wavelength side. Extensive tuning ranges are possible since LBO can be safely operated over a temperature range from + 200 °C to -30 °C, and possibly extending from +300 °C to -40 °C[15]. Figure (5-6) and figure (5-7) shows the signal and idler wavelength temperature tuning dependence respectively.

5.5.4 Linewidth

The spectral linewidth of the signal wave at room temperature has been measured using a MONOSPEX 1000 monochrometer and type 931B photomutiplier. The results shows that when the OPO is operating near 480 nm, the central peak has a full width at half maximum of 0.2 nm (FWHM). Further narrowing of the linewidth is possible using a frequency tripled, injection seeded Nd:YAG laser as pump, when Hanson et al have demonstrated a linewidth of 0.02 nm, corresponding to several axial modes of the resonated signal wave[16].

5.5.5 Characteristics of output beam

The angular divergence of the signal wave at 480 nm was deduced from the spot size which was measured in the far field (for the plane-parallel cavity). It was approximately 10 mrad (FWHM), which is of the same order as that of the UV pump wave. The long term output stability was not measured because of variations in the pump intensities occasioned by the sensitivity of the frequency tripling process to fluctuations of the room temperature. Thermal stabilisation of the two crystal used for frequency tripling is required, but was not implement here. The temporal behaviour (pulse width) of the signal wave has been measured in different cases, and was found

to be generally around 2 ns narrower than the pump pulse width when the pump energy was around oscillation threshold, and sensitive to the pump intensity and OPO cavity length. High intensity in pump or long cavity length generally means a large pulse width.

5.6 Performance of type II non-critical phase matched LBO optical parametric oscillator pumped at 266 nm

Pumping of OPO's with radiation at 266 nm has previously been demonstrated by a few research groups, most recently by Bosenberg et al[17] for the case of type I phase matching in β-barium borate (BBO), but high threshold resulted from this critical phase matching geometry. We were the first to report an optical parametric oscillator based on pumping the new optically nonlinear material lithium triborate with radiation at 266 nm [5], and this device generates what we believe is the shortest signal wavelength (306 nm) yet obtained from an optical parametric oscillator.

As with the OPO pumped at 355 nm, the experimental investigation were carried out with both flashlamp pumped and diode laser pumped Nd:YAG lasers. However similar experimental results were obtained in both cases under conditions of similar pump and cavity geometry, and therefore we do not further distinguish between flashlamp pumped and diode-laser pumped situations.

The 266 nm ultraviolet pump wave was provided by frequency quadrupling the output of a Q-switched Nd:YAG laser. Because the BBO crystal has a small acceptance angle and large walkoff angle, the generated 266 nm wave was significantly elliptical and non-uniform (see Chapter 4 for a fuller characterisation of the UV pump beam), which is believed to somewhat affect the OPO process. The OPO cavity was generally 22 mm long with two plane mirrors coated for high transmission at wavelengths of 266 nm and ~1.7 μm and >95% reflectivity for wavelengths from 300 to 320 nm. The OPO hence was operated singly resonant.

The OPO threshold was measured to be 0.5 mJ (at 266 nm), corresponding to a mean power density of 10 MW/cm^2. The internal and external conversion efficiency as a function of pump energy was investigated, and is shown in figure (5-8). At about 3.5 times threshold, we obtained pump depletions around 25 %. However, the external efficiency (useful signal and idler output) was limited to around 8 %. This can be

largely, but not entirely, accounted for as parasitic loss of the signal wave through Fresnel reflections from the crystal faces in competition with the useful output coupling of this wave via the cavity mirrors (5 % at each mirror). Other possible sources of parasitic loss include crystal absorption, and this requires further study.

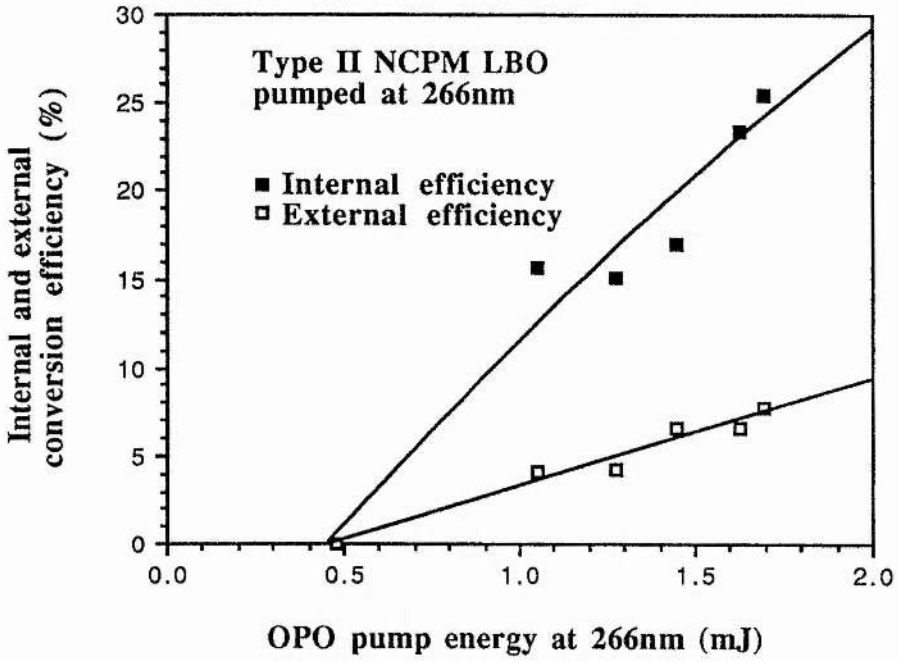

Fig. 5-8 Conversion efficiency (Internal and External) as a function of input pump energy (plane-plane cavity, crystal length 15 mm, mirror reflectivity 95 % at 314 nm).

We investigated the temperature tuning of the device over the limited range 20 °C to 200 °C, and results are given in figure (5-9) and (5-10). The temperature tuning rate measured was around -0.04 nm/°C in the UV, and this implies a rate of about +1.3 nm/°C in the infrared. We measured the wavelength of the signal wave at 20 °C as 313.8±0.2 nm, to be compared with the calculated value of 314.0 nm using the Sellmeier equations given in reference[7].

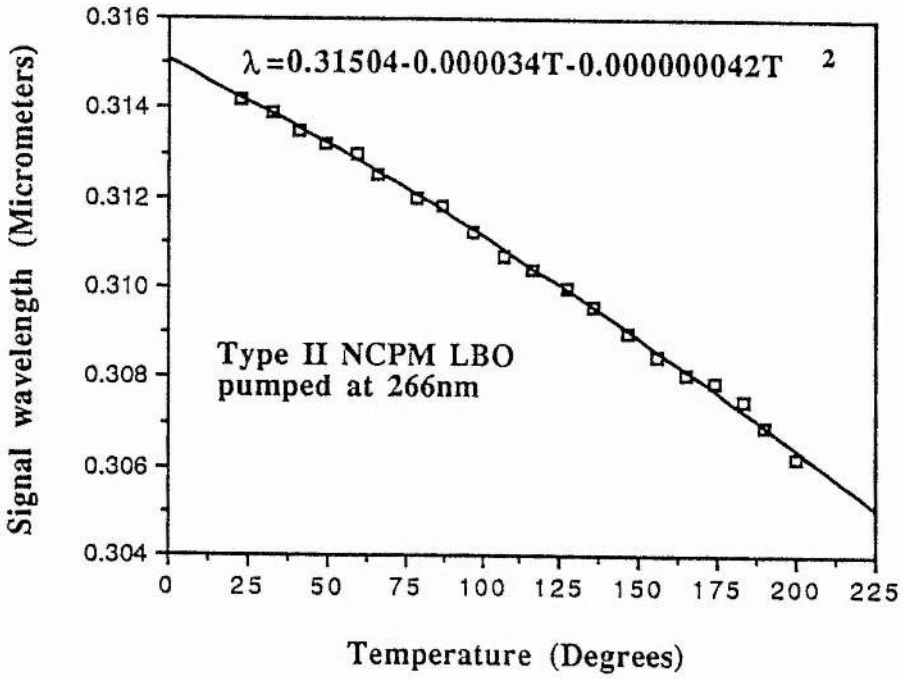

Fig. 5-9 Temperature tuning of signal wave, type II NCPM LBO OPO pumped at 266 nm.

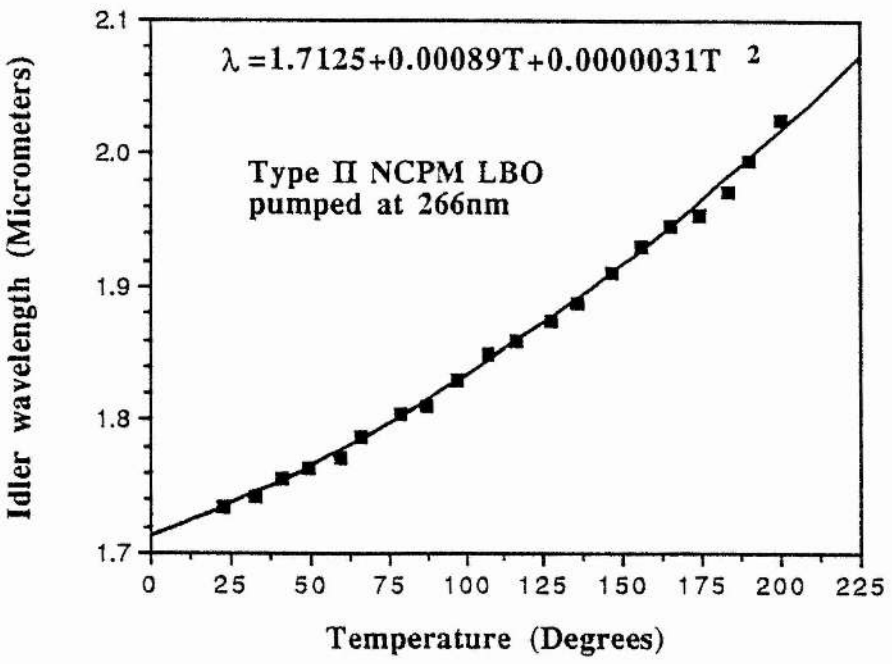

Fig. 5-10 Temperature tuning of idler wave, type II NCPM LBO OPO pumped at 266 nm.

The spectral linewidth of the OPO was very narrow, and was less than the resolution of the monochromator used (0.1 nm). Examination of the output with an 5 mm etalon showed that generally the device oscillated on only 2 or 3 axial modes of the OPO cavity (these modes are spaced by about 0.15 cm^{-1}), and, on occasions, the device operated single axial mode (see figure (5-11)). It might be possible using a single mode pump source and without any line narrowing components and mode control elements, to operate the device on single axial mode. Due to lack of a single axial mode pump source at the time, this prediction has not been experimentally verified.

The experimentally measured tuning rate and linewidth are listed in table (5-3).

Table 5-3 Frequency tuning rate (temperature tuning) and linewidth in type II non-critical phase matched LBO optical parametric oscillator.

Pump wavelength (nm)	Signal wavelength (nm)	Tuning rate (nm/oC)	Linewidth (nm)
355	480	-0.11	~ 0.2
308 [13]	385	-0.07	~ 0.1
266	314	-0.04	< 0.1

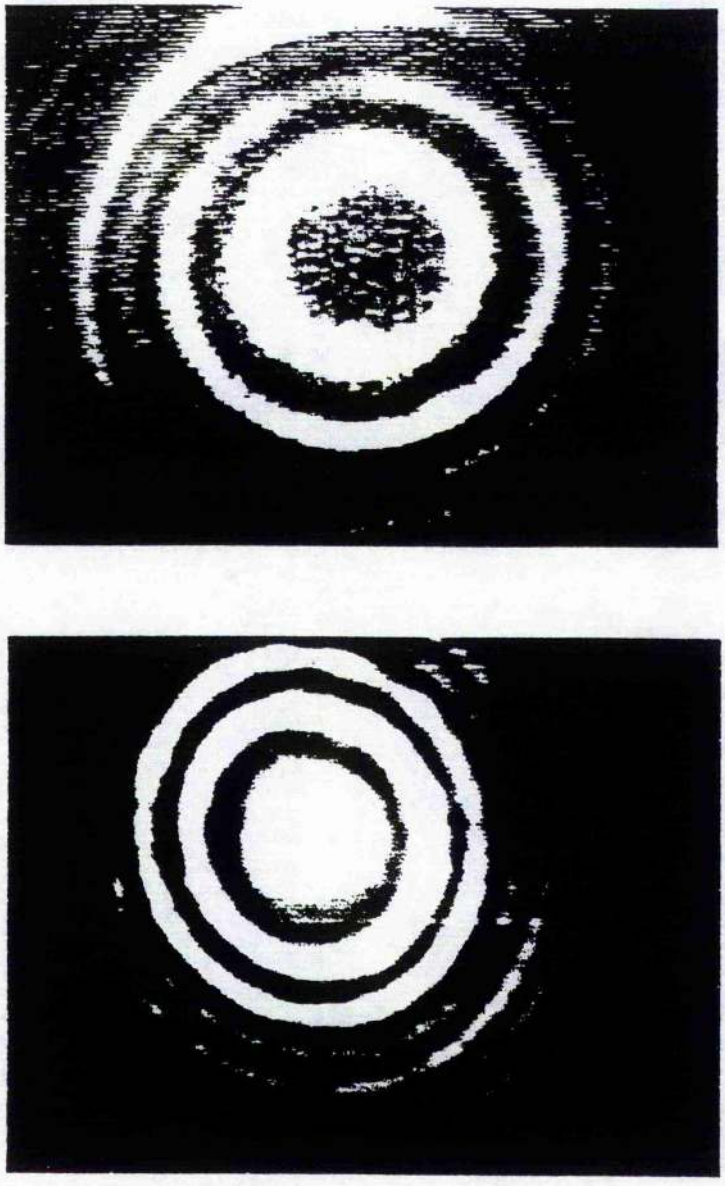

Fig. 5-11 Interference fringes formed by signal wave at 314 nm with a 5 mm etalon. The photograph was taken from a CCD camera.

References

(1) M. Ebrahizadenh, G. Robertson and M. H. Dunn
In conference of Laser and Electro-Optics, (Anaheim, California, USA)
OSA Technical Digest Series, **7**, Post-deadline paper, 659, 1990

(2) M. Ebrahizadenh, G. Robertson and M. H. Dunn
Opt. Lett. **16**, 767, 1991

(3) Y. Cui, M. H. Dunn, C. J. Norrie, W. Sibbett, B. D. Sinclair, Y. Tang and J. Terry
Opt. Lett. **17**(9), 646, 1992

(4) Y. Cui, M. H. Dunn, C. J. Norrie, W. Sibbett, B. D. Sinclair, Y. Tang and J. Terry
In conference of Laser and Electro-Optics, (Anaheim, California, USA)
OSA Technical Digest Series, **12**, Paper CTuR1, 659, 1990

(5) Y. Tang, Y. Cui and M. H. Dunn
in 1991 European Quantum Electronics Conference and Tenth National Quantum Electronics Conference
(Heriot-Watt University, Edinburgh, August 1991)
91 EQEC Technical Digest, Post-deadline paper PD8, 14, 1991

(6) Y. Tang, Y. Cui and M. H. Dunn
Opt. Lett. **17**(3), 192, 1992

(7) S. J. Lin, B. C. Wu, F. L. Xie, and C. T. Chen
Appl. Phys. Lett. **50**(13), 1541, 1991

(8) G. D . Boyd and D. A. Kleinman
J. Appl. Phys. **39**(8), 3597, 1968

(9) S. Guha, F. Wu, and J. Falk
IEEE J. Quantum Electron. **18**(5), 907, 1982

(10) S. J. Brosnan and R. L. Byer
IEEE J. Quantum Electron. QE-**15**(6), 415, 1979

(11) G. Robertson, A. Henderson and M. H. Dunn
Opt. Lett. **16**(20), 1584, 1991

(12) J. E. Bjorkholm
IEEE J. Quantum Electron. QE-7(3), 109, 1971

(13) M. H. Dunn, Y. Cui, A. J. Henderson, G. Roberson, Y. Tang, W. Sibbett, and B. D. Sinclair
J. Opt. Soc. Am. B. (Submitted, Nov. 1992)

(14) J. F. Bjorkholm
IEEE J. Quantum Electron. QE-**7**, 109, 1971

(15) C. T. Chen
Private Communication, July 1991

(16) F. Hanson and D. Dick
Opt. Lett. **16**(4), 205, 1991

(17) W. R. Bosenberg, K. L. Cheng, C. L. Tang
Appl. Phys. Lett. **16**(1), 13, 1989

CHAPTER 6

Critically phase matched lithium triborate optical parametric oscillator pumped at 355 nm

We have discussed in Chapter 3 that the optically nonlinear material LBO can be phase matched in the xy plane, which provides a type I critical phase matching geometry which is broadly tunable from 410 nm to 2.5 μm. Optical parametric oscillators based on this crystal geometry were first reported by Z. Xu et al[1] and again by Y. Wang et al[2] (tunable from 435 nm to 1.922 μm, when pumped at 355 nm). However, we were the first to demonstrate an all-solid-state configuration[3]-[5], in which we obtained a very low energy threshold. This is really very attractive, a compact, efficient and broadly tunable all-solid-state coherent light potentially has many applications. One important thing to mention again is that the LBO crystal is the only material suitable for low energy pump sources and broadly tunable in the visible and near infrared bands (see Chapter 3).

In this chapter we describe the experimental investigation of an all-solid-state type I critically phase matched optical parametric oscillator. Boyd and Kleinman's theory[6][7] has been used in the analysis. We will also briefly discuss the type II critically phase matched LBO optical parametric oscillator pumped at 355 nm. This geometry has been largely ignored, due to its slow tuning behaviour compared to the type I geometry, but the specific properties of the intrinsic line-narrowing may make it useful in particular applications.

6.1 Pump geometry

The all-solid-state pump source is the same as that used previously for the non-critical phase matched OPO case, and was the only pump source used in the critical phase matched studies (please see figure (4-2) and (5-1).

6.2 Type I critical phase matching geometry in LBO

The type I critical phase matching geometry in LBO is illustrated in figure (6-1). The 355 nm pump wave is linearly polarised perpendicular to the z axis (in the xy plane), and both the signal and idler waves are polarised along the z axis (perpendicular to the xy plane), so that the pump is an extraordinary, while the signal and idler are ordinary waves.

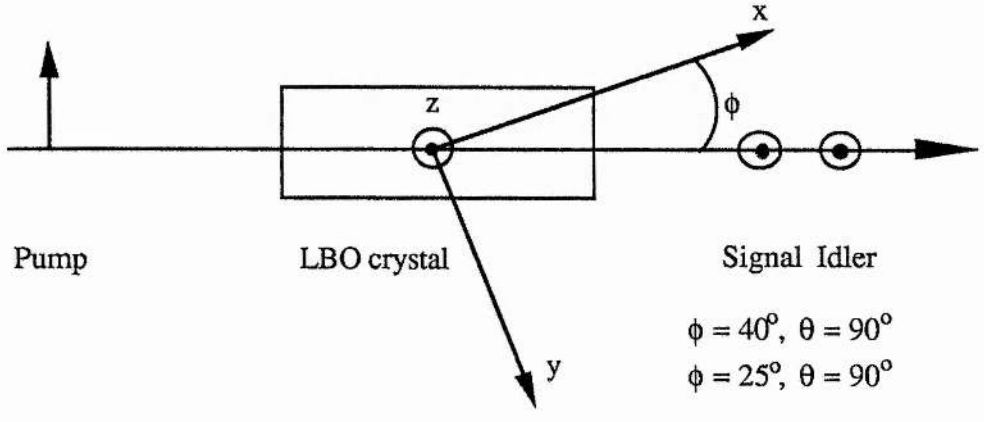

Fig. 6-1 Type I critical phase matching geometry in LBO.

The tuning of the OPO was achieved, in this geometry, by changing the LBO crystal about the z axis, which meant fixing the angle θ at 90° and turning the angle ϕ in the crystal xy plane. Two type I LBO crystals were used in this experiment, both grown and fabricated by FC Castech Inc., Fuzhou, China. One was cut at $\phi = 40°$ with dimensions of 5 x 8 x 15 mm, while the other was cut at $\phi = 25°$ with dimensions 4 x 6 x 13 mm. The former crystal has an aperture of 5 x 8 mm^2, and therefore the internal angle turning range is very large. The experimental investigations have been mainly carried out with this crystal. None of the nonlinear crystals used in these experiments was coated.

The theoretical curves of the Poynting vector walkoff angle, the effective nonlinear coefficient and the acceptance angle under the phase matching conditions have been presented in the Appendix III.

6.3 Cavity

The OPO cavity geometry used in this experiment was similar to the case of the NCPM optical parametric oscillator, where a cavity formed by two simple plane mirrors was used to investigate the OPO tuning behaviour and characterise the OPO output performance, and a cavity formed by two curved mirrors (to match the tightly focused pump wave mode) was used to investigate the minimum oscillation threshold and the frequency conversion efficiency. These mirrors were coated either for high reflection (95 %) at 480 nm or at 580 nm. The former ones have already been used in the experiments on non-critically phase matched LBO optical parametric oscillators; the latter ones designed for the present type I geometry and in particular for a crystal cut at 40°, the signal wavelength is identical to that corresponding to the peak of the reflection. These mirrors were also coated for high transmission at 355 nm, and have only a very low residual reflection for the idler waves. Hence, the OPO oscillated in a singly resonant mode.

The lowest pump threshold and the highest conversion efficiency were obtained with the latter configuration, i.e. with the cavity mirrors have a small radius of curvature and coated at 580 nm. As will be discussed later, this cavity configuration was close to the optimum, with regard to pump spot size and cavity mode size, predicted by the analysis due to Guha et al[7].

6.3.1 Confocal cavity with zero-focal-power mirror

Several sets of curved mirrors were used in these experiments. If a plano-concave configuration is used for the mirror substrate (i.e. plano back surface and concave mirror surface), then the pump beam on passing through such a mirror is subject to a defocusing effect[8]. If the mirror radius of curvature is small, this effect can be very pronounced leading to a requirement to change the primary focusing optic to accommodate such defocusing. Further if the pump light enters the mirror substrate off-axis, prism effects occur which makes alignment of the cavity very difficult. The significance of both of the above effects is that they make it very difficult to obtain good overlap between pump beam and cavity mode, and if it is not achieved then the pump and idler wave fronts will move out of phase with the signal wave fronts as they propagate in the cavity. These spatial phase changes cause an significant phase mismatch that results in reduced interaction and lower conversion efficiency[9]. To avoid these difficulties in alignment of cavity and reduction in frequency conversion efficiency, a zero-focal-power mirror has been introduced for optical parametric oscillators. A specially designed zero-focal-power mirror is such that not only is the radius of curvature of the reflecting face matched to the cavity optimum confocal parameter b, but also the radius of curvature of the back face matches the wave front curvature of the focused pump beam (this condition is closely met by a concentric geometry). Consequently, when the pump beam pass through the mirror, the beam waist position and beam spot size are not changed. Further, the concentric form of these mirrors eliminates prism effects. Such zero-focal-power mirrors with radius of curvature R = -30, +35 mm and R = -15, +20 mm have been used in these experimental investigations (two numbers with R designate the mirror's radii of curvature inside and outside the cavity respectively).

Here an important point to note is that, if a medium is introduced after a focusing lens, then the position of the beam waist in the crystal is shifted. First consider the case when the beam waist is initially in the focal plane of the lens, the position of waist is shifted by an amount $(n-1)(f-a_2)$ on inserting the crystal, where a_2 is the distance from the lens to the crystal face (please see figure (6-2)(2))[10]. However, the beam waist is unchanged in size. Further, the nonlinear crystal normally decreases the effective length of the OPO cavity from the point of view of beam propagation by a factor of $L_n = L\,(1-(1/n))$, where L is the crystal length.

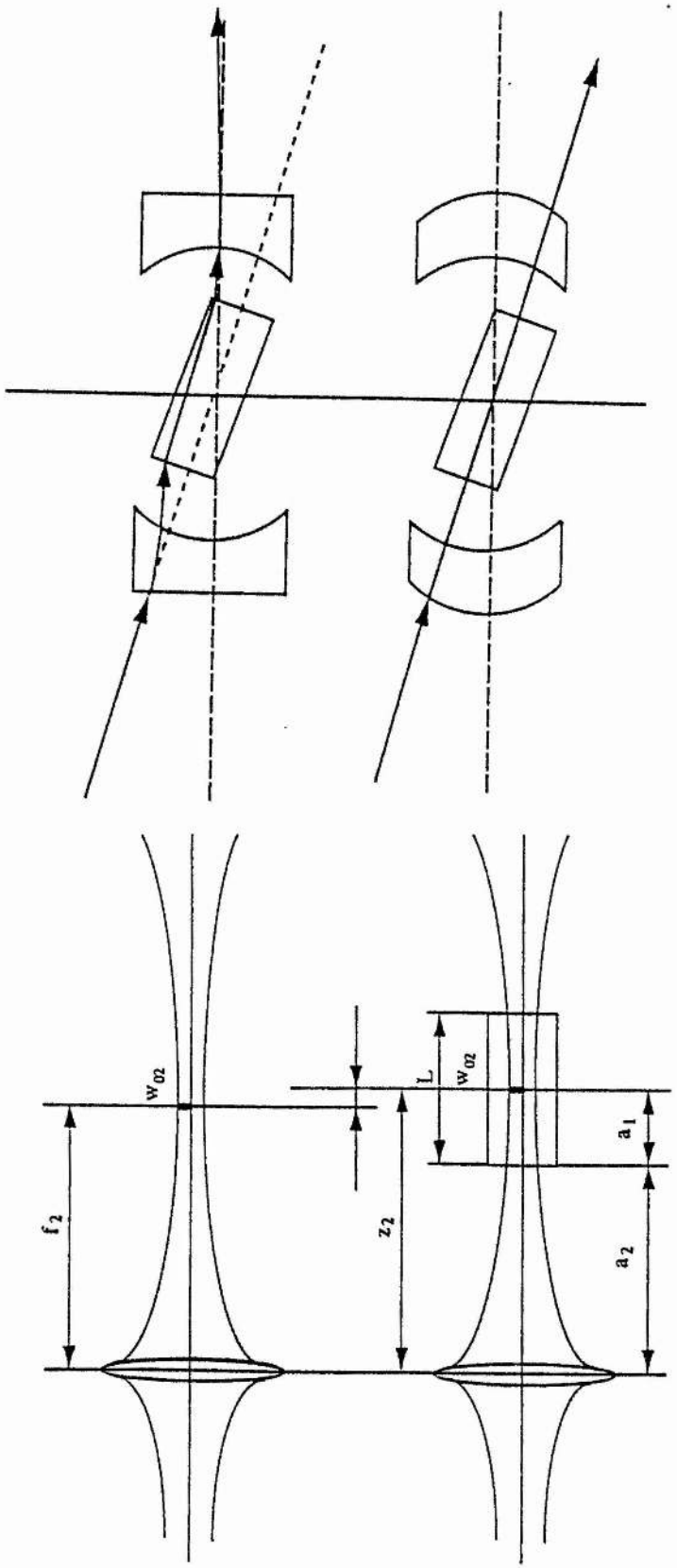

Fig. 6-2 Gaussian beam focusing in the nonlinear optical materials; and the confocal cavity formed by zero-focal-power mirrors.

When using cavities with small radius of curvature mirrors there are certain advantages to the confocal ($L_{cav} = R$) geometry. The beam waist in the cavity reaches a maximum spot size, for a particular mirror set, under the confocal condition, and further the change in spot size with mirror separation goes through a turning point, so spot size is insensitive to mirror separation[11]. A penalty of using the confocal geometry, however, is the need to closely match the radius of curvature of the two mirrors in order to ensure a stable cavity. The zero-focal-power mirror used here relaxed restrictions on the cavity alignment.

6.3.2 Operational performance

An investigation of pump threshold and conversion efficiency has been thoroughly carried out for the OPO cavity formed by curved mirrors . The detailed experimental results are listed in table (6-1), while figure (6-4) and (6-5) in the next section summarise the pump threshold and the pump depletion respectively. However, in this subsection we describe how we have designed the OPO cavity using the theory of Guha et al. The basic parameters of the OPO cavity are as follows:

Type I LBO crystal length	15 mm
Phase matching angle cut at	$\phi = 40^o, \theta = 90^o$
Pump wavelength	$\lambda_p = 0.3547$ μm
Signal wavelength	$\lambda_s = 0.588$ μm
Idler wavelength	$\lambda_i = 0.893$ μm
Walkoff angle	$\rho = 1.05^o$

The walkoff parameter B can be calculated from formula (2-41) as given by Boyd and Kleinman. However, Guha et al[7] define the walkoff parameter slightly differently, such that B(Guha) = B(Boyd and Kleinman)/$\sqrt{2}$. On what follows we use Guha's definition. Therefore, we have that B = 4.25 for the above condition. Following Guha et al, we have calculated a few curves for the optimum h_{sm} value against the signal focusing parameter ξ_s, with different conditions of ξ_p (please see figure (2-5,b)). From these curves we deduce that the optimum focusing parameter ξ_p is around 0.1 while the optimum focusing parameter of the signal wave ξ_s is around 0.56. Hence the confocal parameter of the signal wave b_s = 27 mm, and the signal beam waist in the crystal is then calculated to be w_{os} = 39 μm, while the pump beam waist is 72 μm.

Experimentally a focusing lens with f = 250 mm has been used for tightly focusing the pump radiation into the OPO cavity. The beam waist was measured in the position of the centre of the LBO crystal to be around 100 μm. So, the pump beam confocal parameter b_p = 288 mm, and the focusing parameter ξ_p was determined to be 0.052. In this case the optimum focusing parameter of signal wave ξ_s is around 0.56 as well.

Experimentally an OPO cavity formed by two 30 mm radius of curvature mirrors (zero-focal-power mirrors) has been used to investigate the threshold and the conversion efficiency. For such a cavity the signal wave focusing parameter ξ_s = 0.5, and the spot size was w_{os} = 40 μm.

Table 6-1 Experimental results compared to the theoretical calculated optimum solution, where all of the calculation were carried out under the condition of B = 4.25, and the theoretical optimum parameters were determined by the maximum value in h_{sm}.

	ξ_p	b_p (mm)	w_{op} (μm)	ξ_s	b_s (mm)	w_{os} (μm)	h_{sm}
Theoretical optimum conditions	0.1	150	72	0.56	26.78	0.39	0.0234
Optimum conditions for 100 μm beam spot size	0.052	288	100	0.56	26.78	0.39	0.0218
Experimental conditions	0.052	288	100	0.50	30.00	0.40	0.0217

Values of h_{sm} for (i) optimum focusing conditions as predicted theoretically, (ii) optimum signal beam focusing for a pump beam focusing parameter, ξ_p, is 0.052 as used here, and (iii) the values of ξ_p and ξ_s appertaining to our experimental conditions are given in table (6-1). From this table we can conclude that the experimental parameters closely approach the optimum situation (The value of h_{sm} under experimental conditions is within 10 % of the optimum value). Here, unlike in the non-critically phase matched LBO OPO, further tightly focusing the pump wave or further decreasing the radius of curvature of cavity mirrors will not be helpful in further decreasing the pump threshold or increasing the slope efficiency. This point we will further discuss in the next section.

The importance of matching the OPO cavity mode to the focused pump was investigated by increasing the separation of the OPO cavity mirrors while approximately maintaining the position of the crystal at the focus of the pump. The measured threshold is plotted in figure (6-3) as a function of the effective optical length of the cavity. The results are in agreement with the previous discussions, where the minimum pump threshold and the highest slope efficiency are expected when the cavity length is set around confocal (36 mm). It is also shown in figure (6-3) that when the cavity length departs from the confocal point, the pump threshold increases rapidly. This may be due to higher order spatial mode no longer being degenerate with the TEMoo mode on departure from the confocal condition.

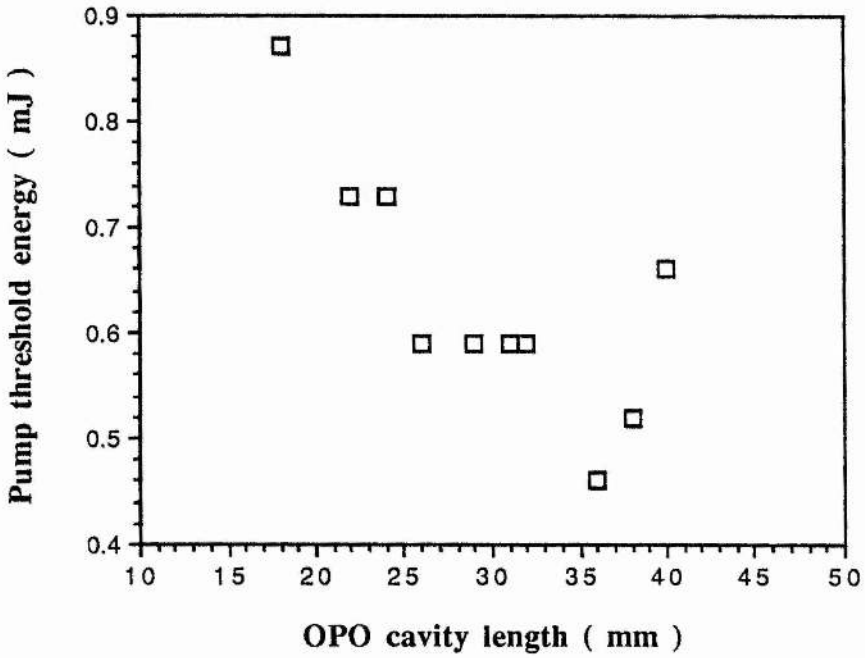

Fig. 6-3 The pump threshold as a function of cavity length.

6.3.3 Explanation of the damage on the cavity mirrors

Optical damage of the coatings of the cavity mirrors limited further investigations of the conversion efficiency with increasing pump energies. Damage occurred when the pump energy reached 0.81 mJ, which was only 1.5 times above pump threshold. By a simple analysis, to be given below, we show that the damage is mainly due to the

oscillated signal wave, and this is consistent with earlier research work by others, where, theoretically and experimentally it has been shown that the circulating power at the oscillated signal wave may be many times the incident pump power in a singly resonant optical parametric oscillator[12]. This is important indeed in an optical parametric oscillator operating near the crystal or mirror damage threshold limit.

In our situation the damage threshold energy density of the coatings given by the manufacturer is 5 J/cm^2, and for a pump pulse width of 10 ns, this means that the damage threshold mean power density is 500 MW/cm^2. Obviously, the pump beam mean power density had not reached this value, which was calculated for the given conditions, i.e. 0.81 mJ energy, 10 ns pulse width, and 100 μm spot size, to be less than 250 MW/cm^2. However, in terms of the experimental results given in figure (6-5), the pump depletion can be assumed to be around 25 % when the pump power closely approached 0.81 mJ. In this case the converted energy is 0.2 mJ, which is composed of 0.12 mJ signal wave and 0.08 mJ idler wave. Further we can assume that about 55 % of the signal wave with a pulse width of ~9 ns is efficiently extracted from the oscillator, and thus, the output signal wave energy is 0.066 mJ, and the mean power is 7.3 KW. We already know that the output coupler of the OPO cavity is 10 % transmitting, and that the signal beam spot size on the cavity mirror is 57 μm. Therefore, the signal wave circulating power in the oscillator is 73 KW, and the mean power density on each mirror is around 350 MW/cm^2. This number is much closer to the manufacturer's damage threshold. From the above analysis we can conclude that the damage was caused by the signal wave in the cavity rather than the pump wave.

6.4 Performance of type I critically phase matched LBO optical parametric oscillator pumped at 355 nm

6.4.1 Pump threshold

The pump threshold and OPO internal conversion efficiency have been comparatively investigated with different cavity geometries and for different signal wavelengths. Table (6-2) shows the pump energy required to reach threshold for different cavity geometries and pump spot sizes. Threshold energy decreases on decreasing the spot size from 300 μm to 100 μm, the cavity throughout being one of a plane-parallel geometry. On the other hand as a result of the detrimental effects of Poynting vector walkoff and increased diffraction losses as the pump spot size is reduced, the threshold

energy density increases. Under these conditions, curved mirrors significantly improve device performance. Choice of the optimum radius of curvature has been discussed in Chapter (6.3.2).

Table 6-2 The pump threshold with different cavity geometry.

Cavity geometry	Plane-plane combination Lc* = 20 mm				R=100mm Lc=18mm	R=30mm Lc=36mm	R=15mm Lc=20mm
Focal length (mm)	Without focusing lens	1000	500	250	250	250	250
Pump beam spot size (μm)	300	250	200	100	100	100	100
Pump threshold energy (mJ)	0.80	0.64	0.59	0.54	0.38	0.33	0.60
Energy density (J/cm^2)	0.28	0.33	0.47	1.71	1.21	1.05	1.91

* Lc is the cavity length.

Figure (6-4) shows the pump threshold as a function of signal wavelength. For a crystal cut at $\phi = 40°$, the signal wavelength corresponding to normal incidence is 588 nm. With the mirror set used here where reflectivities were peaked around 480 nm, it was not possible to operate the OPO at this signal wavelength. Hence the lowering of threshold that we normally observed under such a condition, and which is due to the Fresnel reflections at the crystal faces feeding radiation back along the cavity axis, could not be observed. Fresnel reflections lead to high off-axis loss, therefore increasing pump threshold. From these results we can see that the pump threshold was not changed over a large spectral range of the signal wave (approximately from 460 nm to 530 nm). Indeed, as can be seen in the Appendix III, the increase in d_{eff} and the decrease in the walkoff angle as the crystal is turned away from degeneracy are such as to compensate for decrease in parametric gain due to detuning from degeneracy[10], and as such will act to maintain a constant oscillation threshold across the tuning range.

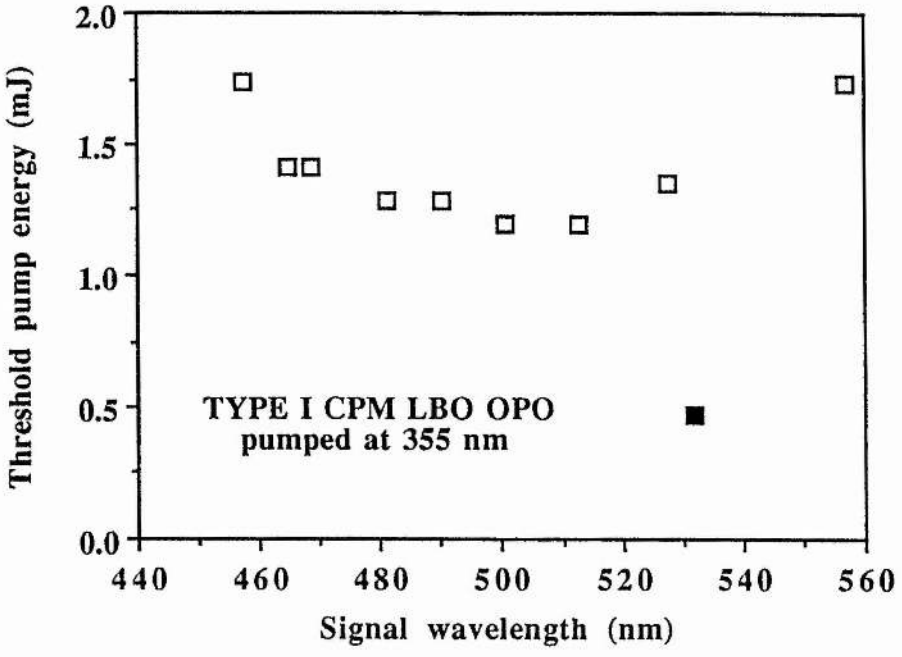

Fig. 6-4 The pump threshold as a function of signal wavelength. LBO crystal was cut at 40°. Cavity mirror coated at 480 nm. The pump spot size was around 300 μm.

As may be seen from figure (6-4) that at the signal wavelength 532 nm (corresponding to the crystal internal angle 36.8°) the pump threshold decreased substantially. The pulse energy of the residual 532 nm wave after the OPO cavity mirror was measured to be 60 μJ. When allowance is made for the polarisation state of this radiation (45° to the required direction for phase matching in LBO) and for the Fresnel loss of the crystal, less than this energy is available for seeding the OPO. Even with such lower available energy (<30 μJ), the pump threshold decreased about three times (from 1.35 mJ to 0.47 mJ).

6.4.2. Conversion efficiency

The pump depletion has been studied with the oscillator oscillating at a signal wavelength of 588 nm as a function of pump energy for the different pump focusing conditions (please see figure (6-5)). For the case (plane cavity geometry) where

additional focusing lenses are not used and the pump beam at 355 nm has an approximately Gaussian beam waist of radius 300 μm at the centre of the LBO crystal, an oscillation threshold of 0.8 mJ is observed and 35 % pump depletion is attained at around 3 times threshold. As the pump beam radius is decreased to 100 μm (plane cavity geometry), the threshold, measured in terms of pump energy, decreases to around 0.54 mJ, and a conversion efficiency in excess of 35 % is reached for a pump energy less than 1.8 mJ before mirror damage begins to limit conversion efficiency. In terms of pump energy density there is an increase in threshold from 0.28 J/cm^2 to 1.72 J/cm^2 as the pump beam size is reduced from 300 μm to 100 μm; this is to be expected since Poynting vector walkoff and diffraction loss are more significant in limiting conversion efficiency at the smaller pump beam size and for a plane cavity geometry. When a curved mirror cavity is used, particularly a confocal cavity geometry, the diffraction loss is reduced, therefore, the pump threshold, not only in terms of the pump energy, but also in terms of the pump energy density, is reduced, and the slope efficiency is increased.

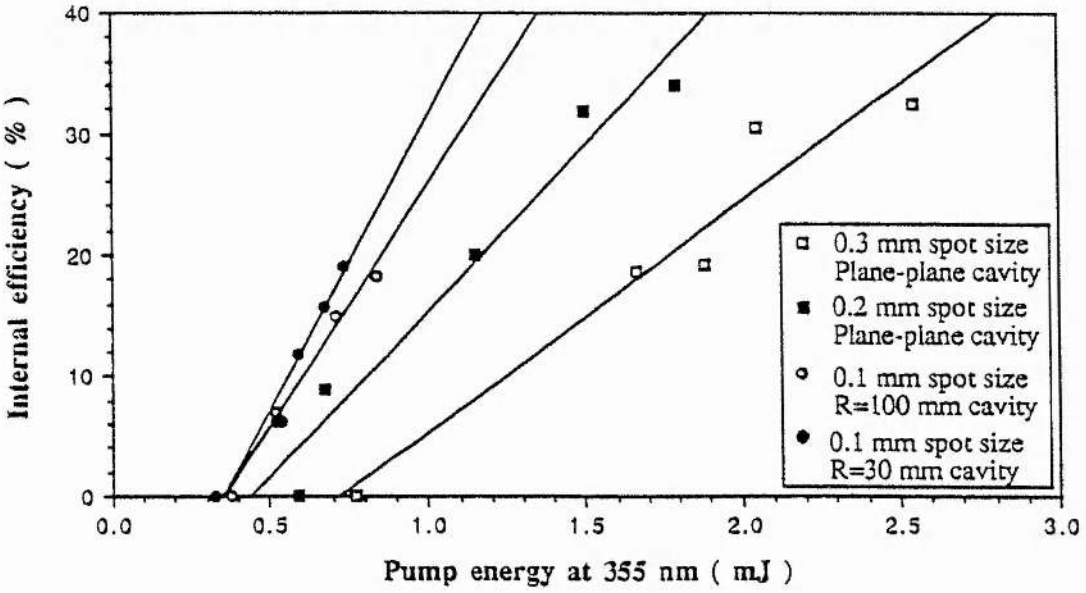

Fig. 6-5 Internal conversion efficiency as a function of pump pulse energy for different pump beam configurations. The open squares represent a plane -plane cavity, no focusing, pump waist 300 μm; the solid squares represent a plane-plane cavity, pump beam focused by 0.5 m lens producing a pump waist of 200 μm; the open circles represent a cavity formed by mirrors with radius of curvature 0.1 m, pump beam focused by 0.25 m lens producing a pump waist of 100 mm; and the solid circles represent a cavity with mirrors of radius of curvature 0.03 m with the same pump configuration.

6.4.3 Angle tuning behaviour

The tuning of the output wavelength of the optical parametric oscillator was measured as a function of the internal angle in the xy plane of the type I LBO crystal, and results are given in figure (6-6). The entire tuning range from 457 nm to 666 nm was achieved by two sets of mirrors and with rotation of the crystal through an internal angle of 14°. In figure (6-6), the solid line is the theoretically calculated curve with the Sellmeier equation coefficients given by Chen et al[13], the open squares were measured using the first crystal cut at 40° and mirrors coated at 580 nm, and the filled squares were measured using crystals cut at both 40° and 25° and using the cavity mirrors coated at 480 nm. The tuning range is limited only by the spectral coverage of the cavity mirrors available to us, and we anticipate no difficulty in obtaining coverage from 420 nm to 2.3 μm, limited only by the infrared absorption when the idler wavelength is longer than 2.3 μm.

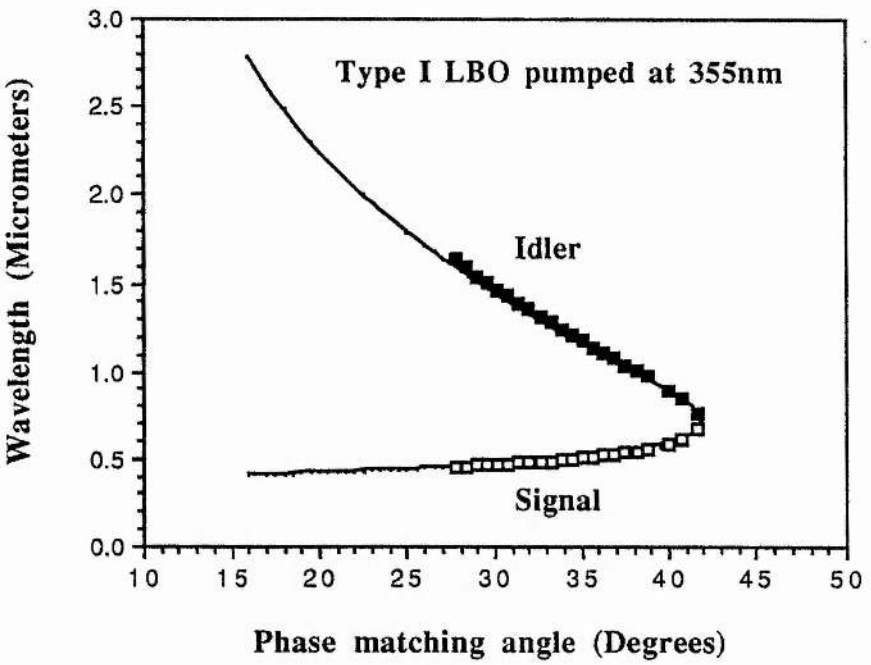

Fig. 6-6 The frequency tuning curve as the function of internal angle. The solid curve is calculated with the revised Sellmeier equation due to Chen[13].

6.4.4 Linewidth

The measured linewidth of the signal wave across the tuning range is shown in figure (6-7). As expected, the linewidth increases substantially as degeneracy is approached. The two values of signal wavelength where linewidth less than those expected from the general trend are observed (represented by solid squares in figure (6-7)) correspond to the case (i) of operation at 532 nm where the OPO is in effect injection seeded by the unconverted second harmonic radiation that reaches the OPO cavity (the linewidth as indicated in the graph is instrumentally limited), (ii) where the crystal is exactly on-axis so that subsidiary cavities are formed between the cavity mirrors and the end faces of the crystal (the crystal has uncoated end faces cut normal to its axis).

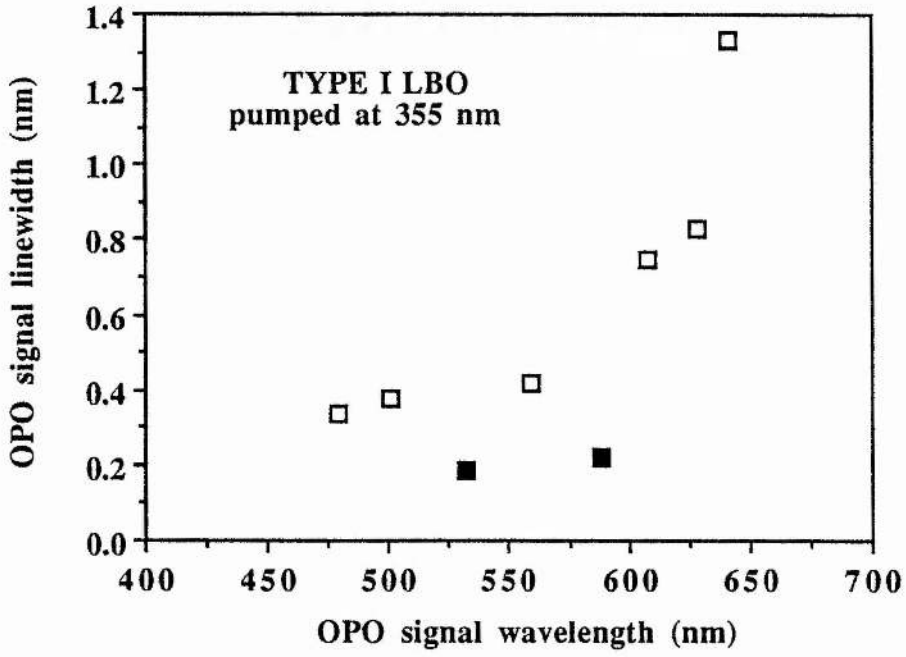

Fig. 6-7 The measured signal wave linewidth as a function of signal wavelength.

6.4.5 Characteristics of output beam

The signal beam divergence was not measured, but, it was estimated to be similar to the NCPM OPO case, namely of order 10 mrad. The signal wave pulse width was measured at 588 nm and with different pump energies. When the pump energy was close to the threshold, the signal pulse width was measured to be around 8 ns (the 355 nm pump pulse width was 10 ns), and to increase progressively as the input pump energy and the conversion efficiency increased. When the pump energy reached 2 mJ, the signal pulse width was measured to be approximately similar to the pump wave.

6.5 Brief discussion of type II critically phase matched LBO optical parametric oscillator pumped at 355 nm

The type II critically phase matched LBO optical parametric oscillator has not been reported until now, due to its slow tuning behaviour, being only tunable in the range from 483 nm to 565 nm (signal) and 1.33 to 0.95 μm (idler), when the device is pumped at 355 nm (please see Appendix III). Understandably in the early stages of the newly developed LBO crystal, most of the research work have been focused on the NCPM geometry and the broad tunable type I CPM geometry. However the type II geometry has some advantages compared to the type I geometry, namely it has a smaller walkoff angle and larger acceptance angle, as expressed in a larger figure of merit. This leads to an intrinsically narrow linewidth, and therefore, the critically phase matched type II LBO optical parametric oscillator may find some particular applications.

We have demonstrated a type II CPM LBO OPO in the early stages of this project. However, the experimental investigation was only very briefly carried out.

The type II CPM LBO crystal used in this demonstration was originally designed for frequency tripling a Nd:YAG laser, and hence was cut at $\theta = 42^{o}$, $\phi = 90^{o}$, with a dimensions of 5 x 5 x 15 mm^3. The tuning of the OPO was achieved by rotating the LBO crystal about the x-axis, which meant fixing the angle ϕ at 90^{o} and changing the angle θ in the crystal yz plane. In this geometry the 355 nm pump laser must be linearly polarised parallel to the x axis and perpendicular to the yz plane, and is hence an ordinary wave. The polarisation direction of the signal wave is in the yz plane, and perpendicular to the x axis, so that it is an extraordinary wave. The polarisation of the infrared idler wave is the same as the pump wave.

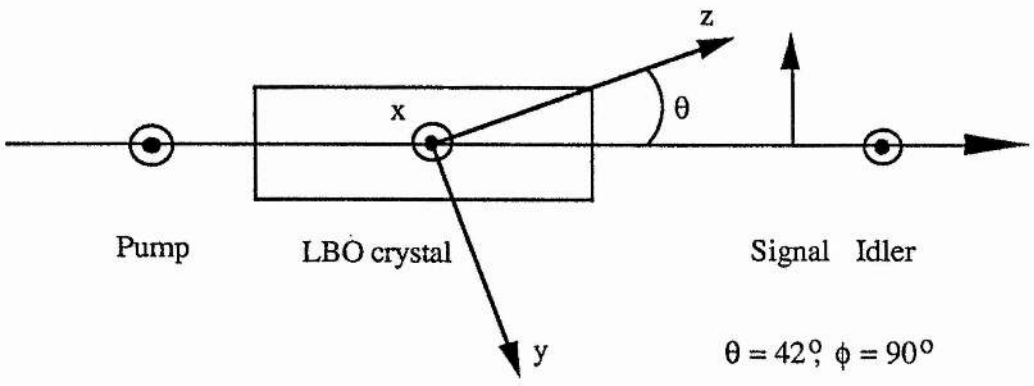

Fig. 6-8 The phase match geometry in type II LBO crystal.

The experimental investigations were carried out with a flashlamp pumped system. The threshold was measured at a signal wavelength of 530 nm (corresponding to a crystal internal angle of 41°) to be < 1 mJ. However the reflectivity of each cavity mirror (plane-parallel cavity geometry, mirror was coated at 480 nm) at this wavelength was around 90 %. The internal and external efficiencies were measured with 2.6 mJ of pump energy at 355 nm, to be 33.6 % and 15 % respectively. The angle tuning behaviour was measured for the signal wave using a monochromator, and the results are plotted into figure (6-9), where the tuning range (501 nm to 535 nm) was limited by the crystal aperture and the mirror coatings. Unfortunately the linewidth was not measured. Experiments by others with the type II BBO crystal[14] have shown that the linewidth in this geometry is a few times less then the type I geometry. Even though the LBO crystal has a smaller birefringence than the BBO crystal, a similar ratio of the linewidths between the two geometries is to be expected.

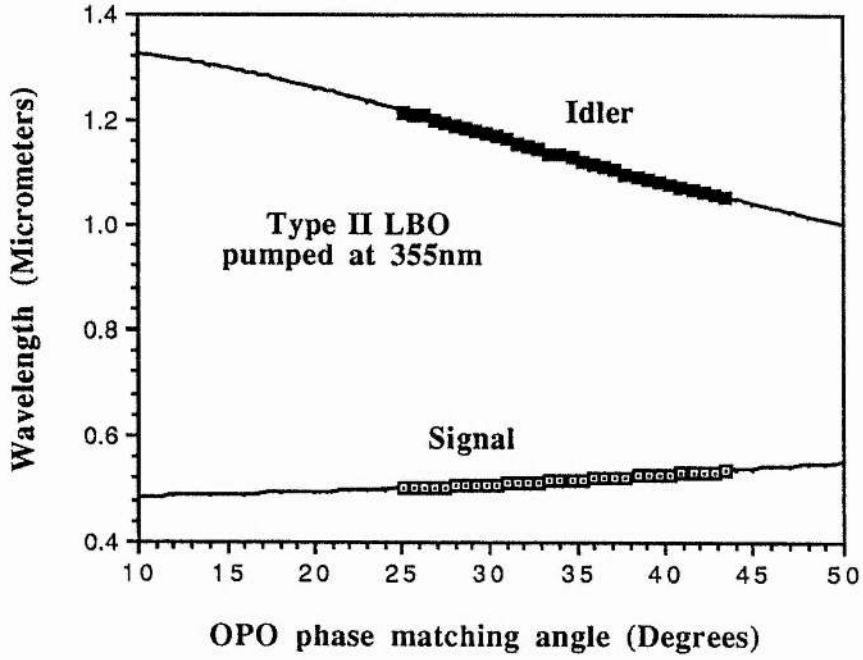

Fig. 6-9 Type II critically phase matched optical parametric oscillator frequency tuning curve against the internal angle.

References

(1) Z. Y. Xu, D. Q. Deng, Y. P. Wang, B. C. Wu, C. T. Chen
In Conference of Lasers and Electro-Optics, (Anaheim, California, USA)
OSA Technical Digest Series 7, Paper CWE 6, 246, 1990

(2) Y. P. Wang, Z. Y. Xu, D. Q. Deng, W. H. Zheng, B. C. Wu, C. T. Chen
Appl. Phys. Lett. **59**(5), 531, 1991

(3) Y. Cui, M. H. Dunn, C. J. Norrie, W. Sibbett, B. D. Sinclair, Y. Tang, and J. A. C. Terry
In Conference of Lasers and Electro-Optics, (Anaheim, California, USA)
OSA Technical Digest Series **12**, Paper CTuR1, 198, 1992

(4) Y. Cui, D. E. Withers, C. F. Rae, C. J. Norrie, Y. Tang, B. D. Sinclair, W. Sibbett and M. H. Dunn
Opt. Lett. **18**(1), 1, 1993

(5) M. H. Dunn, Y. Cui, A. J. Handerson, G. Robertson, Y. Tang, W. Sibbett and B. D. Sinclair
J. Opt. Soc. Am. B. (submitted, Nov.1992)

(6) G. D. Boyd and D. A. Kleinman
J. Appl. Phys. **39**(8), 3597, 1968

(7) S. Guha, F. Wu and J. Falk
IEEE J. Quantum Electron. **18**(5), 907, 1982

(8) R. L. Byer
in " Quantum Electronics : a treatise ", edited by H. Rabin and C. L. Tang
(Academic Press, New York) Vol. **1**, Part B, 587, 1975

(9) L. R. Marshall, J. Kasinski and R. L. Rurnham
Opt. Lett. **16**(21), 1680, 1991

(10) S. K. Kurtz
in " Quantum Electronics : a treatise ", edited by H. Rabin and C. L. Tang
(Academic, New York), Vol. **1**, Part A, 209, 1975

(11) A. Yariv
in "Optical Electronics" 3rd edition, New York, 1985

(12) P. P. Bey and C. L. Tang
IEEE J. Quantum Electron. QE-**8**(3), 361, 1972

(13) S. J. Lin, J. Y. Huang, J. W. Ling, C. T. Chen and Y. R. Shen
Appl. Phys. Lett. **59**(22), 2805, 1991

(14) W. R. Bosenberg and C. L. Tang
Appl. Phys. Lett. **56**(19), 1819, 1990

CHAPTER 7

Conclusions and future work

7.1 Conclusions

We have experimentally investigated the all-solid-state optical parametric oscillator based on the newly developed nonlinear optical crystal lithium triborate. The results presented here have shown the device to be highly practicable. The first demonstrations of the following devices have been made in this work.

- All-solid-state type II NCPM LBO optical parametric oscillator pumped at 355 nm, which was temperature tunable from 457 to 481 nm (signal) and 1.6 to 1.35 μm (idler);

- All-solid-state type I CPM LBO optical parametric oscillator pumped at 355 nm, which was angle tunable from 457 to 666 nm (signal) and 1.6 μm to 768 nm (idler);

- All-solid-state type II NCPM LBO optical parametric oscillator pumped at 266 nm, which was temperature tunable from 306 to 314 nm (signal) and 2.03 to 1.75 μm (idler).

The principal conclusions to be made from the work described in previous chapter are as follows:

The newly developed nonlinear material lithium triborate has been demonstrated to be an excellent nonlinear material for an optical parametric oscillator. It may be phase matched in all three optical principal planes and offers wide tunability across the UV, visible and near infrared spectral bands. LBO has a relatively high effective nonlinear

coefficient, small walkoff angle, large angular acceptance bandwidth and a high optical damage threshold. Hence, it is a superior material for an OPO with a modest pump energy, but tightly focused radiation. Devices with very low pump energy thresholds in a non-critical phase matching geometry (<0.2mJ), and critical phase matching geometry (< 0.4 mJ) have been demonstrated.

Diode laser pumped solid-state lasers exhibit many advantages, and both the optical parametric oscillator and the nonlinear frequency up-conversion process have benefited substantially from the high quality of the pump beam available from such a laser, in particular in terms of increased conversion efficiency. Diode-laser-pumped solid-state lasers display stability, reliability, compactness, and longevity, and proved in many experiments to be excellent sources when applied to nonlinear optics.

Successful operation of the all-solid-state optical parametric oscillator was also due to the accurate theoretical calculations. In this work, the phase matching theory has been systematically verified for the three wave parametric interaction process, and the Guha theory has been successfully used for theoretical analysis of the pump beam geometry and the OPO cavity configurations.

7.2 Further development

Because of time limitations, the experimental investigations of the systems described here have concluded, but there certainly remains much opportunity for further development.

Improvement in conversion efficiency

Several method could be used for further decreasing the pump threshold and increasing the OPO conversion efficiency. It is well known that the doubly resonant optical parametric oscillator has a much lower threshold compared to the singly resonant configurations. In practice, however, this requires a single frequency pump source and careful cavity design and control to assure resonance at both signal and idler waves simultaneously. For these reasons doubly resonant OPO's are not utilised except where necessary, such as for continuous-wave (CW) operation[1]. In our particular case i.e. singly resonant Q-switched pulse pumped optical parametric oscillators, the following considerations might be practically useful.

Firstly, it is possible to utilise the pump pulse energy more efficiently by simply feeding back the pump wave using a high reflecting mirror[2][3]. In this way the pump wave double passes through the OPO gain medium, and significantly reduces the pump threshold hence increasing the OPO conversion efficiency.

Secondly, some compensation of the Poynting vector walkoff may be made. When a critical phase matching geometry is employed in an optical parametric oscillator, this process generally limits the effective medium length or the pump spot size. Earlier research work on this problem has suggested that elliptical focusing can allow the energy density in the beam to be maintained while simultaneously increasing the beam dimension in the appropriate plane to minimize walkoff effects[4]. The two-crystal-walkoff-compensating configuration is another efficient method to compensate for Poynting vector walkoff effect, thereby decreasing the oscillation threshold and increasing the conversion efficiency[5].

Thirdly, there are many improvements which may be made to the OPO cavity geometry. For example, a monolithic ring cavity optical parametric oscillator has been demonstrated to be very efficient, not only in a singly resonant long pulsed OPO[8], but also in a doubly resonant continuous wave pumped OPO[9], with 60 % and 78 % pump depletions demonstrated respectively.

Fourthly, further optimising the focusing parameter using Boyd and Kleinman's theory[10][11] (particularly in a non-critical phase matching geometry) clearly is an option. However, in order to be able to exploit the tighter focusing conditions, improved mirrors with high optical damage threshold are required. At present, the damage thresholds of dielectric coatings, especially for the well developed Nd:YAG laser wavelength at around 1.064 μm, are in most cases lower than the damage threshold of the newly developed nonlinear crystals (for example BBO and LBO etc.).

Fifth, consideration of Fresnel reflection losses of the oscillated wave is important in OPO cavity design. If either the signal wave or idler wave is unwanted, then the unwanted wave should be resonated in the cavity. In this way, the useful wave suffers only single pass loss and the extraction efficiency is increased, without reducing the pump depletion of the device[14]. For the broadly angle tuning geometry, use of an index matching liquid in the cavity can significantly reduce Fresnel losses and increase the OPO conversion efficiency over the entire tuning range.

Line-narrowed OPO

An important property of the LBO crystal is the intrinsically narrow linewidth which results from its low birefringence. Hence, it is suitable to use in line-narrowed OPO's. Hanson et al[15] have demonstrated a line-narrowed OPO using type II non-critical phase matched LBO and a Q-switched, injection seeded, and frequency tripled Nd:YAG pump source. They observed a linewidth of 0.02 nm, which is one order of magnitude narrower than ours. The use of a line-narrowed pump source leads to line narrowed optical parametric oscillator output. The same pump geometry has been used with a BBO OPO by Fan et al[16], and they obtained single axial mode OPO operation with a corresponding OPO linewidth of less than 3 GHz. Different method for line-narrowing OPOs have been used by many research groups. Tang et al have used a grating dispersion method to demonstrate a line-narrowed BBO OPO, whose linewidth was measured to be 0.03 nm[17]. Robertson et al using an excimer laser to pump a BBO OPO with two etalons in the OPO cavity, have demonstrated a linewidth of 1 cm^{-1} (0.02 nm)[18]. More recently Bosenberg et al[19] have demonstrated a single mode KTP OPO using a grating in a grazing incidence configuration as well as Littman configuration[20], and a highly reflecting aluminised mirror as the cavity mirror. The linewidth was measured to be less than 500 MHz(0.02 cm^{-1}). Other methods include the use of beam expansion optics and resonant reflectors, these techniques have been discussed at length elsewhere[21].

7.3. Future direction

In addition to the nano-second pulse pumped optical parametric oscillator recent progress has been made in two other directions. One is the continuous wave pumped (CW) optical parametric oscillator, and the other is the synchronously pumped femto-second pulse pumped optical parametric oscillator. These devices were first demonstrated some time ago, but both were then limited to the near infrared band. Future directions of this project, based on recent achievements may be along these two directions, i.e. investigation of the possibility of development of continuous-wave and femto-second pulsed optical parametric oscillators. These could be based on the newly developed nonlinear optical crystal lithium triborate, and may be tunable in the UV, visible and near infrared bands. These devices will have application fields much wider than Q-switched pulsed optical parametric oscillators. The continuous-wave optical parametric oscillator was first demonstrated by Smith et al[22] in 1968. After that, due

to lack of suitable nonlinear optical materials, it has not been developed rapidly. As a result of demands from research in spectroscopy and on squeezed light, and because of the introduction of newly developed nonlinear materials such as KTP, BBO, LBO, the interest in CW OPO's has increased markedly in recent years. The femto-second pulsed OPO was first demonstrated in 1989 by Tang et al[23]. In their experiments a singly resonant OPO was pumped intra-cavity by femto-second pulses at 620 nm, and the signal wave was continuously tunable from 820 nm to 920 nm, with the idler wave continuously tunable from 2.54 μm to 1.9 μm. Pulse widths of 220 fs were demonstrated. More recently a 62 fs infrared OPO pumped by 765 nm pulses from a Ti:sapphire laser was demonstrated. The signal wave was tunable between 1.2 and 1.34 μm, and the idler wave was tunable from 2.1 to 1.78 μm, with 175 mW average output power[24]. However, all-solid-state continuous-wave optical parametric oscillators and femto-second pulsed optical parametric oscillator have not been demonstrated, perhaps mainly limited by the cost. Theoretically they have been confirmed to be feasible, and each part of the system has already been demonstrated independently.

Other attractive options based on the newly developed nonlinear materials (including the organic materials which were not mentioned in this thesis, but have recently seen substantial development), and the recently well characterised diode-pumped solid-state lasers, are miniature OPOs, microchip OPOs, hybrid OPOs, or even integrated OPOs[25]. These are long term possibilities, and are expected to have many applications.

References

(1) R. L. Byer
in " Quantum Electronics : a treatise " edited by H. Rabin and C. L. Tang, (Acadamic Press, New York) Vol. **1**, Part B, 587, 1975

(2) Y. P. Wang, Z. Y. Xu, D. Q. Deng, W. H. Zheng, X. Liu, B. C. Wu and C. T. Chen
Appl. Phys. Lett. **58**(14), 1461, 1991

(3) Y. P. Wang, Z. Y. Xu, D. Q. Deng, W. H. Zheng, B. C. Wu and C. T. Chen
Appl. Phys. Lett. **59**(5), 531, 1991

(4) D. J. Kuizenga
Appl. Phys. Lett. **21**(12), 570, 1972

(5) W. R. Bosenberg, W. S. Pelouch and C. L. Tang
Appl. Phys. Lett. **55**(19), 1952, 1989

(6) R. L. Byer
Laser Focus World, **25**(3), 77, 1989

(7) D. H. Jundt, G. A. Magel, M. M. Fejer, and R. L. Byer
Appl. Phys. Lett. **59**(21), 2657, 1991

(8) W. J. Kozlovsky, E. K. Gustafson, R. C. Eckardt, and R. L. Byer
Opt. Lett. **13**(12), 1102, 1988

(9) C. D. Nabors, R. C. Eckardt, W. J. Kozovsky, and R. L. Byer
Opt. Lett. **14**(20), 1134, 1989

(10) G. D. Boyd and D. A. Kleiman
J. Appl. Phys. **39**(8), 3597, 1968

(11) S. Guha, F. J. Wu and J. Falk
IEEE J. Quantum Electron. **18**(5), 907, 1982

(12) J. Falk and J. E. Murray
Appl. Phys. Lett. **14**(8), 245, 1969

(13) W. R. Bosenberg, L. K. Cheng, and C. L. Tang
Appl. Phys. Lett. **54**(1), 13, 1989

(14) G. Robertson, A. Henderson and M. H. Dunn
Opt. Lett. **16**(20), 1584, 1991

(15) F. Hanson and D. Dick
Opt. Lett. **16**(4), 205, 1991

(16) Y. X. Fan, R. C. Eckardt, R. L. Byer, J. Nolting and R. Wallenstein
Appl. Phys. Lett. **53**(21), 2014, 1988

(17) W. R . Bosenberg, W. S. Pelouch, and C. L. Tang
Appl. Phys. Lett. **55**(19), 1952, 1989

(18) A. Henderson, G. Robertson and M. H. Dunn
in Conference of Lasers and Electro-Optics, (Baltimore, Maryland, USA)
OSA Technical Digest Series, **10**, Paper 59, 1541, 1991

(19) W. R. Bosenberg and D. R. Guyer
Appl. Phys. Lett. **61**(4), 387, 1992

(20) M. G. Littman and H. J. Metcalf
Appl. Opt. **17**(14), 2224, 1978

(21) S. J. Brosnan and R. L. Byer
IEEE J. Quantum Electron. **15**(6), 415, 1979

(22) R. G. Smith, J. E. Geusic, H. J. Levinstein, J. J. Rubin, S. Singh, and L. G. van Uitert
Appl. Phys. Lett. **12**(9), 308, 1968

(23) D. C. Edelstein, E. S. Wachman, and C. L. Tang
Appl. Phys. Lett. **54**(18), 1728, 1989

(24) Q. Fu, G. Mak, and H. M. van Driel
Opt. Lett. **17**(4), 1006, 1992

(25) G. Colucci, D. Romano, G. P. Bava, and I. Montrosset
IEEE J. Quantum Electron. **28**(3), 729, 1992

APPENDIX I

Conversion efficiency of SHG, THG and relevant theoretical results

1. Conversion efficiency of SHG

The SHG process has been extensively studied theoretically and experimentally in the past. However, more recently, Eimerl gives a closed-form, asymptotic efficiency for SHG conversion that accounts for both drive-influenced phase-mismatch and input wave depletion as follows[1]

$$\eta = \tanh^2 \{ \frac{1}{2} \tanh^{-1} (sn[2\eta_o{}^{1/2}, 1+ \delta^2/4\eta_o]) \} \qquad \text{A-1}$$

Where

$$\eta_o = C^2 I L^2 \qquad \text{A-2}$$

$$C = 5.46\, d_{eff} \,/\, \lambda_1 (n_1 n_2 n_3)^{1/2} \qquad \text{A-3}$$

$$\delta = (1/2)\, \Delta K\, L \qquad \text{A-4}$$

Here, the units of all parameters are designated as follows

Effective nonlinear coefficient	d_{eff}	-------	pm/V
Pump wavelength	λ_1	-------	μm
Phase mismatch	ΔK	-------	cm^{-1}
Crystal length	L	-------	cm
Pump intensity	I	-------	W/cm^2
Coupling parameter	C	-------	$GW^{-1/2}$

sn is a Jacobi elliptic function. The nonlinear drive η_o and phase difference δ are unit-less parameters.

The conversion efficiency depends on the total dephasing. In many applications only beam divergence is significant. The significance of the effect difference from one

nonlinear material to another and is accurately described by the material acceptance angle which we have discussed in Chapter 2. Hence we have

$$\Delta K = \beta_{\theta}' \, \delta\theta + \beta_{\theta}'' \, \delta\theta^2$$

For the critically phase matched situation the first term dominates and ΔK is linear in $\delta\theta$. In the case of NCPM the first term vanishes and ΔK is quadratic in $\delta\theta$.

The sensitivity of the conversion process to the dephasing δ increases as the drive increases. Eimerl has defined the effective dephasing δ_{eff} as given by

$$\delta_{eff} = \delta \exp (\eta_o^{1/2}) \qquad \text{A-5}$$

It might be useful to briefly discuss the conversion efficiency behaviour. If $\eta_o<1$, then the conversion efficiency is

$$\eta = \eta_o \left(\frac{\sin\delta}{\delta}\right)^2 \qquad \text{A-6}$$

Which is the solution for the low conversion efficiencies. If $\eta_o = 1$, this point can be considered as the point where saturation begins and the fundamental pulse is significantly depleted. In this case the conversion efficiency is approximated by

$$\eta \approx \tanh^2 (\eta_o^{1/2}) \frac{\sin^2\delta_{eff}}{\delta_{eff}^{\,2}} \qquad \text{A-7}$$

In the case of perfect phase matching $\Delta K = 0$, so that

$$\eta = \tanh^2 (\eta_o^{1/2}) \qquad \text{A-8}$$

η approaches 1 as the drive tends to infinity.

Eimerl gives other asymptotic efficiency expressions for cases other than those discussed above ($\eta_o >> 1$, $\delta << \pi$), as well as a contour plot of calculated efficiency vs intermediate values of drive and dephasing. These can be found in reference [1].

2. Conversion efficiency of THG

Frequency mixing in the nonlinear media is the other important method for further extending wavelength ranges. Frequency tripling of 1 μm lasers (for example the Nd:YAG laser) are particular cases of mixing, in which the second harmonic wave and the fundamental wave mix in the nonlinear medium and produce a frequency tripled wave ($\omega + 2\omega = 3\omega$). In general such a device consists of a tripling crystal directly following the doubling crystal. Hence, the tripling process involves doubling a fraction of the fundamental radiation of frequency ω in the first doubling crystal, and then mixing the 2ω radiation so produced with the unconverted fundamental radiation in the tripling crystal. In this case, high efficiency for tripling is not necessarily directly proportional to the efficiency of second harmonic generation. Conditions of photon energy conservation and momentum conservation need to be considered. The first condition can be expressed by the rules of Manley-Rowe[2], in which the incremental power gain/loss at λ_3 is accompanied by a concomitant power loss/gain at λ_1 and λ_2 individually, all of which are in proportion to their photon energies, namely

$$+\lambda_1 \Delta P_1 = +\lambda_2 \Delta P_2 = \pm\lambda_3 \Delta P_3 \quad .$$

Where ΔP_i is the incremental change in power at λ_i. For THG, this implies that one fundamental photon plus one second harmonic photon (twice the power) will, under 100% conversion, yield one third harmonic photon at three times the power. Any imbalance of fundamental or second harmonic power in excess of the 1:2 power ratio will not be converted. The momentum conservation condition can be expressed by the phase matching theory, which depends upon what type of geometry is to be employed in the mixing process, and further determines the polarisation states of these two radiations.

Practically there are three different configurations for efficient tripling, namely "polarisation-mismatch scheme", "angle-detuning scheme", and "polarisation-bypass scheme". These have been discussed by Craxton[4]. The first two schemes have been considered for use in our experimental investigations, and the idealised doubler performance for these two tripling schemes is described in figure (4-5).

It has been seen that in the "polarisation-mismatch scheme, a type II doubler is used. In this geometry the incident electric field at ω is linearly polarised at an angle $\theta p = \tan^{-1}(1/\sqrt{2})$ to the o-direction. This ensure that two o-photons are incident for every e-

attainable is 67% when each e-photon combines with one o-photon to give one e-photon at 2ω. Hence, this doubler output is suitably polarized and energy balanced for direct input to a type II geometry tripler.

In the "angle-detuned" scheme, the doubler may be in the type I geometry. In this case the polarisation states of both the generated second harmonic wave and the remaining fundamental wave are ideally matched to the subsequent sum-frequency mixing process in the type II geometry tripler. Hence, the important thing is now only that of energy balance. It also can be satisfied for a suitable choice of doubler thickness, and by detuning with a small angle θ_m, to control the SHG conversion efficiency accurately at 67 %. However, in this case the doubler would be more sensitive to alignment errors, and therefore operationally inconvenient. If the doubler is in a type I NCPM geometry, and temperature phase matching is possible, detuning can be controlled by a small temperature difference ΔT. In this case the difficulties in alignment may be largely ignored.

The Eimerl theory can also be used for the calculation of THG conversion efficiency, where the nonlinear drive is now replaced by the formula given by [3], namely

$$\eta_o = C^2 I_1 I_2 L^2/(I_1+I_2) \qquad \text{A-9}$$

The restrictions and parameters used in designing devices for frequency doubling and tripling are listed in table (A-I-1)

3. Theoretical results

Using the given function (A-1) and the conditions given in table (A-1) we predicted SHG and SFM conversion efficiency against pump intensities by directly solving Jacobi elliptical functions. The pump beam divergence was calculated using the Gaussian beam far field definition. The pump power intensity used here is the average intensity. This approximation avoids calculations involving the Gaussian distribution. The calculation of THG conversion efficiency was carried out with type II SHG/ type II SFM geometry, under the condition that the SHG process be optimized. This mean that (1) the incident fundamental radiation is linearly polarized at 45° to the o-direction, and hence, (2) that ideally only 50 % of the residual fundamental radiation takes part in

frequency mixing process. Another condition used in this calculation is that 60 % of the second harmonic wave takes part in the frequency mixing process. This number was initially from references [5] and [6], and later conformed by our experiments. The results of the calculation of the conversion efficiencies of SHG and THG are plotted into the figure (A-I-1) and (A-I-2).

Table A-I-1 Some relevant parameters of SHG and SFM

Pump:	Nd:YAG laser		
	Pump wavelength	1.064	μm
	Pump energy	10	mJ
	Pulse width	10	ns
	Beam divergence	0.75	mrad
	Focused beam spot size	600	μm
		(Full width at $1/e^2$ peak power)	

	Doubler:	Tripler:
Nonlinear material	KTP crystal (Type II)	LBO crystal (Type II)
	(5 mm length)	(15 mm length)
Phase matching angle (degrees)	23(ϕ)	42(θ)
d_{eff} (pm/V)	3.2	0.8
Walk-off angle (degrees)	0.2	1.028
Acceptance angle (θ) (rad)	0.085	0.0025
Acceptance angle (ϕ) (rad)	0.01	0.042

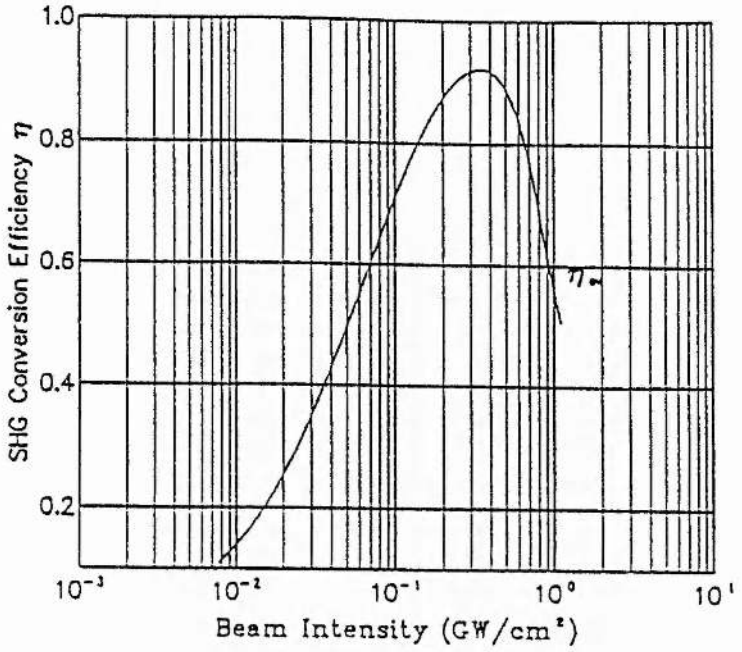

Fig. A-I-1 SHG conversion efficiency against the intensity of the fundamental radiation.

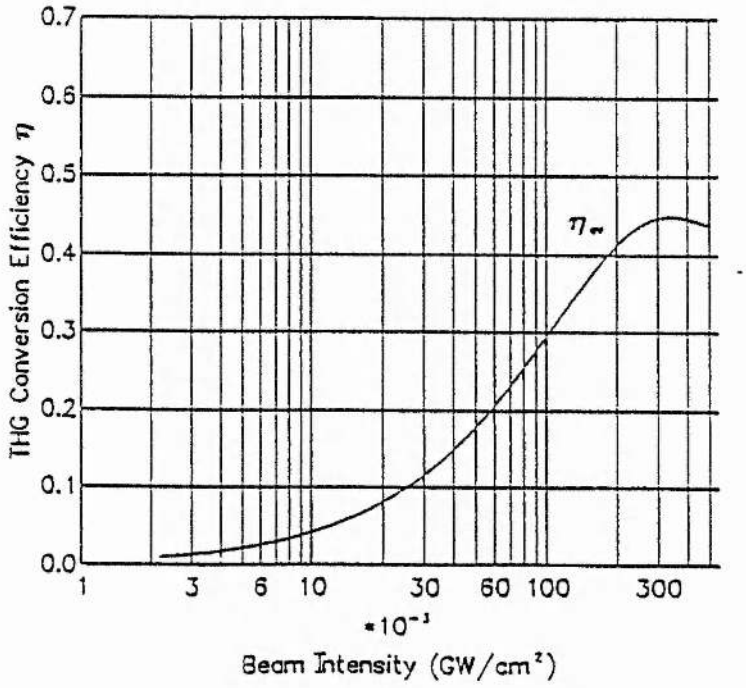

Fig. A-I-2 The overall frequency tripling efficiency against the pump intensity.

References

(1) D. Emierl
IEEE J. Quantum Electron. **23**(5), 575, 1987

(2) J. M. Manley and H. E. Rowe
Proc. IRE, **47**(2), 2115, 1959

(3) D. A. Roberts
IEEE J. Quantum Electron. (submitted, 1992)

(4) R. S. Craxton
IEEE J. Quantum Electron. **17**(9), 1771, 1981

(5) B. C. Wu, N. Chen, and C. T. Chen, D. Q. Deng, and Z. Y. Xu
Opt. Lett. **14**(19), 1080, 1989

(6) A. Borsutzky, R. Brunger, Ch. Huang, and R. Wallenstein
Appl. Phs. B, **52**, 55, 1991

APPENDIX II

Optical properties for various commercial available nonlinear optical materials

LBO (LiB_3O_5, Lithium Triborate)

The Sellmeier dispersion function coefficients [1]

$$n^2 = A + \frac{B}{\lambda^2 - C} - D\lambda^2 + \frac{E}{\lambda^2 - F} + G\lambda^4 \qquad (E = F = G = 0)$$

	A	B	C	D
n_x	2.45316	0.01150	0.01058	0.01123
n_y	2.53969	0.01249	0.01339	0.02029
n_z	2.58515	0.01412	0.00467	0.01850

The orthorhombic system point group	mm2	
(Negative biaxial crystal)		
Crystallographic axes	(a, b, c)	
Optical principal axes	(x, z, y)	
Transparency range	0.16-3.20	μm [2]
Damage threshold	18.9	GW/cm^2
(at 1.054 μm, 1.3 ns)		

$\frac{dnx}{dT}$	$(-1.8\pm0.2) \times 10^{-6}$	$^oC^{-1}$ [3]
$\frac{dny}{dT}$	$(-13.6\pm0.1) \times 10^{-6}$	$^oC^{-1}$ [3]
$\frac{dnz}{dT}$	$(-6.3\pm0.6+(2.1\pm0.8)\lambda) \times 10^{-6}$	$^oC^{-1}$ [3]

(For temperature at 20 °C - 65 °C)

The nonlinear optical coefficients (pm/V) [4]

$d_{31} = 0.97$

$d_{32} = 1.05$

$d_{33} = 0.06$

$d_{15} = 0.89$

$d_{24} = 0.98$

Absorption at 1.064 μm	0.035	%/cm [3]
at 0.355 nm	0.31	%/cm [3]
Shortest SHG wavelength	277	nm [5]
Shortest SFM wavelength	160	nm [5]
	(Limited by crystal transparency range)	

[1] S. J. Lin et al, Appl. Phys. Lett. **59**(13), 1541, 1991
[2] K. Kato, IEEE J. Quantum Electron. **26**(7), 1173, 1990
[3] S. P. Velsko et al, IEEE J. Quantum Electron. **27**(9), 2182, 1991
[4] F. L. Xie et al, Opt. Lett. **16**(16), 1237, 1991
[5] A. Borsutzky et al, Appl. Phys. B**52**, 56, 1991

BBO (β-BaB_2O_4, beta-Barium Borate)

The Sellmeier dispersion function coefficients [1]

$$n^2 = A + \frac{B}{\lambda^2 - C} - D\lambda^2 + \frac{E}{\lambda^2 - F} + G\lambda^4 \qquad (E = F = G = 0)$$

	A	B	C	D
n_o	2.7359	0.01878	0.01822	0.01354
n_e	2.3753	0.01224	0.01667	0.01516

The trigonal system point group (Nagative uniaxial crystal)	3m	
Transparency range	0.189-3.0	μm
Damage threshold (at 1.054 μm, 1.3 ns)	9.9	GW/cm^2
$\frac{dno}{dT}$	-9.3×10^{-6}	$^oC^{-1}$
$\frac{dne}{dT}$	-16.6×10^{-6}	$^oC^{-1}$

The nonlinear optical coefficients (pm/V) [2]

$d_{22} = 1.6 \pm 0.4$ $\qquad$ $d_{22} = 2.2$ [3]

$d_{31} < 0.05 d_{22}$

Absorptions at 266 nm	7	%/cm[4]
Shortest SHG Wavelength	205	nm
Shortest SFM wavelength	190	nm
	(Limited by crystal transparency range)	

[1] K. Kato, IEEE J. Quantum Electron. **22**(7), 1013, 1986
[2] D. Eimerl et al, J. Appl. Phys. **62**(5), 1970, 1987
[3] R. C. Eckardt et al, IEEE J. Quantum Electron. **26**(5), 922, 1990
[4] K. Kato, IEEE J. Quantum Electron. **22**(9), 1455, 1986

KTP ($KTiOPO_4$, Potassium Titanate Phosphate)

The Sellmeier dispersion function coefficients [1]

$$n^2 = A + \frac{B}{\lambda^2 - C} - D\lambda^2 + \frac{E}{\lambda^2 - F} + G\lambda^4 \qquad (E = F = G = 0)$$

	A	B	C	D
n_x	2.9971	0.041030	0.038368	0.012568
n_y	3.0197	0.044090	0.042035	0.012046
n_z	3.3055	0.063289	0.044783	0.013987

The orthorhombic system point group (Positive biaxial crystal)	mm2	
Crystallographic axes	(a, b, c)	
Principal optical axes	(x, y, z)	
Transparency range	0.35-4.5	μm
Damage threshold (at 1.054 μm, 1.3 nm)	4.6	GW/cm^2 [2]
$\frac{dnx}{dT}$	1.1×10^{-5}	$^oC^{-1}$
$\frac{dnz}{dT}$	1.6×10^{-5}	$^oC^{-1}$

The nonlinear optical coefficients (pm/V) [3]

$d_{31} = 6.5$	$d_{31} = 1.93 \pm 0.2$ [1]
$d_{32} = 5.0$	$d_{32} = 3.48 \pm 0.3$ [1]
$d_{33} = 13.7$	$d_{33} =$ ----------
$d_{24} = 7.6$	$d_{24} = 3.3$ [4]
$d_{15} = 6.1$	$d_{15} = 2.6$ [4]

[1] H. Y. Shen et al, IEEE J. Quantum Electron. **28**(1), 48, 1992
[2] FC CASTECH Inc. Trade Literature on LBO, 1991
[3] F. C. Zumsteg et al, J. Appl. Phys. **47**(11), 4980, 1976
[4] R. C. Eckardt et al, IEEE J. Quantum Electron. **26**(5), 922, 1990

$KNbO_3$ (Potassium Niobate)

The Sellmeier dispersion function coefficients [1]

$$n^2 = A + \frac{B}{\lambda^2 - C} - D\lambda^2 + \frac{E}{\lambda^2 - F} + G\lambda^4 \qquad (D = G = 0)$$

	A	B	C	E	F
n_x	4.3898	0.009383630	0.10724149	0.103389333	0.03130828
n_y	4.7984	0.086138365	0.05985156	0.054324401	0.02302662
n_z	4.9375	0.015402446	0.11308698	0.155393874	0.04087914

The orthorhombic system point group (Negative biaxial crystal)	mm2	
Crystallographic axes	(a, b, c)	
Principal optical axes are	(y, z, x)	
Transparency range	0.4-5.0	μm
Damage threshold	0.35	GW/cm^2 [3]
$\frac{dnx}{dT}$	5.83×10^{-5}	$^oC^{-1}$
$\frac{dny}{dT}$	-3.73×10^{-5}	$^oC^{-1}$

The nonlinear optical coefficients (pm/V)

$d_{31} = 15.8$

$d_{32} = 18.3$

$d_{33} = 27.4$

$d_{15} = 16.5$

$d_{24} = 17.1$

Shortest SHG wavelength (at room temperature 20 °C)	425	nm [2]
NCPM temperature tuning range (OPO pumped at 532 nm, temperature varied from 184 to 220 °C)	0.86-1.4	μm

[1] J. C. Baumert et al, SPIE, **492**, 374, 1984
[2] K. Kato, IEEE J. Quantum Eletron. **15**(6), 410, 1979
[3] P. Gunter, Proc. SPIE, **236**, 8, 1981

d-LAP (Deuterated L- Arginine Phosphate)

The Sellmeier dispersion function coefficients[1]

$$n^2 = A + \frac{B}{\lambda^2 - C} - D\lambda^2 + \frac{E}{\lambda^2 - F} + G\lambda^4 \qquad (E = F = G = 0)$$

	A	B	C	D
n_α	2.2352	0.0118	0.0146	0.00683
n_β	2.4313	0.0151	0.0214	0.01430
n_γ	2.4484	0.0172	0.0229	0.01150

The monoclinic system point group	2	
(Negative biaxial crystal)	$n_\gamma > n_\beta > n_\alpha$	
Optical principal axes	(γ, β, α)	
($\beta = 98^\circ$ is the angle between the crystallographic a and c axes, b is the twofold axis.)		
Transparency range	0.25-1.30	μm
Damage threshold	9-13	J/cm^2
$\frac{dn_\alpha}{dT}$	-42.0±0.6 x 10^{-6}	$^\circ C^{-1}$
$\frac{dn_\beta}{dT}$	-24.2±0.8 x 10^{-6}	$^\circ C^{-1}$
$\frac{dn_\gamma}{dT}$	-70.5±0.5 x 10^{-6}	$^\circ C^{-1}$

The nonlinear optical coefficients (pm/V)

[With β(=b)]

$d_{\beta\alpha\alpha}$ = 0.40

$d_{\beta\beta\beta}$ = 0.92

$d_{\beta\alpha\gamma}$ = -0.58

$d_{\beta\gamma\gamma}$ = -0.84

[1] D. Emierl et al, IEEE J. Quantum Electron. **25**(2), 179, 1989

$LiNbO_3$ (Lithium Niobate)

The Sellmeier dispersion function coefficients [1]

$$n^2 = A_1 + \frac{A_2 + B_1 F}{\lambda^2 - (A_3 - B_2 F)^2} + B_3 F - A_4 \lambda^2$$

$$F = (T - T_o)(T + T_o + 546)$$

	A_1	A_2	A_3	A_4	B_1	B_2	B_3	T_o
n_o	4.9048	0.11775	0.21802	0.027153	2.2314×10^{-8}	-2.9671×10^{-8}	2.1429×10^{-8}	24.5
n_e	4.5820	0.09921	0.21090	0.021940	5.2716×10^{-8}	-4.9143×10^{-8}	2.2971×10^{-8}	24.5

The trigonal system point group (Nagative uniaxial crystal)	3m	
Transparency range	0.4-5.0	μm
Damage threshold (at 1.064 μm)	1	GW/cm^2[2]
$\frac{dnx}{dT}$	2.0×10^{-5}	$^oC^{-1}$ [2]
$\frac{dnz}{dT}$	7.6×10^{-5}	$^oC^{-1}$ [2]

The nonlinear optical coefficients (pm/V) [2]

$d_{31} = 4.72$

$d_{32} = d31$

$d_{33} = -45.1$

$d_{24} = d31$

$d_{15} = d24$

$d22 = -d21 = -d16 = 2.4$

[1] G. J. Edwards et al, Opt. Quantum Electron. **16**(4), 373, 1984
[2] E. C. Cheung et al, J. Opt. Soc. Am. **B8**(7), 1461, 1991

$LiIO_3$ (Lithium Iodate)

The Sellmeier dispersion function coefficients [1]

$$n^2 = A + \frac{B}{\lambda^2 - C} - D\lambda^2 + \frac{E}{\lambda^2 - F} + G\lambda^4 \qquad (E = F = G = 0)$$

	A	B	C	D
n_o	3.41400	0.046293	0.037106	0.0076032
ne	2.92282	0.032872	0.033335	0.0042623

The hexagonal system point group (Negative uniaxial crystal)	6	
Transparency range	0.3 - 5.5	μm
Damage threshold (at 1.064 μm, 10 ns and 0.532 nm, 15 ns)	0.5	GW/cm^2
$\frac{dnx}{dT}$	-8.9×10^{-5}	$^oC^{-1}$
$\frac{dnz}{dT}$	-7.8×10^{-5}	$^oC^{-1}$

The nonlinear optical coefficients (pm/V) [2]

$d_{31} = -4.64$ ($d_{31} = -4.1 \pm 0.2$ [3], $d_{31}(LiIO_3) / d_{36}(KDP) = 11$[4])

$d_{32} = d_{31}$

$d_{33} = -4.84$ $d_{33}/d_{31} = 0.8$ [4]

$d_{24} =$ ------

$d_{15} = d_{24}$ $d_{15} = 5.5+0.3$ [5]

$d_{14} = 0.31$

$d_{25} = d_{14}$

[1] H. Y. Shen et al, J. Appl. Phys. **70**(3), 1880, 1991
[2] E. C. Cheung et al, J. Opt. Soc. Am. B**8**(7), 1991
[3] R. C. Eckardt et al, IEEE J. Quantum Electron. **26**(5), 922, 1990
[4] F. R. Nash et al, J. Appl. Phys. **40**(13), 5201, 1969
[5] B. F. Levine et al, Appl. Phys. lett. **20**(8), 272, 1972

$AgGaSe_2$ (Silver Gallium Selenide)

The Sellmeier dispersion function coefficients[1]

$$n^2 = A + \frac{B}{\lambda^2 - C} - D\lambda^2 + \frac{E}{\lambda^2 - F} + G\lambda^4 \qquad (E = F = G = 0)$$

	A	B	C	D
no	6.8544	0.408146368	0.19264	0.0012838
ne	6.6913	0.395833575	0.28365	0.0013430

The tetragonal system point group	42m	
Transparency range	0.73-17.0	μm
Damage threshold	11-30	MW/cm^2
$\frac{dno}{dT} - \frac{dne}{dT}$ $(\lambda = 3.39\ \mu m)$	$30x10^{-6}$	$^oC^{-1}$

The nonlinear optical coefficients (pm/V)[2]

$d_{36} = 43.0$ $\lambda = 10.6\ \mu m$

($d_{36} = 49.3$ $\lambda = 10.6\ \mu m$ [1])

($d_{36} = 39.0$ $\lambda = 2.1\ \mu m$ [3])

Absorption coefficients (at $\lambda = 2.1\ \mu m$)	6.0	m^{-1}
OPO tuning range ($\lambda_p = 2.1\ \mu m$, Type I)	2.5-13	μm

[1] E. C. Cheung et al, J. Opt. Soc. Am. B**8**(7), 1504, 1991
[2] R. C. Eckardt et al, Appl. Phys. Lett. **47**(8), 786, 1985
[3] N. P. Barnes et al, Appl. Opt. **28**(23), 5162, 1989

$AgGaS_2$ (Silver Thiogallate)

The Sellmeier dispersion function coefficients [1]

$$n^2 = A + \frac{B}{\lambda^2 - C} - D\lambda^2 + \frac{E}{\lambda^2 - F} + G\lambda^4 \qquad (D = G = 0)$$

	A	B	C	E	F
no	4.5622	0.223294602	0.09311	2055.8	950
ne	7.8799	0.216152178	0.11066	2410.91037	1030.7

The tetragonal system point group 42m

Transparency range	0.53-12.0	μm
Damage threshold	13	MW/cm^2
(at 1.064 μm, 20 ns)	(>3 GW/cm^2 [4])	
$\frac{dnx}{dT}$	$5x10^{-5}$	$^oC^{-1}$[2]
$\frac{dnz}{dT}$	$5x10^{-5}$	$^oC^{-1}$[2]

The nonlinear optical coefficients (pm/V)

d_{36} = 22 (for 1.064 μm)

(d_{36} = 28.7, for 1.064 μm SHG[2])

(d_{36} = 18 ± 30%, for 10.6 μm SHG[3])

(d_{36} = 31± 5, for 600 nm OPO[5])

Shortest SHG Wavelenth

OPO tuning range 1.2-10 μm [4]

(pump wavelength 1.064 μm)

[1] R. L. Byer, Appl. Phys. Lett. **45**(4), 313, 1984
[2] E. C. Cheung et al, J. Opt. Soc. Am. B**8**(7), 1491, 1991
[3] G. D. Boyd et al, IEEE J. Quantum Electron. **7**(12), 563, 1971
[4] T. Elsaesser etal, Appl. Phys. Lett. **44**(4), 383, 1984
[5] P. Canarelli et al, IEEE J. Quantum Electron. **28**(1), 52, 1992

APPENDIX III

Theoretical calculations of phase matching conditions relating to potassium titanyl phosphate for second harmonic generation, lithium triborate for sum-frequency mixing and optical parametric oscillation

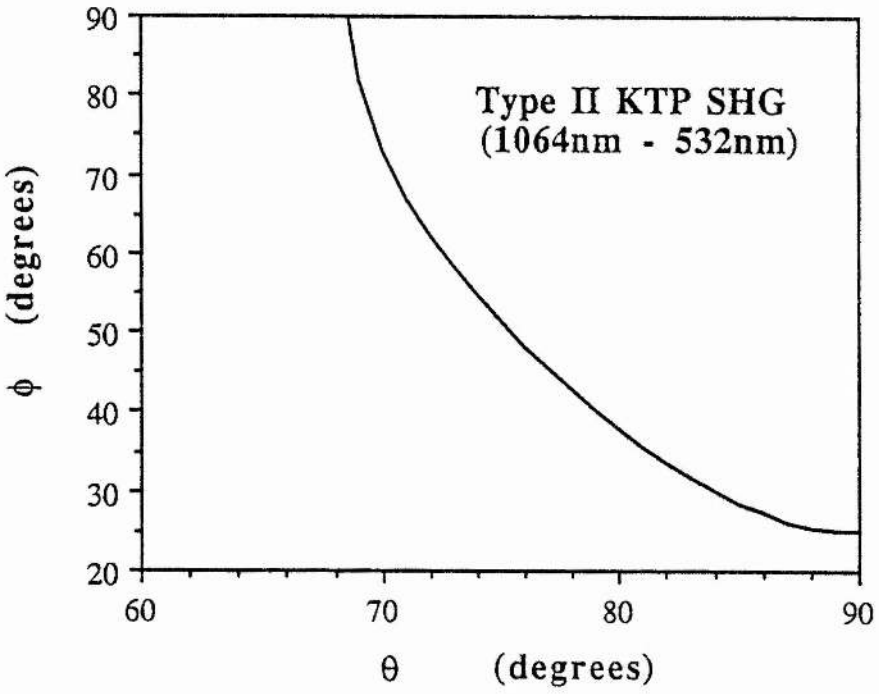

Fig. A-II-1 Phase matching curve for second harmonic generation of 1.064 μm radiation in KTP.

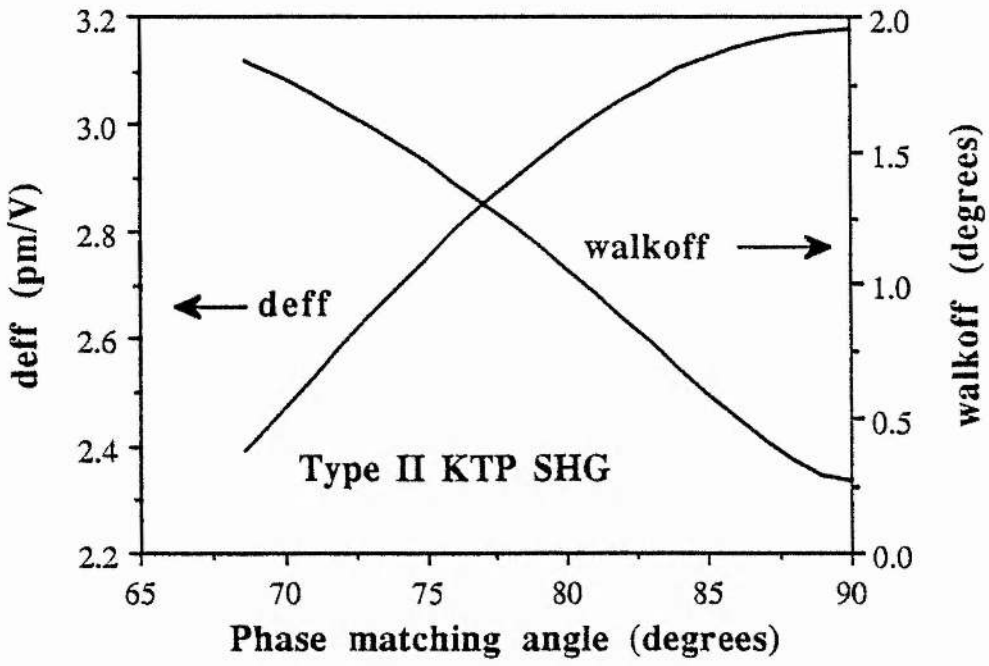

Fig. A-II-2 Effective nonlinear coefficient and walkoff angle in KTP as a function of the θ under phase matching condition for second harmonic generation.

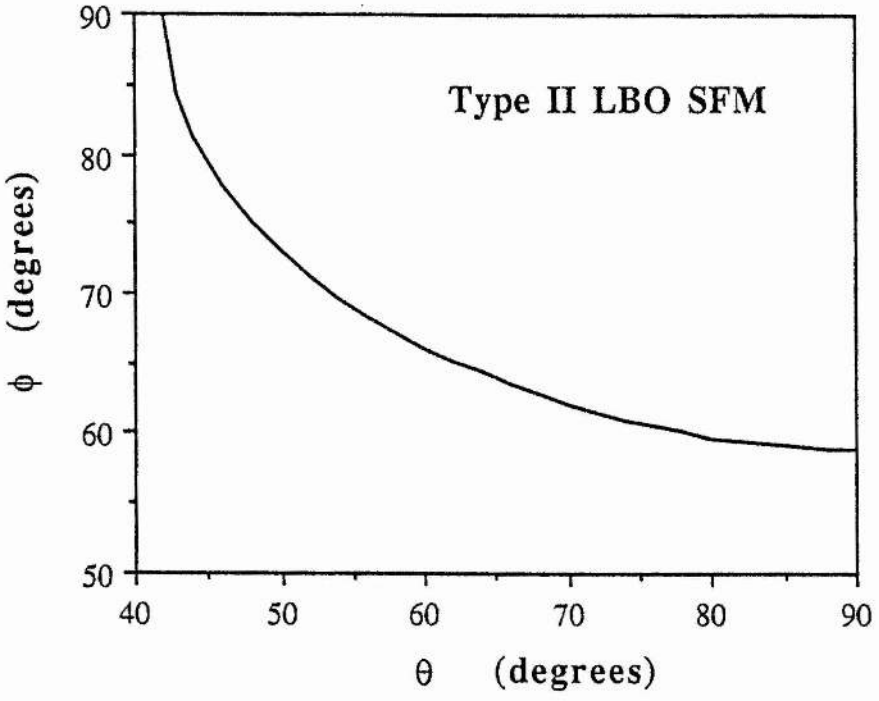

Fig. A-II-3 Phase matching curve for sum-frequency mixing of 1.064 μm and 532 nm radiations in type II LBO.

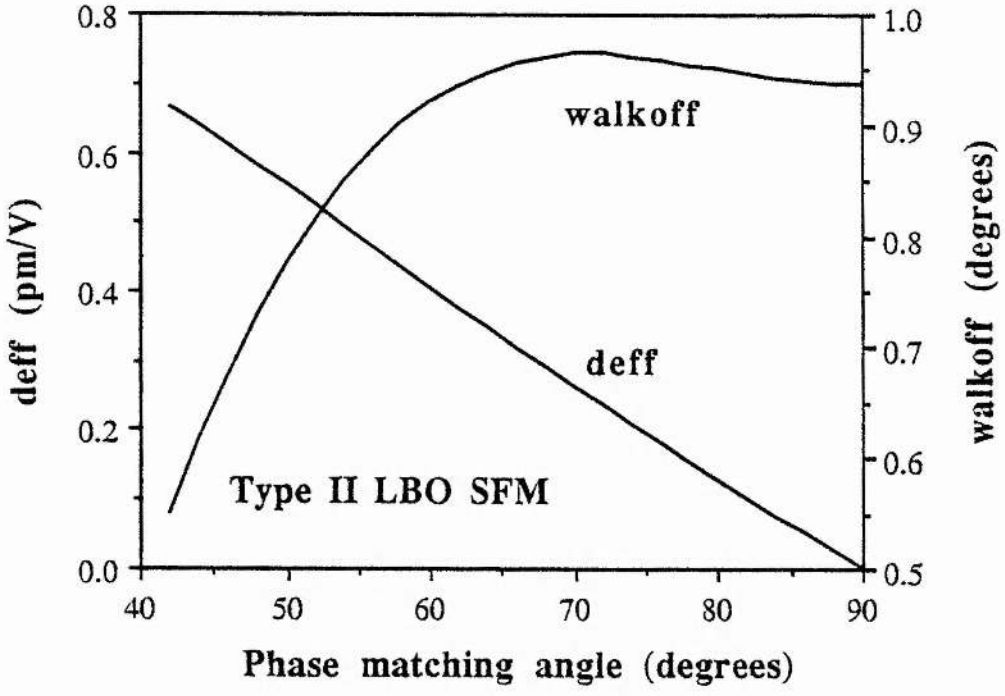

Fig. A-II-4 Effective nonlinear coefficient and walkoff angle for sum-frequency mixing in type II LBO as a function of the θ angle.

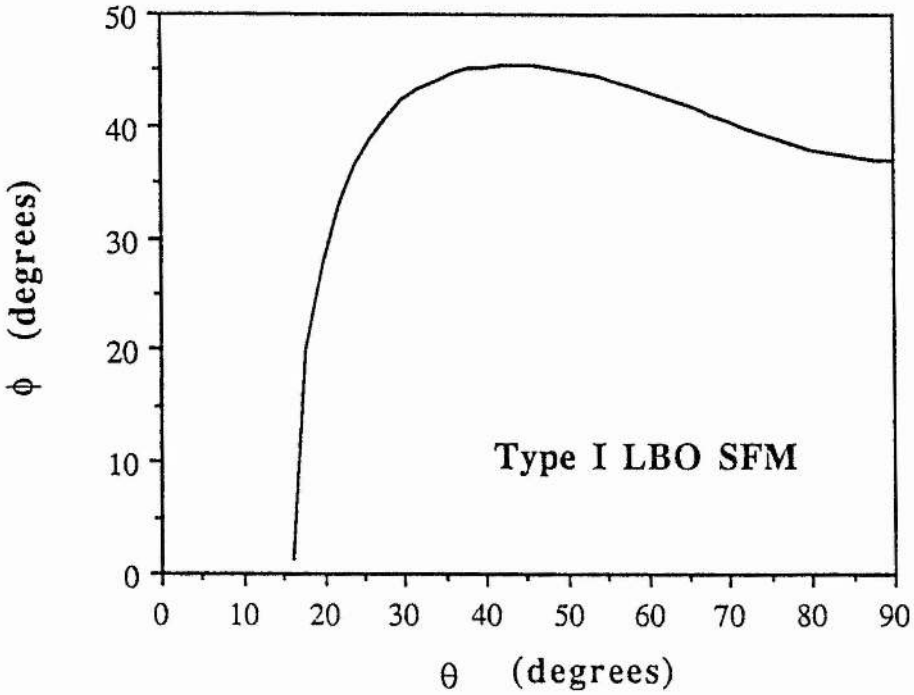

Fig. A-II-5 Phase matching curve for sum-frequency mixing of 1.064 μm and 532 nm radiations in type I LBO.

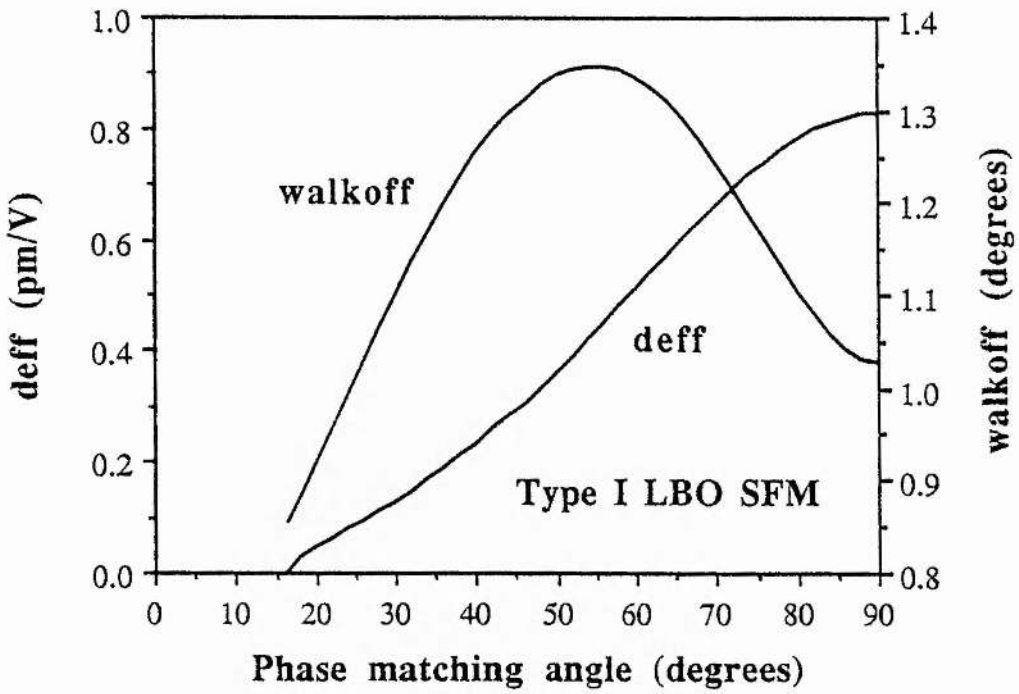

Fig. A-II-6 Effective nonlinear coefficient and walkoff angle for sum-frequency mixing in type I LBO as a function of the θ angle.

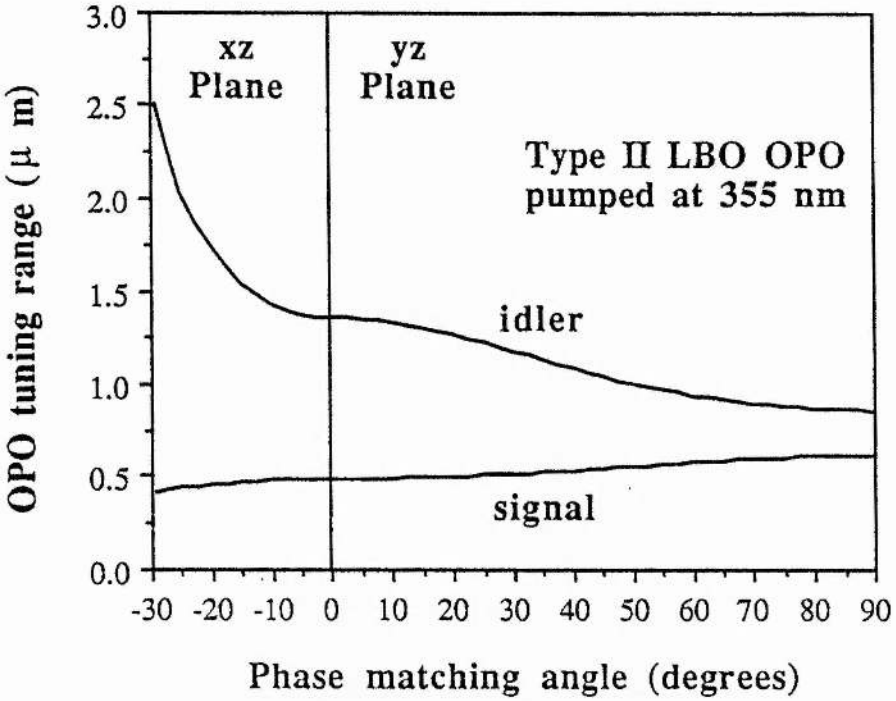

Fig. A-II-7 Signal and idler wave tuning curves in the xz- and yz-principal plane as a function of angle θ for the case of type II LBO OPO pumped at 355 nm.

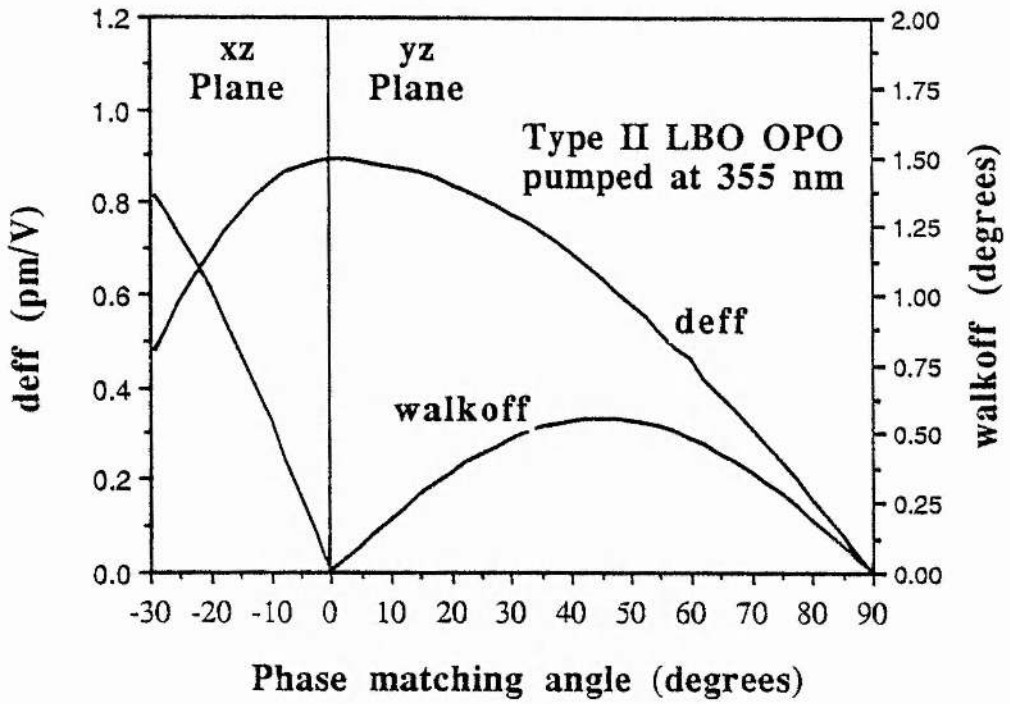

Fig. A-II-8 Affective nonlinear coefficient and walkoff angle for type II LBO OPO as a function of the angle θ.

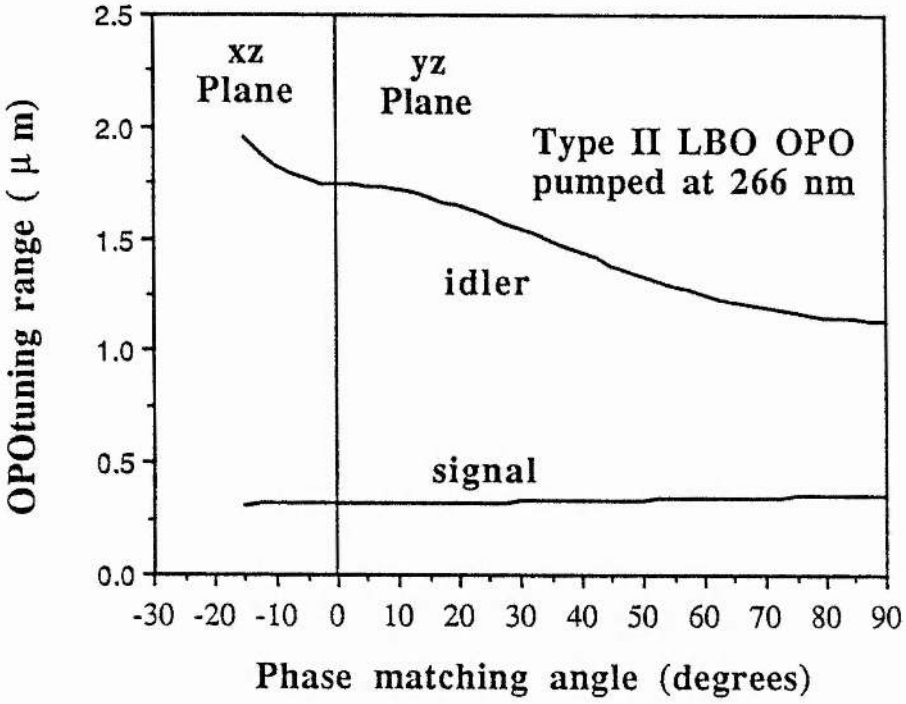

Fig. A-II-9 Signal and idler wave tuning curves in the xz- and yz-principal plane as a function of angle θ for the case of type II LBO OPO pumped at 266 nm.

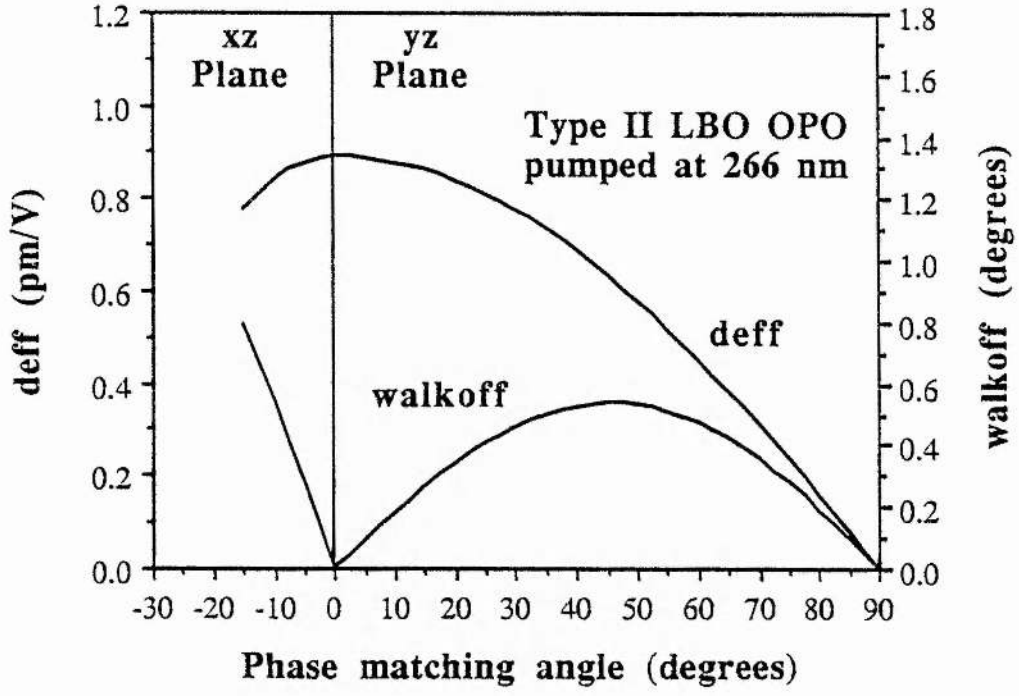

Fig. A-II-10 Effective nonlinear coefficient and walkoff angle as a function of the angle θ for type II LBO OPO pumped at 266 nm.

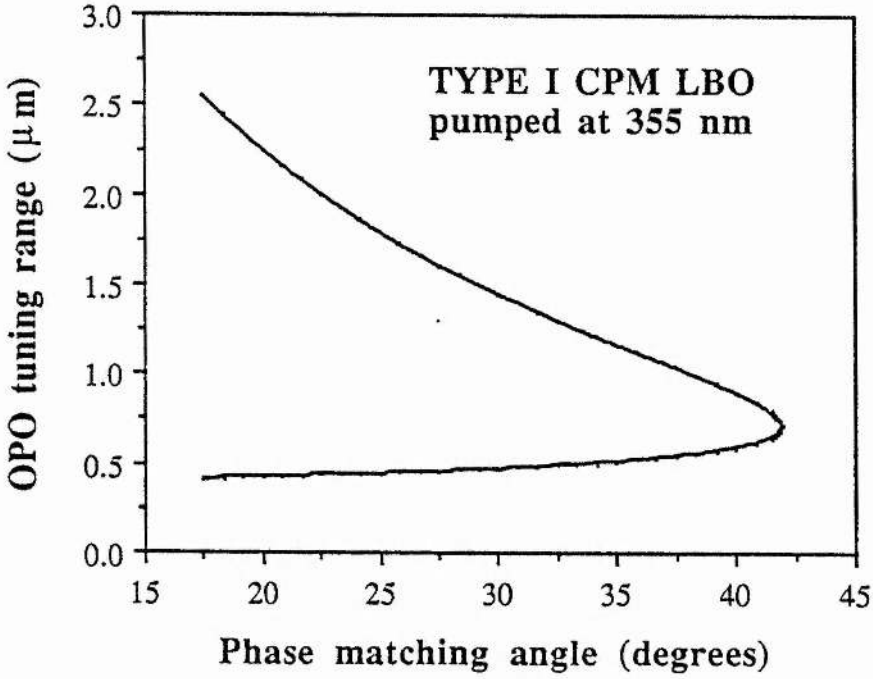

Fig. A-II-11 Signal and idler wave tuning curves in the xy- principal plane as a function of angle ϕ for the case of type I LBO OPO pumped at 355 nm.

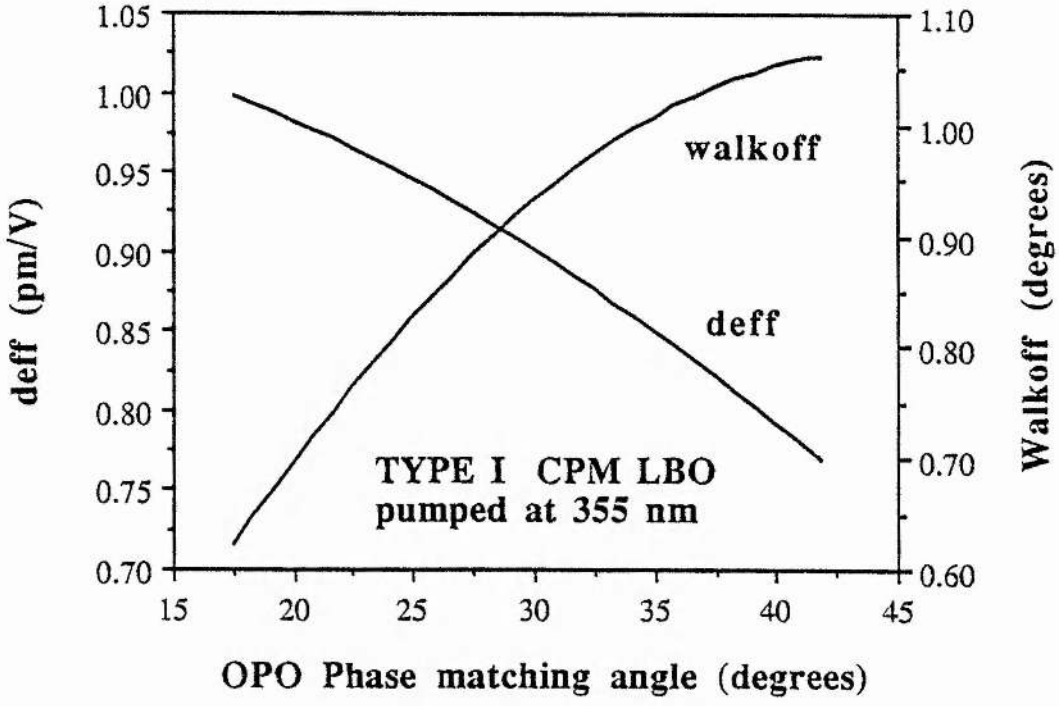

Fig. A-II-12 Effective nonlinear coefficient and walkoff angle as a function of the angle ϕ for type I LBO OPO pumped at 355 nm.

APPENDIX IV

Computer programme

for calculation of optimum focussing parameter h_{sm}

(For definition of the parameters given in the flowchart on the next page see Guha, Wu and Falk's paper, in IEEE J. Quantum Electron. Vol. 18, No. 5, P 907, 1982.)

APPENDIX IV *Computer programme*

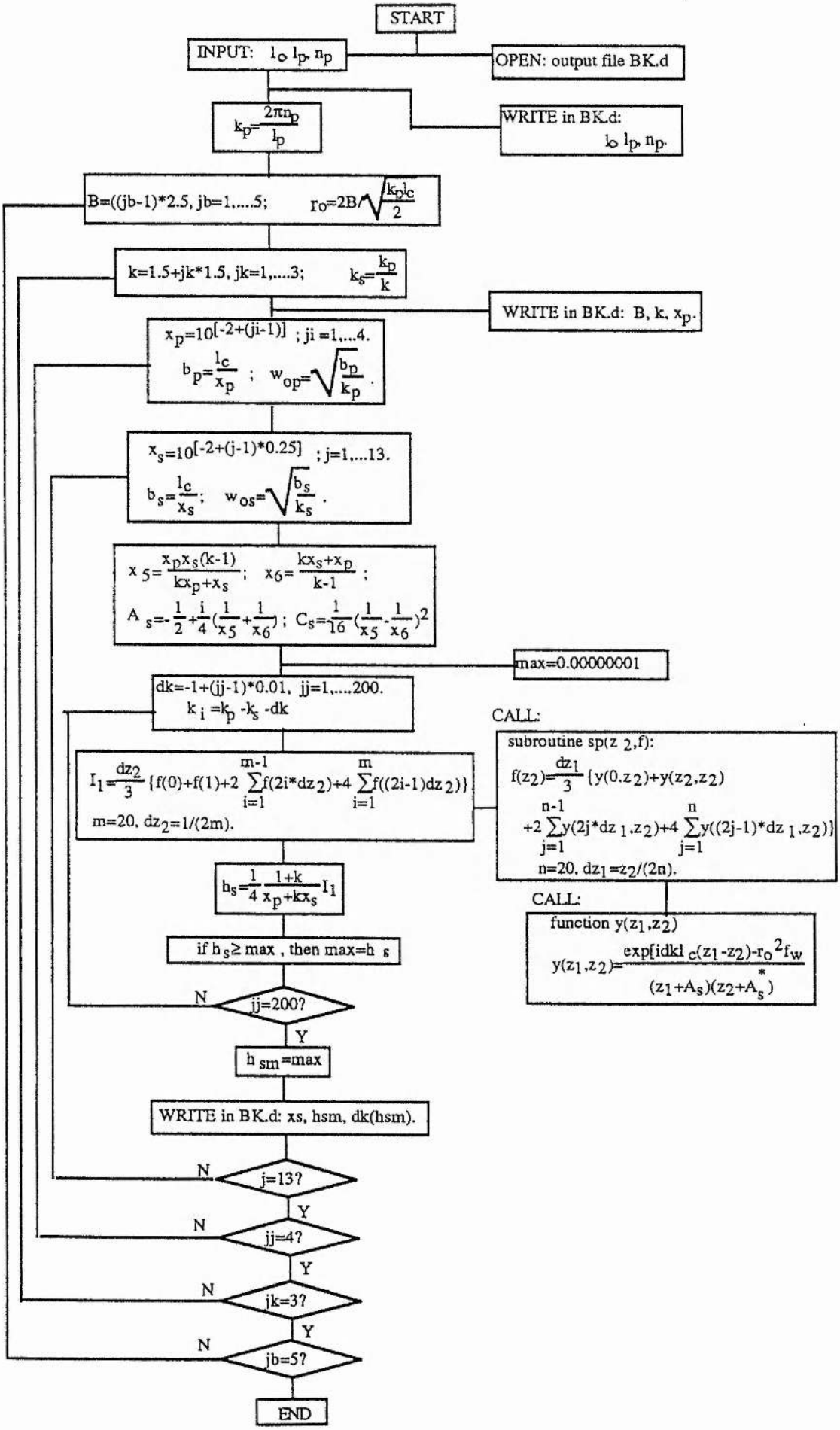

```
c       NewBK.f
        program BODK1
        double complex as
        double precision dz2,e,d,lc,lp,np,b,xp,xs,bp,bs,wop
        double precision r,f,fo,fe,f1,f2,ro,dk,k,kp,ks,ki
        double precision x5,x6,ccs,max,hsm,hs(200),dkL,wos
        integer m
        common  k,dk,lc,bp,bs,wop,wos,ro,as,ccs,ki
        open(12,file='BK.d',status='unknown')
        m=20
        dz2=1.00d00/dble(2*m)
        print*,'Crystal Length = ? (in mm)'
        read(*,*)lc
        print*,'Pump Wavelength = ? (in micrometer)'
        read(*,*)lp
        print*,'Refractive Index of Pump Wave = ? '
        read(*,*)np
        write(12,45)lc,lp,np
45      format('Crystal Length =',f6.2,'(mm)'/'Pump Wave Length =',
     1  f6.4,'(micrometer), Np=',f7.5//)
        kp=2.00d00*3.141592654d00*np*1000.00d00/lp
        do 80 jb=1,5
        b=dble(jb-1)*2.50d00
        ro=2.00d00*b/dsqrt(kp*lc/2.00d00)
        do 70 jk=1,3
        k=1.50d00+dble(jk-1)*1.50d00
        ks=kp/k
        do 30 ji=1,4
        xp=-2.00d00+dble(ji-1)
        xp=10.00d00**xp
        write(12,46)b,k,xp
46      format('B=',f5.2,2x,'K=',f6.3,2x,'xp=',f5.2,2x,//2x,'xs',
     1  6x,'hsm',8x,'dkL')
        bp=lc/xp
        wop=dsqrt(bp/kp)
        do 10 j=1,13
        xs=-2.00d00+dble(j-1)*0.25d00
        xs=10.00d00**xs
        bs=lc/xs
        wos=dsqrt(bs/ks)
        x5=xp*xs*(k-1.00d00)/(k*xp+xs)
        x6=(k*xs+xp)/(k-1.00d00)
        as=DCMPLX(-0.50d00,(1.00d00/x5+1.00d00/x6)*0.25d00)
        ccs=-(1.00d00/x5-1.00d00/x6)**2/16.00d00
        fo=0.00d00
```

```
      max=0.00000001d00
      do 40 jj=1,200
      dk=-1.00d00+dble(jj-1)*0.01d00
      ki=kp-ks-dk
      call sp(1.00d00,f)
      fe=f
      r=0.50d00*(fo-fe)
      do 20 i=1,m
      e=dble(2*i-1)*dz2
      d=dble(2*i)*dz2
      call sp(e,f)
      f1=f
      call sp(d,f)
      f2=f
20    r=r+2.00d00*f1+f2
      r=r/dble(3*m)
      hs(jj)=(1.00d00+k)*0.25d00*r/(xp+xs*k)
      max=DMAX1(hs(jj),max)
40    continue
      hsm=max
      do 60 jj=1,200
      if(DABS(hs(jj)-hsm).le.0.00000000001) then
      dkL=(-1.00d00+dble(jj-1)*0.01d00)*lc
      end if
60    continue
      write(12,22)xs,hsm,dkL
22    format(f5.2,2x,f8.6,2x,f8.4)
10    continue
30    continue
70    continue
80    continue
      print*,'The results have been listed in file BK.d '
      stop 200
      end

      subroutine sp(z2,f)
      integer n
      double precision y,z2,dz1,f,yo,ye,a,b
      n=20
      dz1=z2/dble(2*n)
      yo=y(0.00d00,z2)
      ye=y(z2,z2)
      f=0.50d00*(yo-ye)
      do 10 i=1,n
      a=dble(2*i-1)*dz1
      b=dble(2*i)*dz1
10    f=f+2.00d00*y(a,z2)+y(b,z2)
      f=f*z2/dble(3*n)
      end

      double precision function y(z1,z2)
      double complex fw,as,a4,a5,a3,ib1,cp,cpp,cs,csp,u,v,yo
      double complex ccp,cc
      double precision wop,wos,lc,bp,bs,ki,ccs,dk
      double precision k,z1,z2,z,zp,a,tsp,tpp,ts,tp,ro,b
      common  k,dk,lc,bp,bs,wop,wos,ro,as,ccs,ki
      if(ro.le.0.000000001d00)then
      a=0.00d00
      b=dk*lc*(z1-z2)
```

```
      goto 20
      end if
      zp=z2*lc
      z=z1*lc
      tp=2.00d00*(z-lc/2.00d00)/bp
      ts=2.00d00*(z-lc/2.00d00)/bs
      tpp=2.00d00*(zp-lc/2.00d00)/bp
      tsp=2.00d00*(zp-lc/2.00d00)/bs
      cpp=DCMPLX(1.00d00, tpp)*wop**2
      cp=DCMPLX(1.00d00, tp)*wop**2
      cs=DCMPLX(1.00d00, ts)*wos**2
      csp=DCMPLX(1.00d00, tsp)*wos**2
      ccp=1.00d00/cpp+1.00d00/DCONJG(csp)
      ccp=1.00d00/ccp
      cc=1.00d00/cp+1.00d00/DCONJG(cs)
      cc=1.00d00/cc
      a3=-ki/(ki*ccp+DCMPLX(0.00d00,2.00d00*(z-zp)))
      ib1=1.00d00/cc-DCONJG(a3)
      a4=ki*ccp*(zp-lc/2.00d00)/(cpp*(ki*ccp+DCMPLX(0.0d00,
     1  2.0d00*(z-zp))))
      a5=(DCONJG(csp)+cpp)*(2*(z-zp)+DCMPLX(0.00d00,-ki)*ccp)
      a5=(zp-lc/2.00d00)**2*(2*(z-zp)+DCMPLX(0.00d00,-ki)
     1  *DCONJG(csp))/a5
      fw=DCONJG(a5)+(lc*(z1-0.5d00))**2/cp
     1  -(DCONJG(a4)+lc*(z1-0.5d00)/cp)**2/ib1
      u=DCMPLX(0.00d00,dk*lc*(z1-z2))-ro**2*fw
      a=dble(u)
      b=DIMAG(u)
20    v=(z1+as)*(z2+DCONJG(as))+ccs
      yo=DEXP(a)*DCMPLX(DCOS(b),DSIN(b))/v
      y=dble(yo)
      end
```